Title
Genetic divergence and therapy-driven evolution between initial and recurrent glioma

Permalink
https://escholarship.org/uc/item/8qn3f728

Author
Johnson, Brett Earl

Publication Date
2014

Peer reviewed|Thesis/dissertation

Genetic divergence and therapy-driven evolution between initial and
recurrent glioma

by

Brett E. Johnson

DISSERTATION

Submitted in partial satisfaction of the requirements for the degree of

DOCTOR OF PHILOSOPHY

in

Biomedical Sciences

in the

GRADUATE DIVISION

of the

UNIVERSITY OF CALIFORNIA, SAN FRANCISCO

DEDICATION AND ACKNOWLEDGMENTS

For Timber and Copper. Much love and many thanks.

The work presented in this dissertation was made possible with the help and support of many amazing collaborators. Specific acknowledgment is deservedly given to Tali Mazor, Susan Chang, Barry Taylor, and Joseph Costello.

The text of chapters two and three of this dissertation are a reprint of the material as it appears in B. E. Johnson *et al.*, Mutational analysis reveals the origin and therapy-driven evolution of recurrent glioma. *Science (New York, NY)* **343**, 189 (Jan 10, 2014).

Genetic divergence and therapy-driven evolution between initial and recurrent glioma

Brett E. Johnson

ABSTRACT

Low-grade gliomas are slow-growing tumors that often undergo malignant progression to an aggressive high-grade glioblastoma (GBM) with a significantly worse prognosis. Treatment options after surgical resection include temozolomide (TMZ), an alkylating chemotherapeutic which is cytotoxic but can induce C>T/G>A transition mutations when DNA mismatch repair is deficient. However, the extent and clinical impact of TMZ-associated mutagenesis is poorly understood. To investigate the genomic evolution of recurrent tumors and the contribution of TMZ-induced mutagenesis to their mutational landscape, we sequenced the exomes of 23 initial low-grade gliomas and their patient-matched recurrences resected up to 11 years later. We identified a diverse set of evolutionary trajectories that included unexpected losses of canonical driver mutations and radical differences in the genetic relatedness of initial-recurrent tumor pairs. Notably, we found that the recurrent tumors of six patients treated after surgery with TMZ became hypermutated and subsequently recurred as GBM. In each, TMZ-associated mutations altered the function of key cancer genes in pathways involved in malignant progression, including activating mutations in *MTOR* and *PIK3CA*, and inactivating mutations in *CDKN2A*, *PTEN*,

and *RB1*. These findings suggest that this widely used chemotherapeutic agent has the potential to accelerate tumor evolution with unintended clinical and biological consequences. The ongoing evolution of the genetic landscape in all recurrences emphasizes the need for a longitudinal approach to personalized cancer genomics.

TABLE OF CONTENTS

LIST OF TABLES

LIST OF FIGURES

CHAPTER 1.

INTRODUCTION

1.1 LOW-GRADE GLIOMAS AT DIAGNOSIS

1.1.i Histological classification of low-grade gliomas

Gliomas are the most prevalent group of primary brain tumors and are graded clinically and histologically according to the international standard of the World Health Organization (WHO) (*1*). Grade I tumors show little indication of proliferation and are generally treated with surgical resection. These include well-circumscribed pilocytic astrocytomas, pleomorphic xanthoastrocytomas, and gangliomas. Grade II tumors are diffuse and infiltrative, show nuclear atypia and a small amount of proliferative potential, and often require additional treatment beyond an initial surgical resection. The term "low-grade glioma" is imprecise and has many possible definitions. In this dissertation, low-grade glioma refers to the grade II astrocytomas, oligodendrogliomas, and the mixed cell-type oligoastrocytomas in adults. Grade III tumors have increased levels of proliferation and display additional histological signs of anaplasia. Common grade III tumors include anaplastic astrocytomas and anaplastic oligodendrogliomas. The fraction of tumor cells staining positive for Ki-67, a marker of actively dividing cells (*2*), is called the proliferation index, and can be used to differentiate between grade II and grade III lesions (*3*). Grade IV tumors are malignant with histological features such as pseudopalisading necrosis and microvascular proliferation. Direct evidence of the high proliferative rate can be found in the presence of mitotic figures. Glioblastoma multiforme (GBM) is the main form of the fast-growing and highly aggressive grade IV tumors.

While the average overall survival of patients with grade II astrocytomas is 5-10 years, the overall survival for patients with grade II oligodendrogliomas is 10-15 years (*4, 5*). In addition to histological subtype, prognostic factors for patients with low-grade gliomas include the age at diagnosis, Karnofsky performance score (KPS), and the extent of resection (*5-8*). Higher tumor grades are also accompanied by significantly worse prognoses. For patients with grade III and IV tumors the overall survival drops to 2-3 and only 1 year, respectively (*9*).

1.1.ii Characteristic mutations of low-grade gliomas

The histological subtyping of low-grade gliomas results in a stratification of distinct mutational profiles as well. Grade II astrocytomas and oligodendrogliomas each have a set of frequent genetic events that help define them. Common across all histologic subtypes of low-grade gliomas, however, are mutations in the cytosolic *isocitrate dehydrogenase 1* (*IDH1*) or the mitochondrial *isocitrate dehydrogenase 2* (*IDH2*). Isocitrate dehydrogenases convert isocitrate to alpha-ketoglutarate. Mutations in approximately 75% of grade II astrocytomas and 87% of grade II oligodendrogliomas occur exclusively at arginine 132 of *IDH1* or arginine 172 of *IDH2*, the highly conserved binding sites for isocitrate (*10*). These mutations are somatic, heterozygous, and confer a neomorphic enzyme activity converting alpha-ketoglutarate to 2-hydroxyglutarate (2HG) (*11*). The oncometabolite 2HG is a competitive inhibitor of the many alpha-ketoglutarate-dependent dioxygenases (*12*), and its accumulation leads to the inhibition of TET-mediated DNA demethylation and the enrichment of transcriptionally repressive histone marks (*13*). Mutations in *IDH1* and *IDH2* are thus linked to a glioma CpG island

methylator phenotype (G-CIMP) and widespread transcriptional changes (*14*), including the inhibition of genes associated with gliogenic differentiation (*15*). In acute myeloid leukemia, mutations in *IDH1* and *IDH2* are mutually exclusive with mutations in *TET2*, but result in similar epigenetic defects, suggesting a central role for TET enzymes in low-grade gliomas as well (*16*). As mutations in IDH genes are early events in the development of low-grade gliomas (*17*), this represents one model of how *IDH1* and *IDH2* mutations lead to tumorigenesis. On the other hand, low-grade gliomas with wild-type *IDH1* and *IDH2* genes also tend to lack any of the mutations that further characterize either astrocytomas or oligodendrogliomas (*18*), suggesting they have different initiating events. Their genetic landscapes remain largely unexplored but actively under investigation in The Cancer Genome Atlas (TCGA) project, an NIH funded national effort to identify common driver mutations in many tumor types.

IDH-mutant grade II astrocytomas are further characterized by mutations in *TP53* and *alpha thalassemia/mental retardation syndrome X-linked (ATRX)*. Mutations in *TP53* are found in 50-80% of grade II astrocytomas (*19, 20*). *TP53* encodes a protein that plays a key role in a diverse set of cellular processes including the DNA damage response, cell cycle arrest, apoptosis, and senescence. With antiproliferative activity across a broad set of stresses, *TP53* is one of the most frequently inactivated genes in human cancer (*21*). Approximately 70% of grade II astrocytomas also have mutations in *ATRX*, a gene that encodes a chromatin remodeling protein belonging to the SWI/SNF family of DNA helicases (*19, 22*). Inactivating mutations in *ATRX* are thought to permit the homologous recombination necessary for tumor cells to maintain their telomere length

through a telomerase-independent mechanism called the alternative lengthening of telomeres (ALT) (*23*). Mutations in *IDH1/2*, *TP53*, and *ATRX* tend to co-occur in the vast majority of grade II and III astrocytomas, suggesting astrocytic tumors without these mutations either genetically belong to another histological subtype or represent an unstudied subtype of astrocytoma (*22*).

Grade II oligodendrogliomas frequently contain co-deletion of the chromosomal arms 1p and 19q and mutations in the promoter of *telomerase reverse transcriptase* (*TERT*). Up to 80% of grade II oligodendrogliomas show 1p/19q co-deletion, likely mediated by an unbalanced translocation (*20, 24, 25*). These deletions are thought to involve the unmasking of tumor suppressor genes *homolog of Drosophila capicua* (*CIC*) on 19q and *far-upstream binding protein 1* (*FUBP1*) on 1p (*26*). Mutations in these two genes have been identified in 53% and 15% of oligodendrogliomas, respectively, and appear to be largely restricted to gliomas with oligodendroglial histology (*22*). The majority of oligodendrogliomas also contain a mutation in the core promoter of *TERT* (*19*). These promoter mutations are thought to activate the transcription of *TERT*, which encodes for the catalytic subunit of telomerase (*27*). The inactivation of *ATRX* function and the up-regulation of *TERT* expression are two routes by which cancer cells can maintain their telomere length. In low-grade gliomas, *ATRX* and *TERT* promoter mutations occur in a mutually exclusive fashion (*19*).

Grade II oligoastrocytomas have a histologically mixed appearance, with cells appearing similar to either astrocytomas or oligodendrogliomas intermixed together. In

contrast, the genetic alterations present within each individual oligoastrocytoma places it within one of two distinct groups of *IDH1*-mutant tumors (*28*). Some oligoastrocytomas contain 1p/19q co-deletion and *TERT* promoter mutations making them genetically similar to oligodendrogliomas, while others contain *TP53* and *ATRX* mutations making them similar to astrocytomas (*19*). This mixture of genetic profiles may be partially indicative of the difficulties of distinguishing between low-grade gliomas based purely on histological and clinical features (*22*).

Germline variants also play a role in the development of low-grade glioma. The SNP rs55705857 was identified as a variant strongly associated with the risk of developing a glioma with mutant *IDH1* or *IDH2* (odds ratio, OR=4.8) (*29*). This SNP is located within a conserved region of 8q24.21 that might encode for a novel microRNA, but the mechanism by which variants in this region could contribute to gliomagenesis is unknown.

1.1.iii Treatment options for low-grade gliomas

Surgery remains the primary method of intervention for low-grade gliomas, with the extent of the resection playing a critical role in the life expectancy of the patient (*8*). More extensive resections are associated with increased overall survival as well as progression free survival (*5, 30*). Delaying surgery when a gross total resection can not be achieved is occasionally advocated, which involves a biopsy followed by resection only if the tumor shows signs of growth or malignant progression on follow-up magnetic resonance (MR) imaging. However, early surgical resection has been associated with a

longer overall survival when directly compared with this type of watchful waiting strategy (*31*).

Despite the clear benefits of surgical resection, low-grade glioma tumor cells infiltrate into normal brain tissue and are generally not surgically curable (*32*). Thus, low-grade glioma may be considered a chronic disease and many patients receive either adjuvant treatment immediately after surgery or at the first sign of recurrence. Factors such as preoperative tumor diameter $\geq$ 4 cm, astrocytoma or oligoastrocytoma histology, and residual tumor $\geq$ 1 cm according to MR imaging have been shown to predict a significantly worse progression free survival (*33*). However, the exact definition of a patient with a high-risk for developing a recurrent low-grade glioma is unclear (*34*). In the absence of poor prognostic factors, a strategy of watchful waiting with observation by MR imaging is often employed after an initial gross total resection (*8*).

Radiation therapy is a common tool in the postoperative management of patients with low-grade gliomas. Radiation therapy uses high-energy radiation to kill tumor cells, but can have adverse and delayed consequences on normal brain tissue leading to impaired cognition (*32*). In low-grade glioma patients, there is no difference in progression free survival or overall survival when comparing low and high doses of radiation (*6, 35*). Additionally, a prospective trial showed no benefit in overall survival when comparing low-grade glioma patients who received immediate radiation therapy against those who delayed treatment until signs of tumor progression (*36*). Currently, radiation therapy is primarily considered in the context of treating tumor recurrence (*8*).

Chemotherapeutics such as temozolomide (TMZ) or the trio of procarbazine, lomustine, and vincristine (PCV) are also frequently used to treat low-grade glioma patients. The results from phase II trials suggest that TMZ treatment is associated with improved quality of life, better seizure control, and longer progression-free survival in patients with low-grade gliomas (*37-39*). Similarly, treatment with PCV is associated with better tumor control and regression of residual tumor (*40, 41*), although TMZ is better tolerated and orally administered (*42*). While TMZ treatment at the time of recurrence or progression has shown a high response rate (*39, 42, 43*), a clear increase in overall survival has not been demonstrated for the upfront treatment of low-grade glioma patients with these chemotherapies (*8*). Notably, RTOG 9802 is a clinical trial of high-risk low-grade gliomas comparing radiation therapy and PCV against radiation therapy alone. Initial results suggested the addition of PCV confers a longer progression free survival, but not a benefit to overall survival (*35*). These results may have been reported too early to find any overall survival benefit, however, and contain no analysis of molecular markers (*44*). An updated analysis of the data from this trial is forthcoming, and an initial press release has indicated a significant improvement in overall survival of 5.5 years for patients treated with PCV and radiation (13.3 years median survival) compared to those treated with radiation alone (7.8 years median survival).

Biomarkers predictive of response to adjuvant chemotherapy can help to restrict treatment to those patients that will clearly benefit. Despite potential clinical benefits, alkylating agents like procarbazine and TMZ are carcinogenic and exposure to this

class of systemic therapies is associated with an increased risk of developing treatment-related leukemias (*45*). Several biomarkers with relevance in high-grade gliomas have been assessed for efficacy in low-grade glioma populations with variable success. First, 1p/19q co-deletion is a common feature of gliomas with oligodendroglial histology. Both PCV and TMZ have shown efficacy in grade III anaplastic oligodendrogliomas and anaplastic oligoastrocytomas, with 1p/19q co-deletion predicting both better progression free survival and substantially longer overall survival (*46-48*). Similar results have been seen in low-grade gliomas, where 1p/19q co-deleted tumors treated with TMZ had increased response rates and a longer duration of response (*49, 50*). Second, DNA methylation of the promoter of O^6-methylguanine-DNA methyltransferase (MGMT) predicts a clear survival benefit in GBM patients treated with TMZ (*51*). Interestingly, this association is potentially limited to grade III and IV gliomas that do not contain *IDH1* mutations (*52*). The situation is less clear in patients with low-grade gliomas, where conflicting studies have found MGMT promoter methylation to be either a favorable predictor (*53*) or not associated with (*54*) improved progression free survival after treatment with TMZ. Third, mutations in *IDH* genes are a favorable prognostic factor for patients with GBMs (*55*). Again, some studies report *IDH* mutations in low-grade gliomas correlate with a higher rate of response to TMZ (*56*) while others have found them not to be predictive (*54, 57*). The results of RTOG 9802 and other additional clinical trials are needed to clarify the predictive role of these biomarkers and to identify the patients with low-grade gliomas that do not benefit from adjuvant chemotherapy.

1.2 LOW-GRADE GLIOMAS AND MALIGNANT PROGRESSION

1.2.i Causes of malignant progression

Low-grade gliomas are highly recurrent and can be thought of as a chronic disease. Even in the context of a gross total resection, infiltrating tumor cells remain beyond the surgical margin and can give rise to a recurrent tumor (*32*). When initially low-grade tumors recur after surgical resection they may undergo malignant progression, the histological upgrading from grade II to grade III or IV. Grade II astrocytomas can progress to either grade III anaplastic astrocytoma or grade IV GBM. Grade II oligodendrogliomas can generally only progress to grade III anaplastic oligodendrogliomas, though grade IV glioblastoma with oligodendroglioma component is a recognized WHO entity (*3*). In each of these cases, malignant progression is accompanied by a significantly worsened prognosis for the patient (*4*). Both the incidence and timing of this malignant progression are highly variable. The frequency of malignant progression reported in clinical studies ranges from 17 to 73% while the median interval after initial resection stretches from 2.1 to 10.1 years (*8*). Despite this variability, nearly all patients are expected to eventually undergo malignant progression if they live long enough (*28*). Thus, the molecular mechanisms governing malignant progression are of considerable clinical interest.

Although the clinical courses of patients diagnosed with low-grade glioma are heterogeneous and unpredictable, several factors have been associated with an increased risk of malignant progression. In a study measuring the growth rate of untreated low-grade gliomas, tumor volume was found to be the most significant

predictor of malignant progression within the following 12 months (*58*). While larger tumors were more likely to undergo malignant progression, this association also held true in studies where the tumor was resected, suggesting tumor growth rate may be the more important factor. Amongst patients with hemispheric low-grade gliomas, malignant progression free survival was predicted both by preoperative tumor volume and the extent of the resection (*5*). Similarly, a lower extent of resection was found to be significantly associated with the malignant progression of low-grade gliomas in the insula (*59*). Thus, a large preoperative tumor volume, high growth rate, and subtotal resection place a patient initially diagnosed with a low-grade glioma at high risk of malignant progression upon recurrence.

1.2.ii Genetic alterations associated with malignant progression

The malignant progression from low-grade to high-grade glioma includes increases in the cellularity and proliferation index of tumor cells. Underlying genetic alterations in two key pathways frequently accompany this increase in clinical aggressiveness and may be responsible for driving these changes. These include copy number alterations and mutations that result in either the hyper-activation of the v-akt murine thymoma viral oncogene homolog (AKT) and mammalian target of rapamycin (mTOR) signaling pathway or deregulation of retinoblastoma (RB) mediated control of the G1/S checkpoint of the cell cycle (*28, 60*).

Activation of the AKT-mTOR signaling pathway drives cellular growth, metabolism, proliferation, and survival. Phosphoinositide 3-kinases (PI3K) are activated by upstream

signals from receptor tyrosine kinases (RTKs) and are opposed by the activity of phosphatase and tensin homologue (PTEN). Increased signaling through RTKs or loss of PTEN activity lead to the activation of AKT, which promotes cell survival and proliferation through the inhibitory phosphorylation of many downstream proteins. Activation of AKT also drives signaling through mTOR by inhibiting tuberous sclerosis protein 1 (TSC1) and 2 (TSC2), which are negative regulators of the activity of the mTORC1 complex. When uninhibited, the mTORC1 complex phosphorylates its two major downstream targets, p70 ribosomal protein S6 kinase (RPS6K) and eurkaryotic translation initiation factor 4E binding protein 1 (4E-BP1), which together drive protein translation and cell survival (*61*).

Genetic alterations that drive signaling through the AKT-mTOR pathway have been identified in 88% of GBMs (*60*). These include amplification of RTKs such as EGFR (45%), inactivating mutations or homozygous deletions in NF1 (18%) or PTEN (36%), and activating mutations in PI3K (15%), that all result in the hyperactivation of AKT. These genetic alterations are far less common in lower grade tumors (*28, 62*). Indeed, there is a significant positive correlation between the activation status of the AKT pathway and glioma grade (*63*). Furthermore, the introduction of an activated form of AKT into mouse astrocytes and neural progenitors contributes to the development of GBMs (*64*).

The inactivation of RB-mediated cell cycle control enables the increased proliferation rate associated with malignant progression. *CDKN2A* is a gene that encodes for p16,

which binds to cyclin dependent kinase 4 (CDK4) and cyclin dependent kinase 6 (CDK6) and inhibits their kinase activity. When CDK4/CDK6 bind cyclin D and are not inhibited, they phosphorylate the Rb protein, and the transcription factor E2F1 is freed from binding with Rb. E2F1 is thus no longer sequestered in the cytoplasm and can move to the nucleus and promote the transcription of genes necessary for the progression through the G1-S phase of the cell cycle (*65*).

Genetic alterations impacting different components of the RB pathway are common in high-grade gliomas, and result in the increased transcription of E2F regulated genes. Chromosomal deletion or mutation of *CDKN2A* occurs in 50% of grade III anaplastic astrocytomas (*28*) and grade IV GBMs (*60*). DNA hypermethylation of the *CDKN2A* locus is also common in oligodendroglial tumors (*66*). Homozygous deletion or mutation of RB1 itself has been found in 11% of GBMs. The amplification and subsequent overexpression of *CDK4* or *CDK6* is another mechanism that can bypass cell cycle control by p16, and has been identified in approximately 18% of GBMs. Overall, genetic alterations in the RB pathway were identified in 78% of GBMs assessed by the TCGA (*60*). The functional importance of these genetic events on high-grade tumor development has also been shown in experimental models. In a mouse model of oligodendroglioma driven by *EGFR* overexpression, the heterozygous deletion of *CDKN2A* made the resulting tumors high grade (*67*). Similarly, the inactivation of Rb in mouse astrocytes leads to the development of anaplastic astrocytomas (*68*).

Together, these data clearly implicate genetic alterations in the RB and AKT-mTOR pathways as central events in the increased cellularity and proliferation index that characterize the transition from low-grade to high-grade glioma. Lacking from much of this published data, however, is the longitudinal characterization of these key genetic alterations in tumors from the same individual before and after malignant progression.

1.3 HYPERMUTATION OF GLIOMAS

1.3.i Induction of mutations by alkylating agents

Alkylating chemotherapeutic agents such as TMZ and procarbazine are known mutagens. In experimental systems, TMZ treatment produces a dose-dependent increase in the levels of N7-methylguanine and O^6-methylguanine (*69*). While N7-methylguanine is the major DNA adduct induced by TMZ and other alkylating agents, O^6-methylguanine has been identified as the relevant mutagenic lesion (*70*). The methylation of the O^6 position of guanine changes the normal hydrogen bonding of guanine with cytosine and causes it to preferentially pair instead with thymine during DNA replication (*70*). The DNA mismatch repair (MMR) machinery recognizes the mispairing of guanine with thymine and repairs the daughter strand, but leaves behind the O^6-methylguanine in the template strand. This leads to repeated attempts by the MMR pathway to repair the same mismatched base over and over. This "futile cycling" results in DNA double-strand breaks that activate the apoptosis pathway and are thought to be the basis for the cytotoxicity of alkylating agents (*71*). If the MMR pathway is not active, the mispairing of guanine with thymine leads to C:G>T:A transition mutations upon DNA replication.

There is a strong similarity between the mutational profiles of cells exposed to alkylating agents *in vitro* and clinical tumor samples from glioma patients treated with alkylating agents. Experiments have shown that O^6-methylguanine almost exclusively induces C:G>T:A transitions (*72*). Similarly, the *in vitro* exposure of cells to TMZ results in a dose-dependent increase of C:G>T:A transition mutations predominantly at non-CpG sites (*69*). In contrast, most spontaneous mutations arise through the deamination of methylated cytosine, leading to an elevated rate of C:G>T:A mutations at CpG dinucleotides. A study of the patterns of somatic mutation in human cancer genomes found that some recurrent GBMs treated with alkylating agents had the highest mutation prevalence of all samples studied, with approximately 77 mutations per Mb (*73*). These hypermutated GBMs were only identified in patients after alkylating agent therapy and displayed a pattern of C:G>T:A transitions predominantly at non-CpG sites (*74, 75*). This suggests most mutations in hypermutated recurrent GBMs are caused by alkylating agent therapy (*60*).

Alkylating agents have mutagenic properties and are thus known to be carcinogens. Patients who receive systemic therapy with alkylating agents are at risk of developing treatment-related leukemias (*45*). Both treatment-related myelodysplasia (MDS) and treatment-related acute myeloid leukemia (AML) are associated with a four-fold increase in the rate of *TP53* mutations with a distinct mutational spectrum when compared to *de novo* MDS and AML (*76*). While these secondary leukemias are rare in adult brain tumor patients, this is likely because these malignancies usually appear

three to five years after treatment, which is longer than the average overall survival of patients with grade III or IV gliomas (*69*). The potential for secondary malignancies to develop is not surprising, as these mutagens are also used to induce tumors in model organisms. N-ethyl-N-nitrosourea (ENU) is a highly mutagenic alkylating agent that preferentially alkylates A:T base pairs, leading to A:T>T:A transversions, A:T>G:C transitions, and G:C>T:A transitions (*77*). The injection of ENU into pregnant rats consistently results in the development of neural tumors in the rat's offspring (*78*). These tumors are predominantly astrocytomas, oligodendrogliomas, and oligoastrocytomas that often display anaplasia and other histological features of high-grade gliomas (*79*). While these model gliomas have not been fully sequenced, their origins suggest they are likely hypermutated. The high rate of mutagenicity across alkylating chemotherapeutic agents makes their use in managing low-grade gliomas a particularly sharp double-edged sword.

1.3.ii Mutations in the DNA mismatch repair pathway

MMR pathway dysfunction arises when key members are inactivated by gene silencing, mutation, or copy number loss. These include *MutS homolog 2* (*MSH2*), *MutS homolog 3* (*MSH3*), *MutS homolog 6* (*MSH6*), *MutL homolog 1* (*MLH1*), and *PMS2 postmeiotic segregation increased 2 (S. cerevisiae)* (*PMS2*) (*80*). In the MMR pathway, the MSH2 protein heterodimerizes with either the MSH3 or MSH6 protein to form a complex that recognizes DNA mispairing (*81*). The MLH1 and PMS2 proteins heterodimerize, are recruited to the site of the mismatch, and facilitate the coupling of downstream proteins involved in excision and replacement (*81*).

Resistance to alkylating agents like TMZ arises in cells deficient in MMR, where DNA damage no longer leads to apoptosis (*80*). In experimental systems using human cell lines, inactivation of the MMR pathway allowed for cell growth under otherwise cytotoxic concentrations of alkylating agents, and the reintroduction of wild-type components of the MMR machinery re-sensitized these cells to alkylating agents (*82, 83*). Additionally, resistant clones isolated from a GBM cell line treated with TMZ showed the acquisition of *MSH6* mutations that were undetectable prior to treatment (*75*).

Gliomas are highly recurrent and frequently become refractory to TMZ treatment. The mechanism of their resistance *in vivo* may be partially through inactivation of the MMR pathway. Indeed, analyses of recurrent GBMs have shown an association between patients treated with TMZ or other alkylating agents, high rates of C:G>T:A transition mutations, and MMR pathway mutations (*60*). These mutational patterns were distinct from spontaneous mutations in mice or human cells without MMR activity (*74*). Non-silent mutations in *MSH6* have been identified in 26% of GBMs after alkylating agent therapy (*75*), but are rare in primary, untreated GBMs (*84*) and their patient-matched pre-treatment tumors (*75*). When assessed by immunohistochemistry (IHC), approximately half of TMZ treated GBMs lost *MSH6* expression when compared to their pre-treatment tumors, showing *MSH6* inactivation was specifically associated with recurrence after TMZ treatment (*84*). The sequencing of additional members of the MMR pathway has identified mutations in *MLH1*, *MSH2*, and *PMS2* in hypermutated recurrent GBMs, suggesting multiple genetic paths to alkylating agent resistance and

hypermutation (*60*). Interestingly, gliomas with mutations in the MMR pathway showed no evidence of the microsatellite instability that is a hallmark of colorectal cancer arising from germline MMR pathway mutations (*74, 75*).

1.3.iii DNA methylation of MGMT

MGMT is a DNA repair protein capable of removing the O^6-methyl adducts induced by TMZ and other alkylating agents. After transferring the alkyl group to an internal cysteine residue, MGMT is irreversibly consumed. The amount of O^6-methylguanine that can be repaired is therefore directly proportional to the amount of MGMT protein within a cell, and an excess of O^6-methylguanine can deplete MGMT (*85*).

MGMT is a critical regulator of the cytotoxicity of alkylating agents. Cells with high levels of MGMT are capable of repairing more O^6-methylguanine, leading to fewer mismatched bases, less "futile cycling" by the MMR system, and fewer pro-apoptotic signals. The best clinical response to TMZ and other alkylating agents is therefore expected in tumor cells with low levels of MGMT and a functional MMR pathway (*86*). Support for this hypothesis can be found in the treatment of GBMs with TMZ, where some gliomas display DNA hypermethylation of the promoter region of *MGMT* that is associated with transcriptional silencing *(87-89)*. This loss of transcription leads to a lower abundance of MGMT protein, the sensitization of glioma cells to TMZ treatment, and a clear survival benefit in GBM patients (*51*). While *MGMT* promoter methylation is associated with an improved response to TMZ treatment, many patients with low-grade gliomas, regardless of *MGMT* status, are still considered for TMZ therapy, especially in

cases with subtotal surgical resections or when deferring the use of radiation therapy is preferable.

MGMT may also play an important role in modulating the mutagenicity of alkylating agents. The amount of MGMT protein within a cell influences the abundance of O^6-methylguanine available to generate mismatches. This is supported by a survey of nervous system tumors that found *MGMT* silencing by promoter DNA hypermethylation was associated with a higher likelihood of C:G>T:A transition mutations in the *TP53* gene (*90*). Despite this, an analysis of 17 GBMs found MGMT protein level assessed by immunohistochemistry was unchanged between initial and recurrent tumors treated with TMZ (*84*). The MGMT promoter methylation status of GBMs in two additional studies was found to be not concordant with their hypermutator phenotype (*60, 74*). Some hypermutated GBMs had a hypermethylated MGMT promoter while others did not. Interestingly, *MGMT* promoter hypermethylation was associated with a shift in the dinucleotide context of alkylating agent induced C:G>T:A mutations away from CpG sites (*60*). While the complete loss of MGMT activity may not be necessary for hypermutation to occur, this suggests that MGMT may influence which DNA adducts exist long enough to generate mutations.

1.4 CANCER GENETICS

1.4.i Evolution of cancer genomes

Sporadic cancers are fundamentally genetic diseases, arising from the clonal outgrowth of single cells that have acquired mutations and epigenetic alterations. The clonal

evolution theory of tumor progression applies evolutionary principles to the expansion of tumor cell populations to explain how changes in biological properties happen during tumor development (*91*). This begins when the founding clone undergoes neoplastic transformation leading to unrestricted cell growth. Genetic instability then gives rise to additional genetic alterations in daughter cells, a subset of which acquire advantageous mutations which allow them to outcompete neighboring cells. This process then repeats itself, where continued cell division and mutagenesis enable the competition and selection of successive rounds of daughter cells. The resulting tumor is not homogenous, but a collection of cancer cells with a diverse set of genetic alterations and biological properties. There is extensive support for this theory (*92*) and it has become a field of intense interest in modern cancer genomics (*93*). For example, the sequencing of spatially distinct regions of heterogeneous tumors has enabled the construction of phylogenetic trees that directly demonstrate the ancestral relationships of subclonal populations (*94*). Similarly, sequencing of primary tumors and their distant metastases has provided insight into the evolutionary timing of the subclones that give rise to these separate lesions (*95*).

Mutations acquired during the clonal evolution of a tumor that have no impact upon selection are said to be "passenger" mutations, while those that promote cell growth or increased fitness are called "driver" mutations. These driver mutations can take the form of activating mutations in oncogenes or inactivating mutations in tumor suppressor genes. Early investigation of the patterns of tumor evolution postulated that tumors must acquire two-independent genetic events at one gene locus during development in order

to fully inactivate a tumor suppressor gene (*96*). This two-hit hypothesis was later proven in retinoblastoma with inactivation of the *RB1* gene (*97*).

There is some evidence that clonal evolution also underlies the development of low-grade gliomas and their recurrences. Most notably, the recurrence of low-grade astrocytomas has been shown to involve the clonal expansion of cells with *TP53* mutations (*98, 99*). Additionally, driver mutations in the RB and AKT-mTOR pathways can be identified in many secondary GBMs but few low-grade gliomas, suggesting the malignant progression from low-grade to high-grade glioma is accompanied by the expansion of subclones with these genetic alterations (*28, 60*). Hypermutated recurrent GBMs have also been shown to acquire mutations in the MMR pathway undetected in their initial pre-treatment tumors, suggesting gliomas with resistance to alkylating agents arise through the expansion of subclones with advantageous mutations (*74*). This hypermutation of tumor cell populations may also drive more rapid clonal evolution by increasing mutational heterogeneity (*74, 100*).

1.4.ii Intratumoral heterogeneity in low-grade gliomas

Intratumoral genetic heterogeneity necessarily results from the clonal evolution of cancer cell populations and may contribute to tumor adaptation and therapeutic resistance. This has been shown in chronic lymphocytic leukemia, where clonal evolution after treatment led to the expansion of subclones with driver mutations (*101*). The presence of subclonal driver mutations was also identified as an independent risk factor for rapid disease progression.

Gliomas are a histologically heterogeneous group of tumors that display varying levels of intratumoral genetic heterogeneity. A survey of gliomas across many grades and histologies used florescence in situ hybridization (FISH) of frequently altered chromosomal regions to identify two or more genetically distinct subclones in the vast majority of tumors (*102*). In this study, high-grade gliomas showed more complex and heterogeneous genetic alterations with higher numbers of subclones. This finding is similar to earlier work that concluded copy number alterations lead to intratumoral heterogeneity in high-grade but not in low-grade gliomas (*103*).

Indeed, many studies support genetic intratumoral heterogeneity in GBMs. Karyotyping of individual clones from eight malignant gliomas revealed between three and 21 genetically distinct subpopulations (*104*). Additionally, the microdisection of multiple regions from 10 GBMs followed by comparative genomic hybridization (CGH) showed discrete areas with distinct copy number alterations (*105*). Intratumoral heterogeneity can also manifest within a single region, where GBMs with the amplification of multiple RTKs were identified as having intermixed and clonally related subpopulations each with only a single amplified RTK (*106*).

Low-grade gliomas can display intratumoral heterogeneity as well. The extensive microdissection of a single low-grade oligoastrocytoma followed by flow cytometry and cytogenic analysis showed multiple, spatially distinct subclones can exist within low-grade gliomas (*107*). This analysis found regional clustering of genetically distinct

subclones that suported a model of tumor progression in which advantageous genetic alterations resulted in clonal expansion, followed by successive rounds of mutation and expansion, with the most successful subclones undergoing migration as well. Additionally, the microdissection and sequencing of 11 gliomas found separate *TP53* driver mutations in the low and high-grade components of the same tumors (*108*). Culturing low-grade glioma cells also reveals their potential for heterogeneity, where subpopulations of cultured cells have been shown to replicate their chromosomes without cytokinesis, generating shifts in chromosome number and laying the foundation for heterogeneous tumors (*109*).

1.5 AIMS OF THIS STUDY

Grade II astrocytomas can recur after an initial surgery without a change in tumor grade or may unpredictably undergo malignant progression to a higher grade. The initial goal of this study was to aid in the prediction of which patients initially diagnosed with a low-grade glioma would have a subsequent high-grade recurrence. To do this, we set out to analyze the natural history and genomic evolution between patient-matched initial and recurrent gliomas. This goal, while clinically important, was several steps ahead of our current understanding of low-grade gliomas and their evolutionary trajectories. When we began, there were giant gaps that needed to be filled in. First, complete exomes from low-grade gliomas had not been published, and thus their complete mutational burden unknown. Second, the full extent of genetic intratumoral heterogeneity in low-grade gliomas was unknown. Up to this date, most investigations were focused on gross copy number alterations or mutations within specific genes. Third, primary data on the

changes in mutational burden that accompany tumor progression were scarce and only existed for select exons of a small number of genes. Previous studies of glioma evolution used unpaired tumors of different grades to infer the genetic events that occur during malignant progression (*110-113*). Even amongst other tumor types, analyses of full exomes from paired initial and recurrent solid tumors were rare. Finally, the extent and impact of TMZ-associated mutagenesis on gliomas was poorly understood. Alkylating agents and their mutagenicity have been studied for decades, but a direct *in vivo* demonstration of the changes in a tumor's mutational profile before and after therapy was completely lacking. During the course of the experiments detailed in Chapter 3, each of these gaps revealed themselves, needed to be addressed, and so became aims of this study.

CHAPTER 2.

MUTATIONAL ANALYSIS REVEALS THE ORIGIN AND

THERAPY-DRIVEN EVOLUTION OF RECURRENT

GLIOMA

2.1 ABSTRACT

Tumor recurrence is a leading cause of cancer mortality. Therapies for recurrent disease may fail, at least in part, because the genomic alterations driving the growth of recurrences are distinct from those in the initial tumor. To explore this hypothesis, we sequenced the exomes of 23 initial low-grade gliomas and recurrent tumors resected from the same patients. In 43% of cases, at least half of the mutations in the initial tumor were undetected at recurrence, including driver mutations in *TP53*, *ATRX*, *SMARCA4,* and *BRAF*, suggesting recurrent tumors are often seeded by cells derived from the initial tumor at a very early stage of their evolution. Notably, tumors from 6 of 10 patients treated with the chemotherapeutic drug temozolomide (TMZ) followed an alternative evolutionary path to high-grade glioma. At recurrence, these tumors were hypermutated and harbored driver mutations in the RB and AKT-mTOR pathways that bore the signature of TMZ-induced mutagenesis.

2.2 MAIN TEXT

The genetic landscape of tumors is continually evolving, which can be an impediment to the clinical management of cancer patients with recurrent disease (*92, 100*). In contrast to the clonal evolution of hematological malignancies (*101, 114*) and solid tumor metastases (*94, 95, 115*), the local regrowth of solid tumors after surgery occurs under a unique set of evolutionary pressures, which are further impacted by adjuvant therapies. Through acquisition of new mutations, residual tumor cells can progress to a more aggressive state. Grade II astrocytic gliomas are particularly troublesome from this perspective. While surgery is the standard of care, these invasive brain tumors typically

recur (*8*). Many remain grade II at recurrence, while others progress to a higher histological grade with a poor prognosis (*4*). The incidence and timing of malignant progression is variable and unpredictable (*8*).

We undertook genome sequence analysis of initial and recurrent human gliomas to address two questions: (i) what is the extent to which mutations in initial tumors differ from their subsequent recurrent tumors?; and (ii) how does chemotherapy with TMZ, a drug commonly used in the treatment of glioma, affect the mutational profile of recurrent tumors? We sequenced the exomes of 23 grade II gliomas at initial diagnosis and their recurrences resected from the same patients up to 11 years later (Table 2.1). We selected initial tumors of predominantly astrocytic histology that capture the full spectrum of glioma progression (histological grade II-IV at recurrence) and adjuvant treatment history. Tumor and matched normal DNA were sequenced to an average 125-fold coverage, enabling the sensitive detection of mutations down to a 10% variant frequency, small insertions/deletions, and DNA copy number alterations (CNAs) (Figure 2.1) (Table 2.2) (*116, 117*).

We identified an average of 33 somatic coding mutations in each initial tumor, of which an average of 54% were also detected at recurrence (shared mutations) (Figure 2.1). The shared mutations included those in *IDH1*, *TP53*, and *ATRX* in most but not all cases (Figure 2.2) (*17, 22, 118*). All other somatic mutations were identified only in the initial tumor or only in the recurrent tumor from a given patient (private mutations) and thus presumably arose later in tumor evolution. For example, mutations in *SMARCA4*

were private to the initial or recurrent tumor in six of seven patients and therefore may confer a selective advantage in the context of pre-existing early driver events (*119, 120*). Overall, the initial and recurrent gliomas displayed a broad spectrum of genetic relatedness (Figure 2.3) (Table 2.3). At one end of this spectrum were four patients whose tumors showed a pattern of linear clonal evolution; we infer that the recurrent tumors in these patients were seeded by cells bearing ≥75% of the mutations detected in the initial tumors (as in patient 27, Figure 2.4). At the other end of the spectrum, tumors from three patients showed branched clonal evolution; we infer that the recurrent tumors in these patients were seeded by cells derived from the initial tumor at an early stage of its evolution, as the recurrent tumors shared ≤25% of mutations detected in the initial tumors. Patient 17 was an extreme example of branched clonal evolution, as the initial and recurrent tumors shared only the *IDH1* R132H mutation (Figure 2.5). This further implicates *IDH1* mutations as an initiating event in low-grade gliomagenesis (*17*). Indeed, *IDH1* mutation was the only shared mutation in every patient, an observation that supports the current interest in IDH1 as a therapeutic target (*15*). Paired tumors from the remaining 16 patients formed a continuum between linear and branched clonal evolution. Together, these data illustrate the extent to which genetically similar low-grade gliomas diverge after surgical resection, and that recurrences may emerge from early stages in the evolution of the initial tumor.

Many solid tumors, including glioblastoma (GBM) display intratumoral heterogeneity (*121, 122*). For example, geographically distinct parts of the tumor may have different mutations. Intratumoral heterogeneity could be a confounding factor in estimates of

genetic divergence when only one relatively small fraction of a tumor is sampled. To explore the extent of intratumoral heterogeneity in our cases, we first analyzed the *BRAF* V600E mutation that was subclonal in the initial tumor of patient 18 and undetectable in the recurrent tumor by either exome sequencing or droplet digital PCR (Figure 2.6 and 2.7). *BRAF* V600E was present in three of six additional samples from geographically distinct regions of the initial tumor, while seven additional samples of the recurrence all lacked this mutation. This suggests the *BRAF*-mutant clone did not expand, despite the proliferative advantage typically conferred by this mutation. This contrasts sharply with the selection and outgrowth of subclonal drivers during the evolution of chronic lymphocytic leukemias (*101*).

Beyond the actionable *BRAF* mutation, we sequenced the exomes of additional, geographically distinct samples from three cases to further determine the extent to which apparently private mutations might be misclassified due to intratumoral heterogeneity. For patient 17 in which all mutations except *IDH1* were private, intratumoral heterogeneity was observed in the initial and recurrent tumor. From the mutational profiles however, we inferred that three samples of the initial tumor and four samples of the recurrence all derived from a common tumor cell of origin that possessed only an *IDH1* R132H mutation (Figure 2.8) (Table 2.4). Moreover, the recurrent tumor contained driver mutations in *TP53* and *ATRX* distinct from those observed in the initial tumor. We found no evidence of these new *TP53* or *ATRX* mutations in the initial tumor at allele frequencies of ~0.1% (Figure 2.7 and 2.9), implying convergent phenotypic evolution (*94*) via a strong ongoing selection for loss of

these genes. The initial and recurrent tumors likely did not arise independently, as they also shared three somatic non-coding mutations (Figure 2.10). Thus, the initial and recurrent tumors were only distantly related and, despite the local and relatively rapid recurrence (Figure 2.11), exonic mutations other than *IDH1* R132H were only transiently present during the course of this patient's disease. Finally, we sequenced the exomes of additional distinct samples of the initial and recurrent tumors from patients 26 and 27, broadening our assessment of the impact of intratumoral heterogeneity on the reported genetic divergence. We found only a small minority of private mutations were actually shared events (7%) (*117*). Intratumoral heterogeneity therefore could not explain the majority of the genetic divergence between the initial and recurrent tumors in our cohort, including the driver mutations in initial tumors that were undetected in their recurrence.

To investigate whether sequential recurrences from a single patient could each be traced to the same evolutionary stage of the initial tumor, we sequenced the exomes of the second and third recurrent tumors from patient 04 and constructed a disease phylogeny by clonal ordering (Figure 2.12 and 2.13) (Table 2.4) (*94, 123*). The initial tumor and three sequential local recurrences were clonally related, as indicated by the shared phylogenetic branch containing early driver mutations in *IDH1* and *TP53*. We infer that the tumor cells seeding the second recurrence branched off from the initial tumor at a slightly earlier evolutionary stage than the cells seeding the first recurrence. In contrast, the third recurrent tumor was a direct outgrowth of the second recurrence. These results show that branched and linear patterns of clonal evolution occurred at differing times in the same patient and are therefore not intrinsic properties of the tumor.

Beyond maximal, safe, surgical resection, there is currently no standard of care for patients with low-grade glioma, and options include surveillance, adjuvant radiation alone, TMZ alone, or radiation and TMZ. TMZ is an alkylating agent that induces apoptosis in glioma cells and is sometimes used to defer or delay the use of radiation. However, there is currently no information on whether treatment of grade II astrocytomas with TMZ confers longer overall survival (*8*). As TMZ is also mutagenic (*69*), we sought to determine how adjuvant chemotherapy with TMZ affects the mutational profile of recurrent tumors by comparing the initial low-grade gliomas to their post treatment recurrence. While the initial tumors and most of the recurrent tumors in our cohort had 0.2-4.5 mutations per megabase (Mb) (*60, 73*), six of the ten patients treated with TMZ had recurrent tumors that were hypermutated; that is, they harbored 31.9-90.9 mutations per Mb (Table 2.5). Overall, 97% of these were C>T/G>A transitions predominantly occurring at CpC and CpT dinucleotides, a signature of TMZ-induced mutagenesis distinct from non-hypermutated tumors (Figure 2.14) (*60, 69, 74*). We classified C>T/G>A transitions in each hypermutated tumor as TMZ-associated if they were undetected in the matched initial tumor, which was resected before TMZ treatment (Figure 2.15). Although it is difficult to definitively attribute any single mutation to TMZ exposure, comparing the C>T/G>A mutation rates in each tumor pair suggested that >98.7% are due to TMZ-induced mutagenesis. To determine whether intratumoral heterogeneity in initial tumors resulted in the misclassification of some mutations as TMZ-associated, we sequenced the exomes of three additional geographically distinct samples of the untreated initial tumor from patient 18. For mutations classified as TMZ-

associated, sequencing reads with the mutation were rare in the additional exomes and were found at rates no higher than expected by chance (1.7±0.08%; p-value=0.5, Wilcoxon) further suggesting they are induced by TMZ.

Resistance to TMZ develops in part through the acquisition of mutations that inactivate the DNA mismatch repair (MMR) pathway. MMR pathway dysfunction and continued TMZ exposure can in turn result in hypermutation (*60, 74, 75, 84*). Indeed, we found that hypermutated tumors acquired somatic mutations in MMR genes that were not detected in their initial tumors, as well as aberrant DNA methylation of O^6-methylguanine-DNA methyltransferase (*MGMT*) (Figure 2.7 and 2.16) (Table 2.1).

The introduction of thousands of *de novo* mutations may drive the evolution of TMZ-resistant glioma cells to higher states of malignant potential (*74, 100*). Indeed, all six recurrent tumors that showed evidence of TMZ-induced hypermutation underwent malignant progression to GBM, a high-grade tumor with a worse prognosis (*4, 8*). To investigate this hypothesis and identify TMZ-associated mutations that may drive the outgrowth of GBM from low-grade glioma, we focused on the RB and AKT-mTOR signaling pathways which are associated with high-grade gliomas (Figure 2.17) (*28, 60, 63, 124*). In each hypermutated recurrence, TMZ-associated mutations affected genes coding for essential signaling molecules in these two pathways. For example, in the RB pathway we identified a TMZ-associated RB1 c.2520+1G>A splice site mutation found previously in the germline of patients with hereditary retinoblastoma (*125, 126*). Transcriptome sequencing confirmed this mutation triggered aberrant splicing,

premature termination, and loss of the RB1 C-terminal domain necessary for growth suppression (Figure 2.18A) (*127*). Recurrent tumors from patient 05 and patient 10 each had a TMZ-associated *CDKN2A* P114L mutation that prevents it from inhibiting CDK4 or inducing cell cycle arrest (*128*). The same mutation has been reported in other tumor types (*129*) and in the germline of patients with familial melanoma (*130*). Gene set enrichment analysis further confirmed deregulation of RB1-mediated cell cycle control upon tumor recurrence (Figure 2.18B), suggesting that TMZ-associated mutations compromise the function of the RB tumor suppressor pathway.

We also investigated TMZ-associated mutations that may activate the AKT-mTOR signaling pathway. We identified a TMZ-associated mutation *PIK3CA* E542K in the recurrent tumor of patient 18 that drives Akt hyperactivation and induces mTOR-dependent oncogenic transformation (*131*). Similarly, the TMZ-treated second recurrence of patient 24 had TMZ-associated mutations in *PTEN* (A121T and G165R) at residues critical to its phosphatase activity (*132*) that are recurrently mutated in GBM (*129*). Finally, we validated *in vitro* that a TMZ-associated *MTOR* S2215F mutation in the recurrent tumor of patient 01 was constitutively activating (Figure 2.19), similar to the previously identified *MTOR* S2215Y (*133*). Moreover, adjacent regions of this recurrence showed heterogeneous mTORC1 activity (Figure 2.20 and 2.21). Microdissection revealed that while these adjacent regions shared a subset of the mutations found in the initial tumor, *MTOR* S2215F and other TMZ-associated mutations were present only in the region that stained strongly for mTORC1 activation, which also had higher Ki-67, implying that the TMZ-associated mutations conferred a

proliferative advantage. A distal second recurrence harbored the same TMZ-associated mutations and stained strongly and homogeneously for mTORC1 targets (Figure 2.22). Although both regions of the first recurrence were GBM, the hypermutated subclone underwent *in vivo* selection, invaded distally, and seeded the second recurrence (Figure 2.23 and 2.24). Across our cohort, AKT-mTOR pathway mutations corresponded with elevated phospho-4E-BP1 and RPS6 *in vivo,* indicating hyper-activated mTORC1 in recurrent GBMs relative to their initial tumors (Figure 2.22).

There was no evidence that the mutations in the RB and AKT-mTOR signaling pathways preceded TMZ treatment, based on analysis of additional geographically distinct samples of initial tumors from four of the six patients with hypermutated recurrent tumors (Table 2.6). Non-hypermutated recurrent tumors that progressed to GBM also acquired genetic changes in these signaling pathways, but through alternative mechanisms. In contrast, none of the grade II-III recurrences acquired mutations in these pathways. These data suggest a connection between TMZ treatment, driver mutations in oncogenic signaling pathways, and malignant progression.

In summary, through direct comparison of the genomic landscape of gliomas at initial diagnosis and recurrence, we were able to infer the mutational character of the infiltrating tumor cells that give rise to recurrence and that adjuvant therapy with TMZ is intended to eliminate. Recurrences did not typically arise from cells bearing the full set of mutations found in the initial tumor, as would be expected from a local recurrence in

the absence of selective pressure from adjuvant chemotherapy. This finding complicates the use of tumor genomics to design precision therapies targeting residual disease. We also demonstrated an alternative evolutionary path of low-grade glioma that is largely determined by adjuvant chemotherapy with TMZ. This extends earlier studies of primary GBMs (*74, 75*), unpaired recurrent tumors (*60*), and a cell culture model (*69*). Future basic and clinical studies must weigh the initial antitumor effects of TMZ against the potential risk of inducing new driver mutations and malignant progression. Ultimately, a better understanding of the invading cells that give rise to recurrent tumors and the effect of adjuvant therapeutics on their evolution will facilitate the development of new strategies to delay or prevent recurrence and malignant progression.

FIGURE 2.1
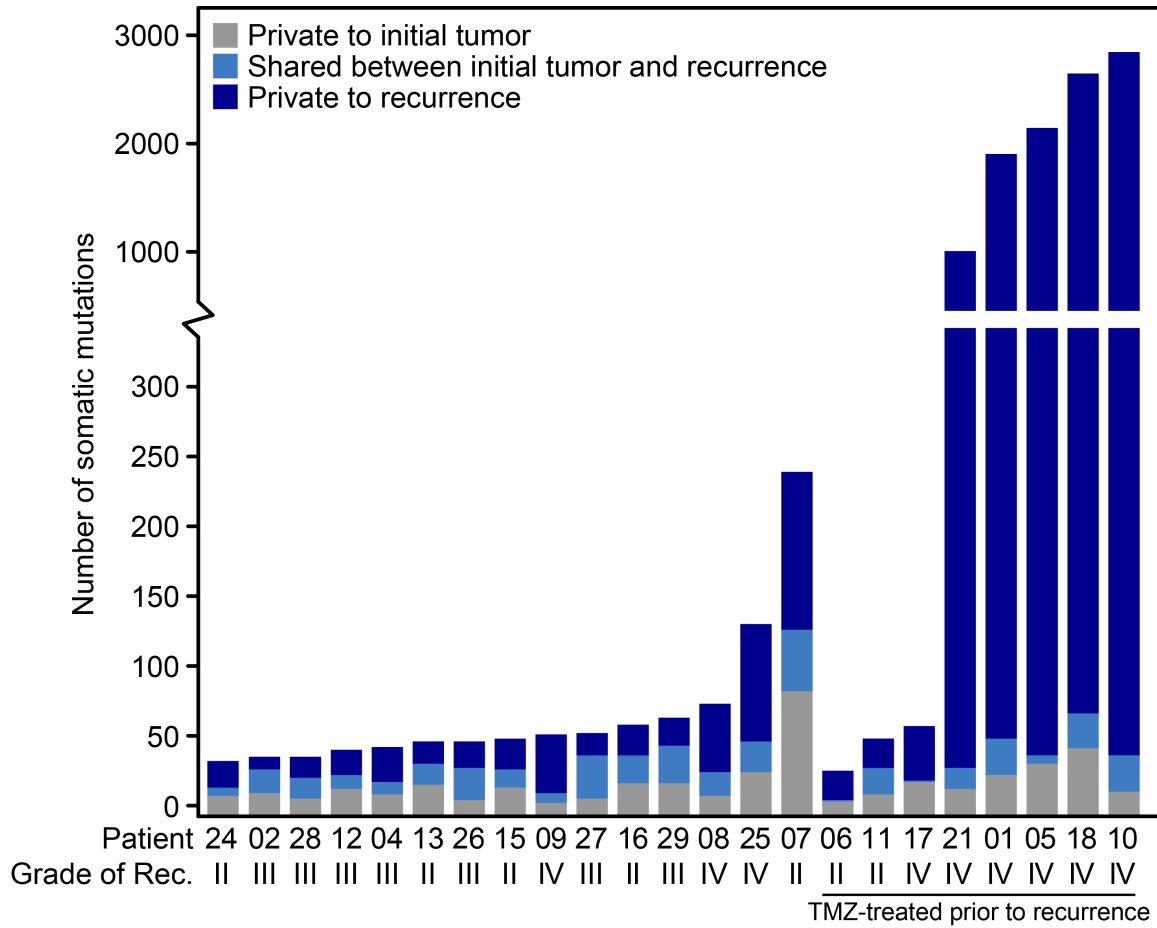
Figure 2.1 Genetic landscapes of low-grade gliomas and their patient-matched recurrences. Total number of mutations private to or shared between the initial and first recurrent glioma of 23 patients.

FIGURE 2.2
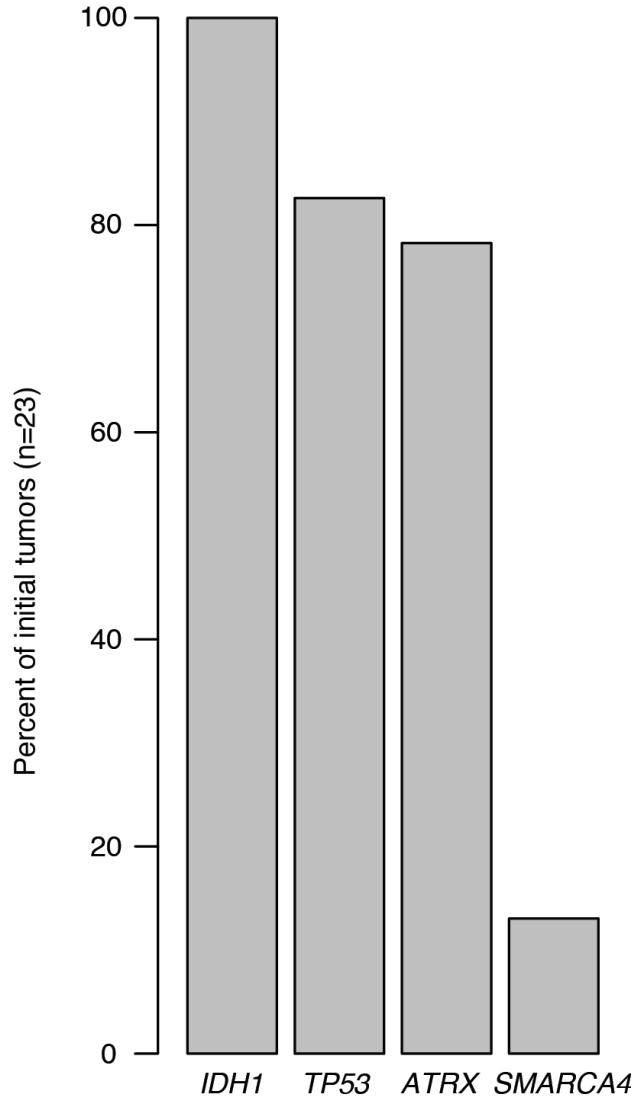
Figure 2.2 Commonly mutated genes in grade II glioma. The three genes most commonly mutated in grade II glioma at initial diagnosis are each identified in >75% (23/23, 19/23, 18/23) of this cohort. The next most commonly mutated gene, *SMARCA4*, is identified in 13% (3/23) of the initial tumors in this cohort. 13 additional genes are identified in 9% (2/23) of the cohort.

FIGURE 2.3
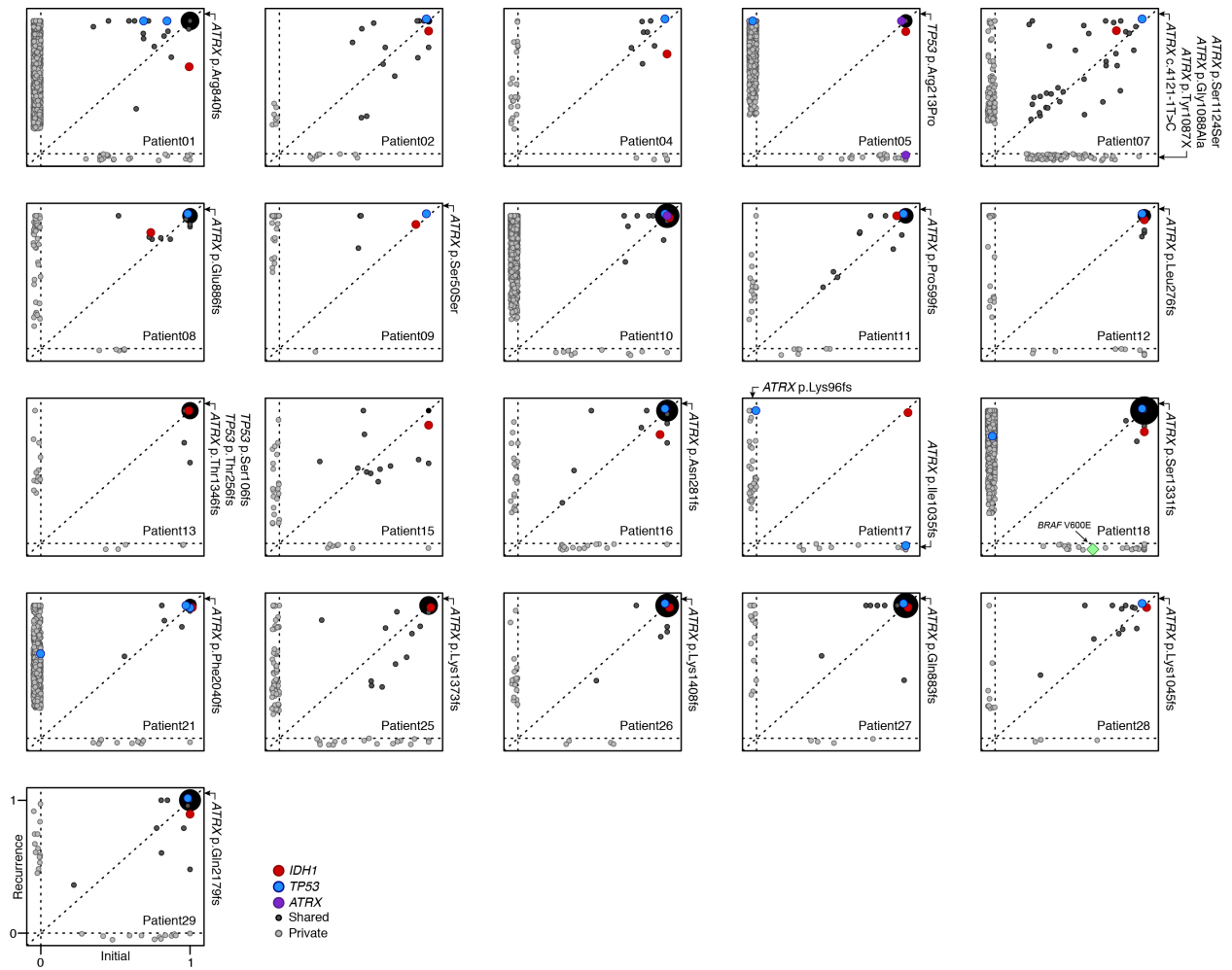
Figure 2.3 Tumor cell fraction of somatic mutations in paired initial and recurrent tumors. Mutations private to tumors at initial diagnosis (x-axis), private to recurrent tumors (y-axis) or shared between the two tumors are shown as a function of the fraction of tumor cells containing the mutation. Those mutations clonal in both tumors are represented by a single point whose radius is scaled by the log count of such mutations. Key mutations are colored as indicated. Data from patients 06 and 24 were not available.

FIGURE 2.4
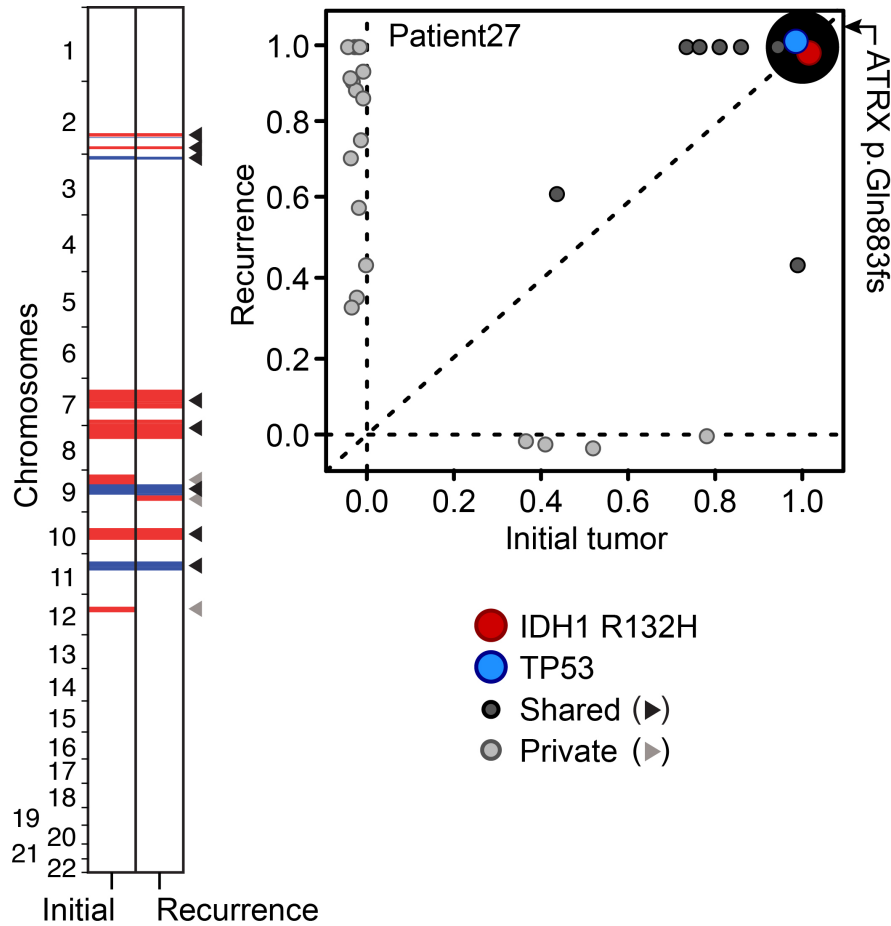
Figure 2.4 Genetic relationship between the initial and recurrent gliomas from patient 27. Shared and private somatic mutations in paired initial and recurrent tumors (x and y axes respectively) as a function of the estimated fraction of tumor cells carrying the mutant allele. Mutations present in all the cells in both tumors are represented by a single point whose radius is scaled by the log count of such mutations. Shared and private CNAs are indicated (red and blue are gains and losses respectively, white is copy-neutral).

FIGURE 2.5
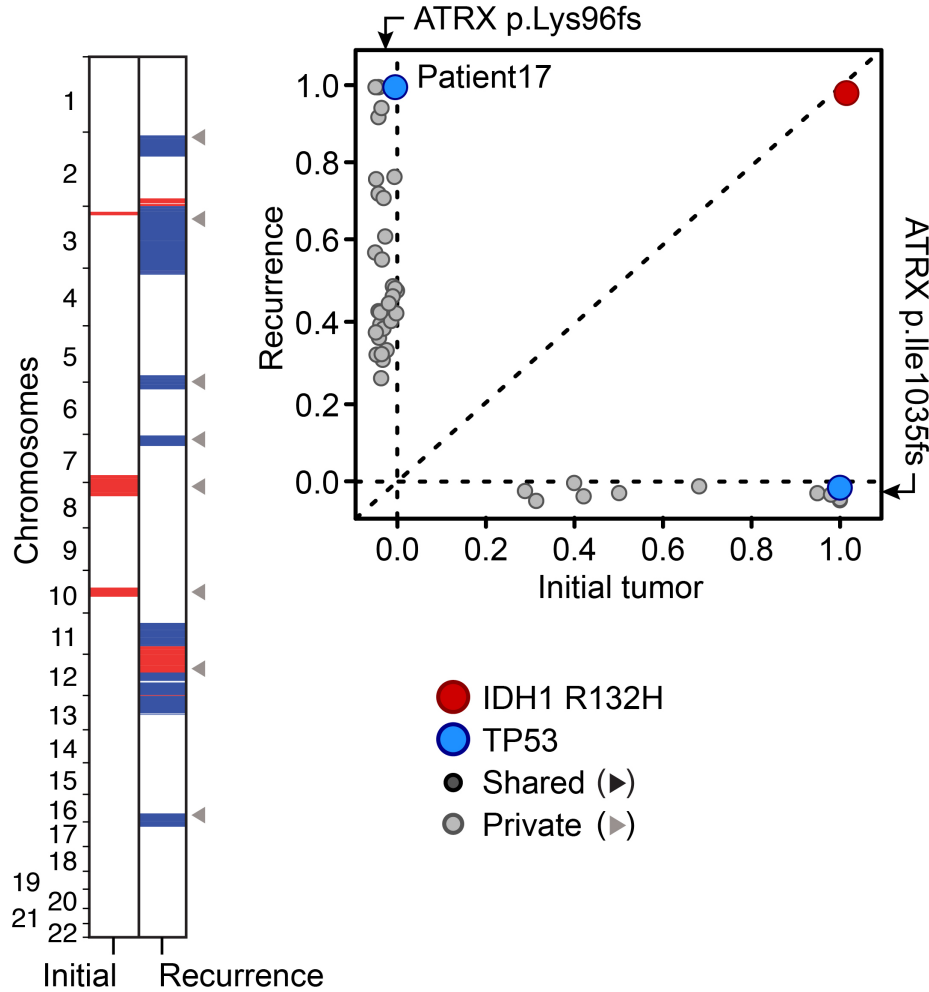
Figure 2.5 Genetic relationship between the initial and recurrent gliomas from patient 17. Shared and private somatic mutations in paired initial and recurrent tumors (x and y axes respectively) as a function of the estimated fraction of tumor cells carrying the mutant allele. Mutations present in all the cells in both tumors are represented by a single point whose radius is scaled by the log count of such mutations. Shared and private CNAs are indicated (red and blue are gains and losses respectively, white is copy-neutral). Clonal *TP53* and *ATRX* mutations in the initial tumor were not identified in the recurrent tumor, but different clonal mutations in these two genes were acquired.

FIGURE 2.6
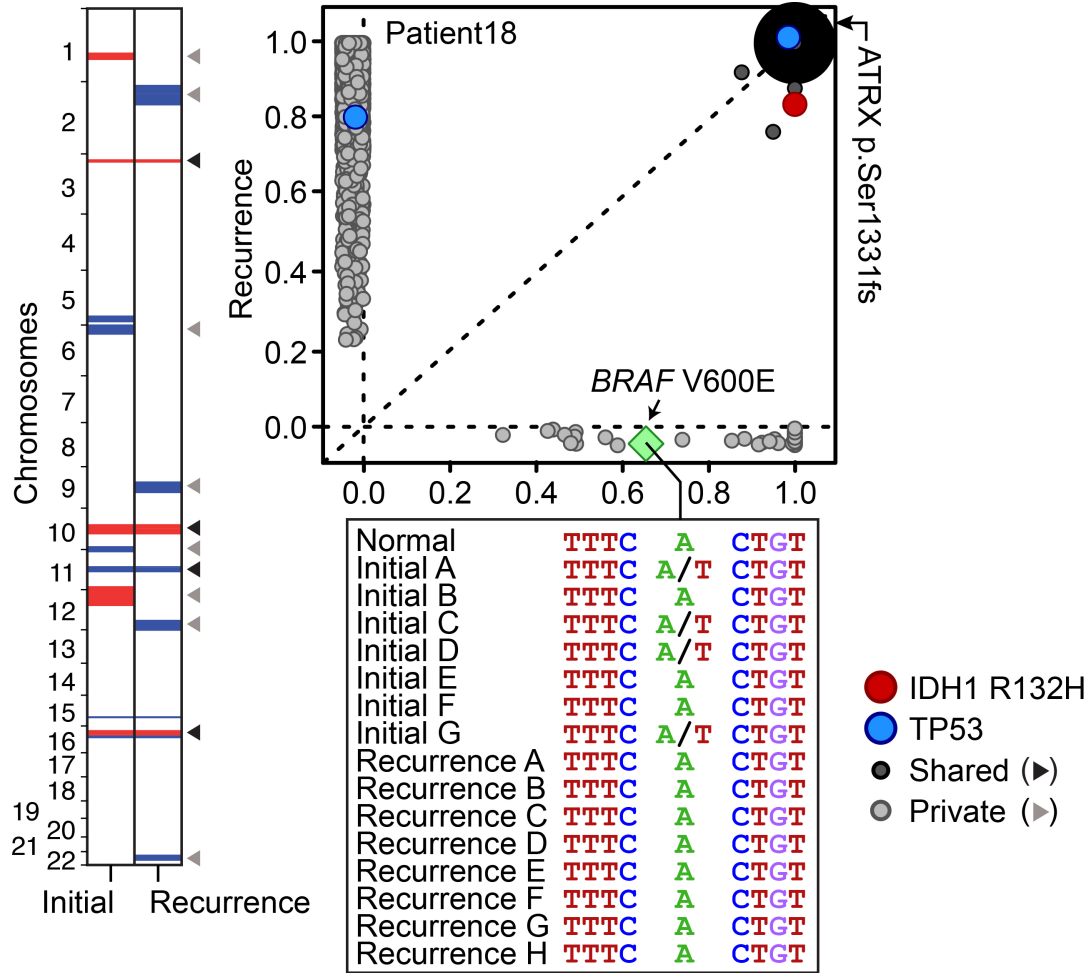
Figure 2.6 Genetic relationship between the initial and recurrent gliomas from patient 18. Shared and private somatic mutations in paired initial and recurrent tumors (x and y axes respectively) as a function of the estimated fraction of tumor cells carrying the mutant allele. Mutations present in all the cells in both tumors are represented by a single point whose radius is scaled by the log count of such mutations. Shared and private CNAs are indicated (red and blue are gains and losses respectively, white is copy-neutral). Inset shows the DNA sequence encompassing *BRAF* V600E in the normal tissue and in 15 geographically distinct samples of the initial and recurrent tumors.

FIGURE 2.7
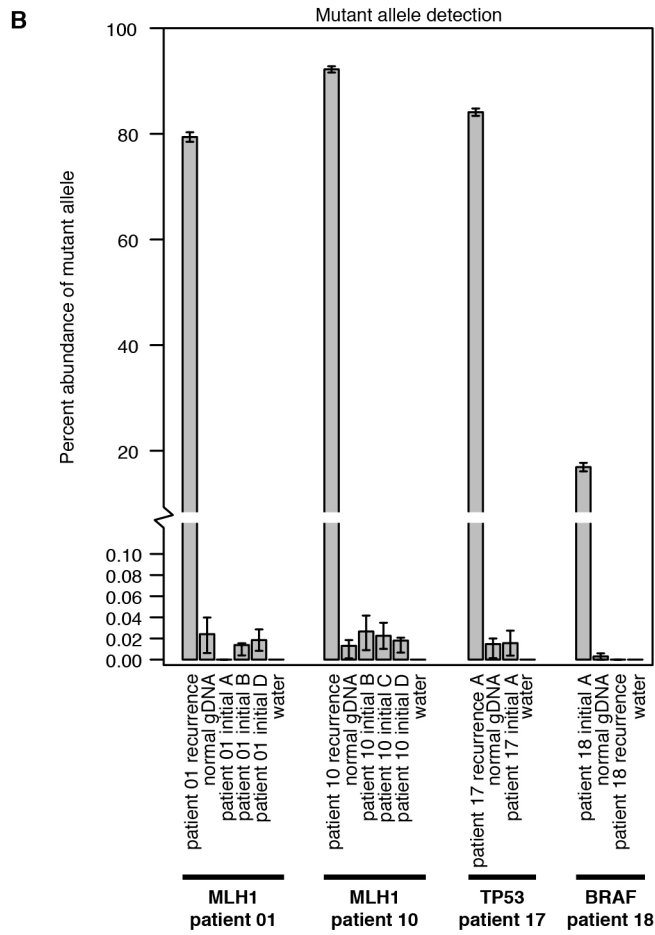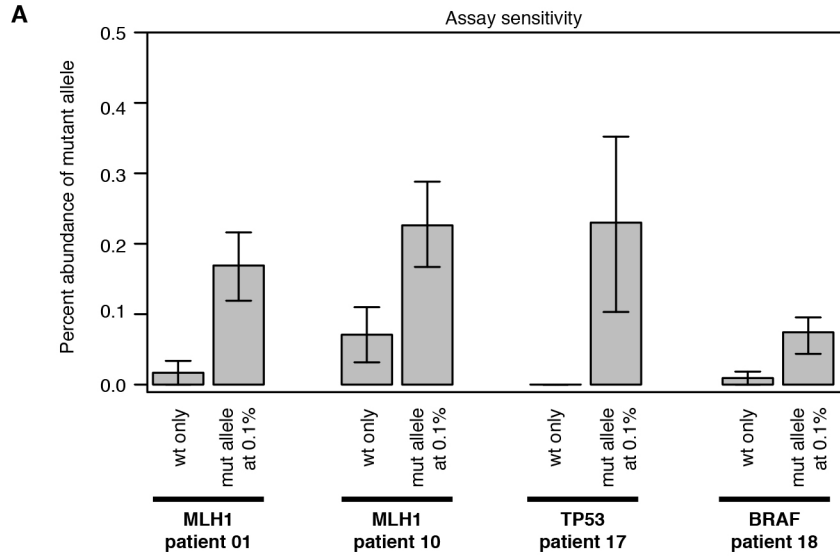
Figure 2.7 Sensitive detection of mutant alleles. (A) Droplet digital PCR assays against 4 mutations identified as private to either an initial (BRAF in patient 18) or recurrent (MLH1 patient 01, MLH1 patient 10, TP53 patient 17) tumor can detect the mutant allele down to a frequency of 0.1% (0.1% samples run in triplicate). The background positive level ranges from 0.01% to 0, allowing for sensitive detection of the mutant allele at 0.1%. **(B)** Geographically distinct samples of patient-matched tumor in which the mutation was not originally identified show no evidence of the mutant allele. Three distinct samples of the initial tumor from patients 01 and 10, one sample of the initial tumor from patient 17 and one sample of the recurrent tumor from patient 18 (all test samples run in quadruplicate), show background-level signals indicating that the mutant alleles are not present at a sensitivity of 0.1%. All error bars indicate the standard deviation from the Poisson calculation of allele concentrations.

FIGURE 2.8
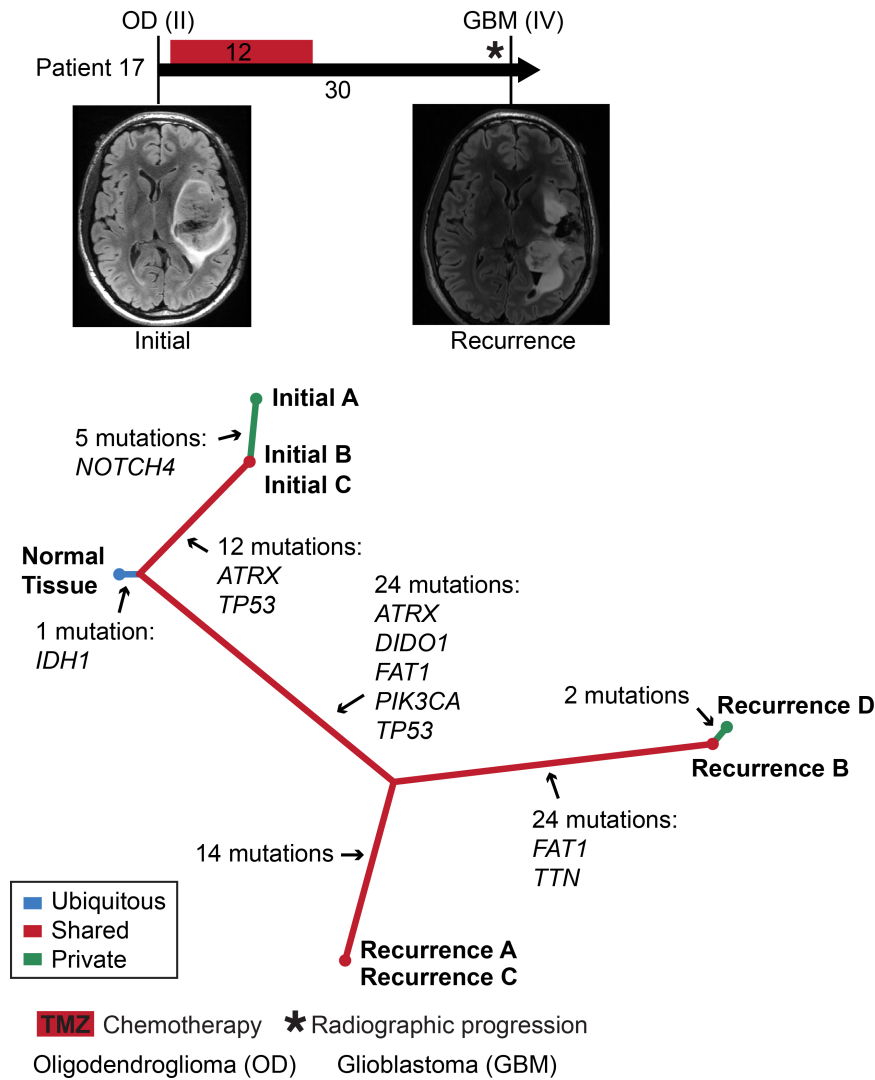
Figure 2.8 The temporal and spatial pattern of clonal evolution in the tumors of patient 17. A timeline of treatment history for patient 17 (top, intervals labeled in months). Vertical bars correspond to the time of tumor resection and are labeled with the tumor diagnosis and grade. Representative MRIs are also shown. A phylogenetic tree (bottom) depicts the patterns of clonal evolution of these tumors inferred from the pattern and frequency of somatic mutations, highlighting genes frequently mutated in cancer.

FIGURE 2.9

A

B
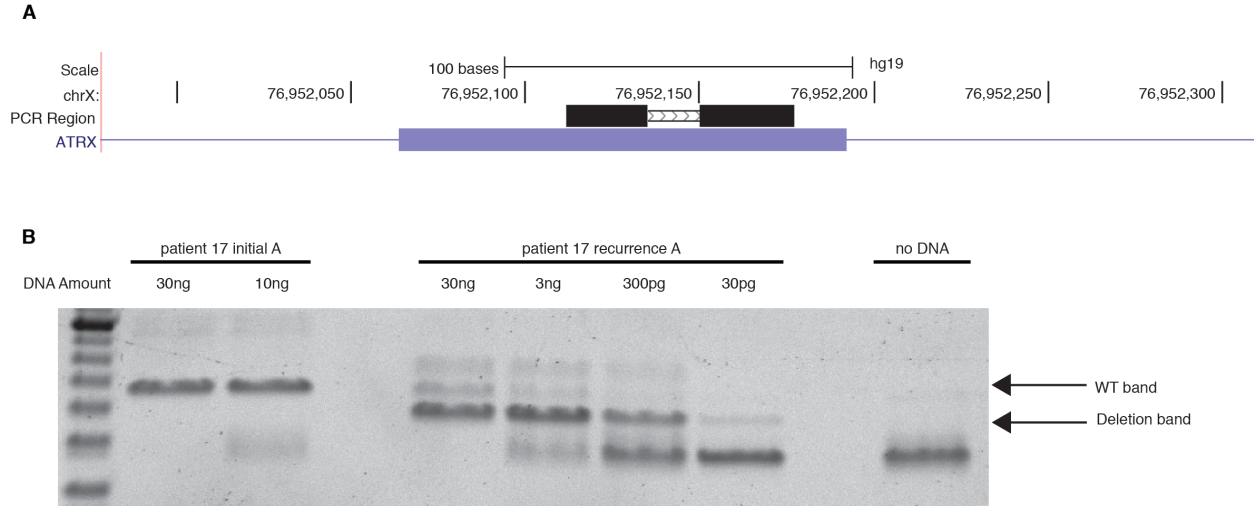
Figure 2.9 Sensitive PCR analysis of an ATRX deletion in patient 17. (A) The position of the amplicon used to assess the 8bp deletion starting at chrX:76952141 identified by exome sequencing as private to the recurrence of patient 17. **(B)** A PCR analysis of this region using primers that flank the deletion and allow for amplification of both the wild-type (65bp) and deletion (57bp) alleles. The PCR product corresponding to the allele with a deletion was observed in patient 17 recurrent DNA with 30ng down to 30pg of template DNA. However, no such deletion-specific PCR product was observed with 30ng or 10ng of input from the initial tumor sample.

FIGURE 2.10
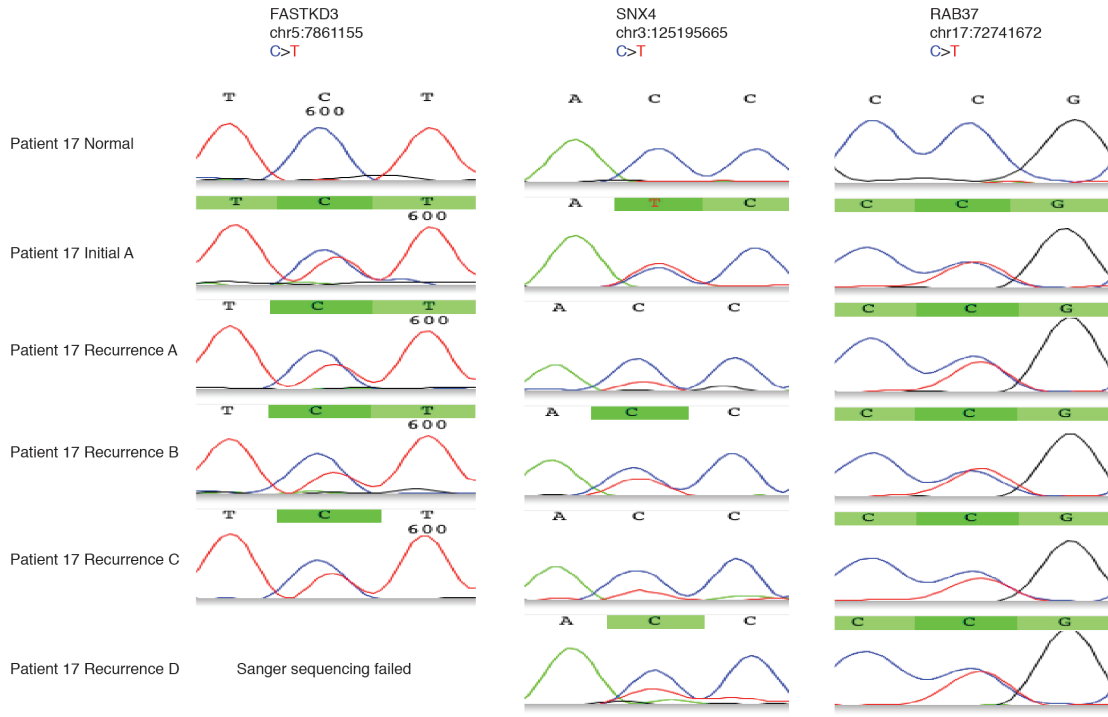
Figure 2.10 Shared non-coding mutations in patient 17. Sanger sequencing confirms that at least three non-coding mutations are shared between the initial and recurrent tumors of patient 17. This indicates that these tumors diverged early in their evolutionary history from a nearest common ancestor that includes these three non-coding mutations and the shared *IDH1* R132H coding mutation.

FIGURE 2.11

Patient 17
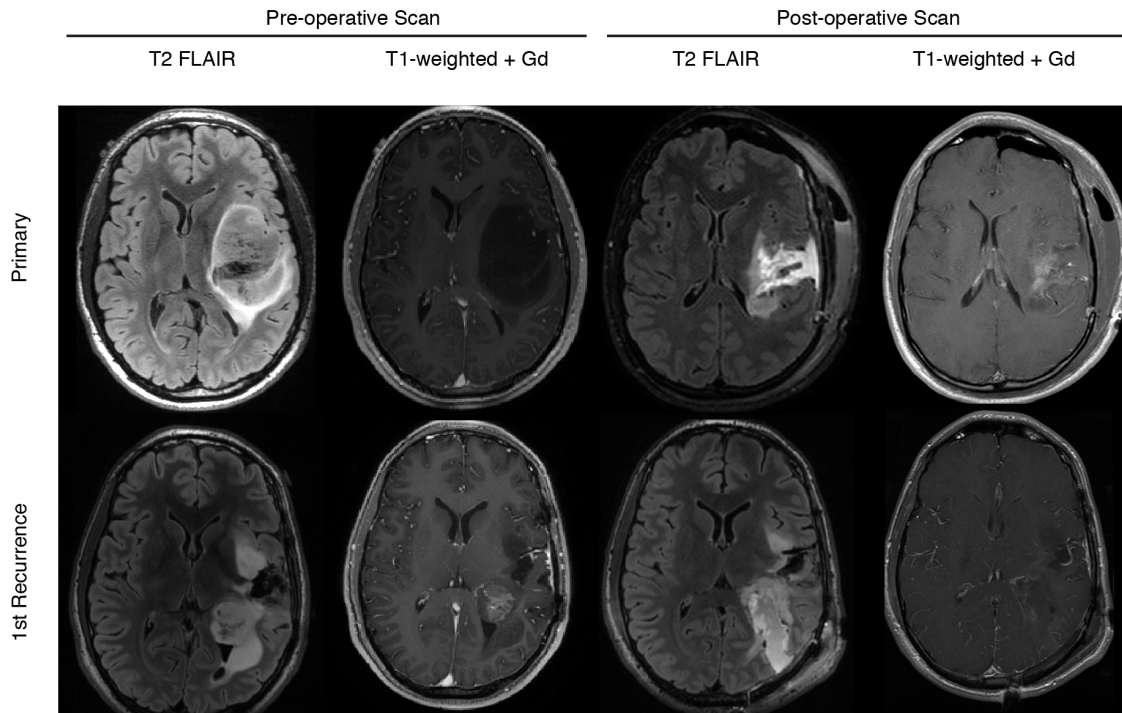
Figure 2.11 Pre- and post-surgical MR imaging of patient 17. T1- and T2-weighted images representative of the tumor region before and after the initial resection and recurrence. Imaging for the initial resection demonstrated a large T2 hyperintense non-enhancing mass situated in the left insula with significant mass effect on the left lateral ventricle. After a near gross total resection the pathological diagnosis was a WHO grade II oligodendroglioma. Significant T2-hyperintensity and tissue shifts were observed post resection. At the time of recurrence, an enhancing mass centered in the left posterior temporal and parietal white matter was noted with interval growth, avid heterogeneous enhancement, and MR features consistent with upgrade to a high-grade neoplasm. Abnormal susceptibility and T1-hyperintensity with focal reduced diffusion (not shown) in the center of the mass was consistent with central necrosis. Surrounding masslike T2

hyperintensities without contrast enhancement were seen in the left insular white matter, extending into the left temporal lobe, left parietal lobe, and left corona radiata and were consistent with residual low-grade neoplasm. Gross total resection was performed on the enhancing portion of the left parietal mass and determined pathologically to be grade IV glioblastoma multiforme.

FIGURE 2.12
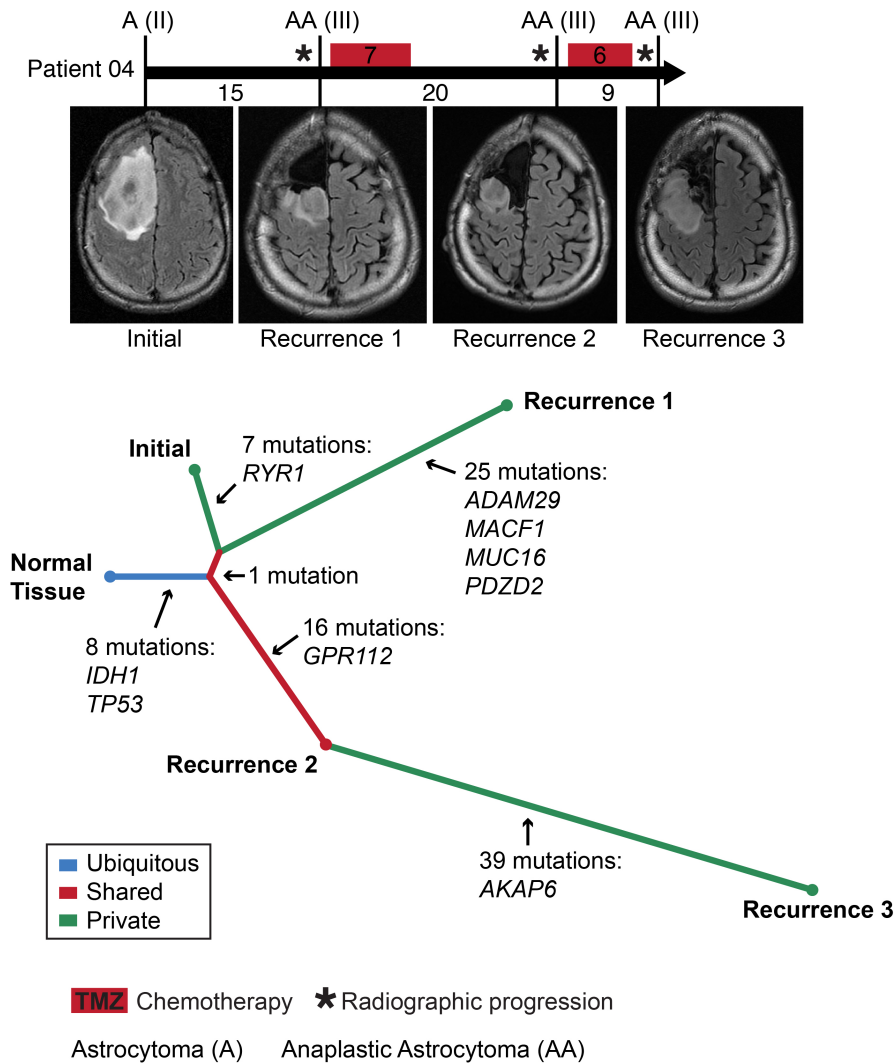
Figure 2.12 The temporal and spatial pattern of clonal evolution in the tumors of patient 04. A timeline of treatment history for patient 04 (top, intervals labeled in months). Vertical bars correspond to the time of tumor resection and are labeled with the tumor diagnosis and grade. Representative MRIs are also shown. A phylogenetic tree (bottom) depicts the patterns of clonal evolution of these tumors inferred from the pattern and frequency of somatic mutations, highlighting genes frequently mutated in cancer.

FIGURE 2.13

Patient 04
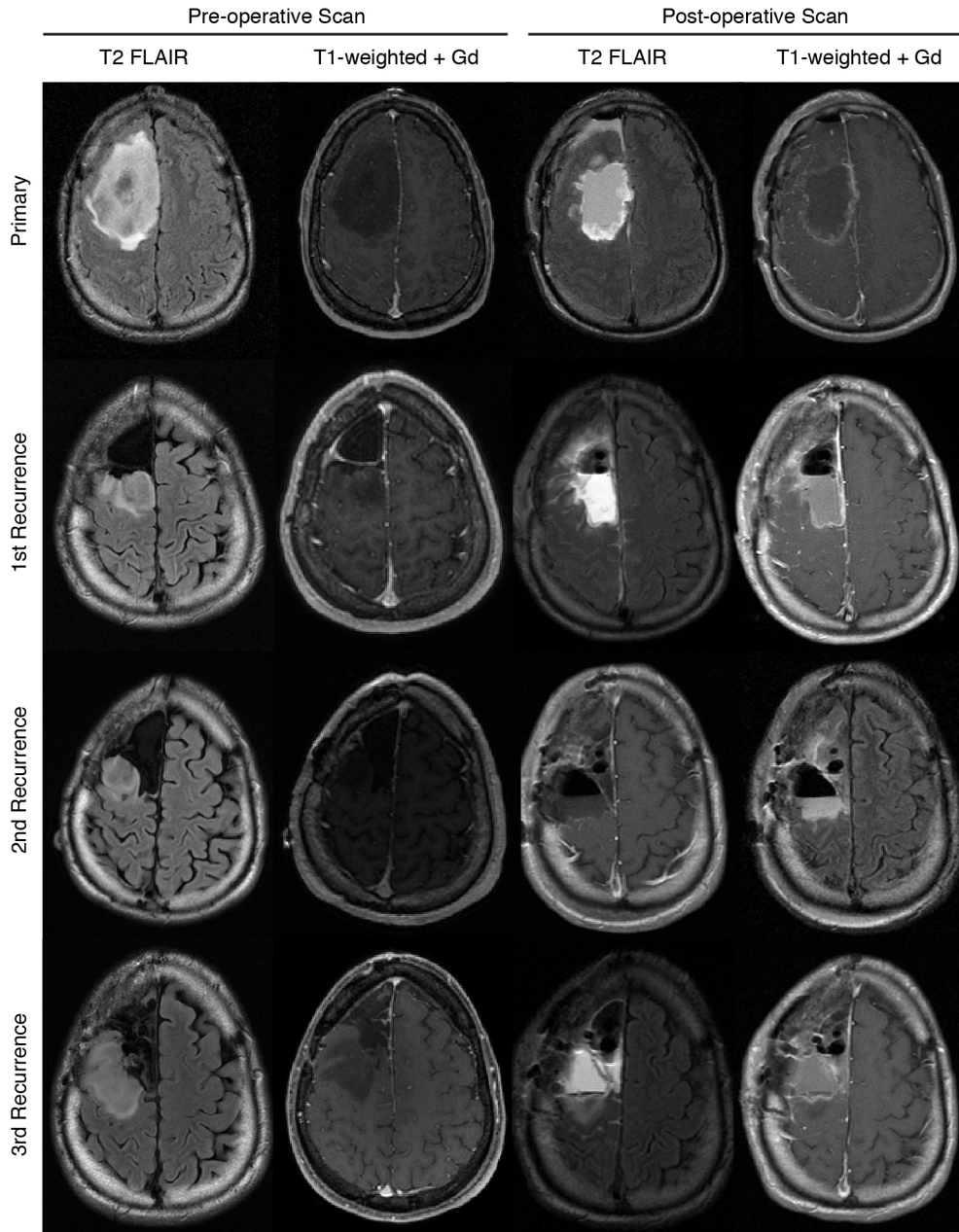
Figure 2.13 Pre- and post-surgical MR imaging of patient 04. T1- and T2-weighted images representative of the tumor region before and after the initial resection and subsequent three recurrences. Imaging for the initial resection demonstrated a large T2 hyperintense non-enhancing mass situated in the right frontal lobe with significant mass

effect. Perfusion imaging and spectroscopic imaging (not shown) were suggestive of low-grade neoplasm, confirmed after gross total resection to be a grade II astrocytoma. Upon first recurrence, an abnormal T2 lesion was observed along the posterior resection cavity, extending superiorly and inferiorly to the level of the lateral ventricles, with corresponding T1 hypointensity, characteristic of highly cellular recurrent tumor. After a gross total resection, pathology analysis indicated the tumor had upgraded to a grade III anaplastic astrocytoma. At the time of the second recurrence, a mass-like non-enhancing lesion was identified in the posterior superior lateral aspect of the resection cavity with similar imaging characteristics as the previous recurrence. A gross total resection was obtained surgically, but with limited posterior margins due to proximity with the motor tracts. The lesion remained pathologically grade III. At the time of the third recurrence, there was continued interval progression of a mass-like T2 hyperintensity within the right middle frontal and precentral gyri posterior to the surgical cavity. Signal abnormality further involved the anteromedial margins of the cavity infiltrating inferiorly into the ipsilateral corona radiata. Surgical resection was limited to 80-85% due to infiltration of the motor tracts, and the tumor tissue was confirmed to remain grade III.

FIGURE 2.14
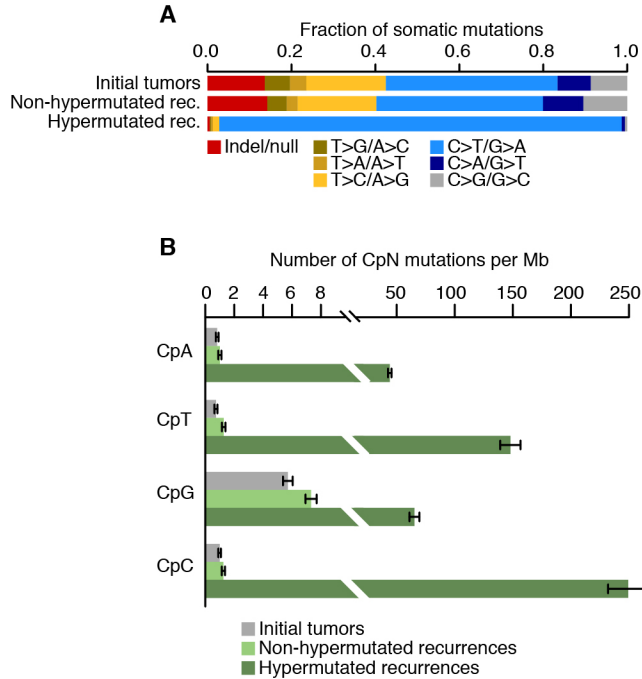
Figure 2.14 The spectrum and context of somatic mutations in hypermutated and non-hypermutated gliomas. (A) The spectrum of somatic mutation types observed in initial tumors as well as both non-hypermutated and hypermutated recurrences indicates a massive increase in the C>T/G>A mutation rate in only the latter. **(B)** Somatic mutation rates for each CpN dinucleotide context indicates a propensity for C>T/G>A mutations to arise outside the CpG and CpA dinucleotide contexts.

FIGURE 2.15
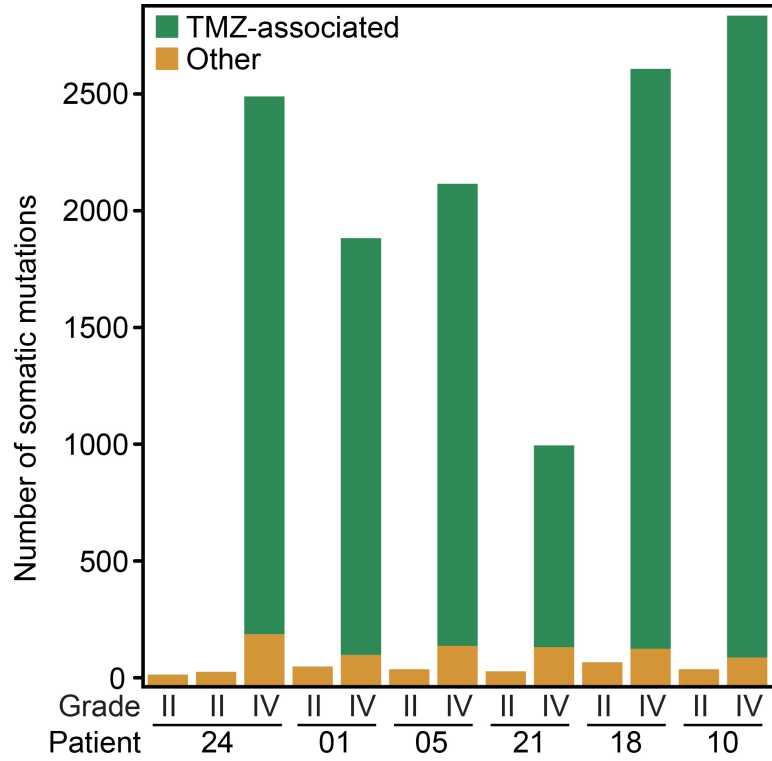
Figure 2.15 The number of TMZ-associated mutations and other mutations identified in the six patients with hypermutated recurrent tumors.

FIGURE 2.16

A

131,265,400   131,265,700

CpG island

MGMT

Bisulfite region

B

Patient 01
CpGs 1-23

Initial (18%)

Recurrence1 (50%)

Patient 18

Initial (40%)

Recurrence (75%)

■ Unmethylated
■ Methylated

Patient 05

Initial (20%)

Recurrence (51%)

Patient 21

Initial (48%)

Recurrence (55%)

Patient 10

Initial (71%)

Recurrence (79%)

Normal brain (NB)

NB1 (1.6%)

NB3 (1.8%)
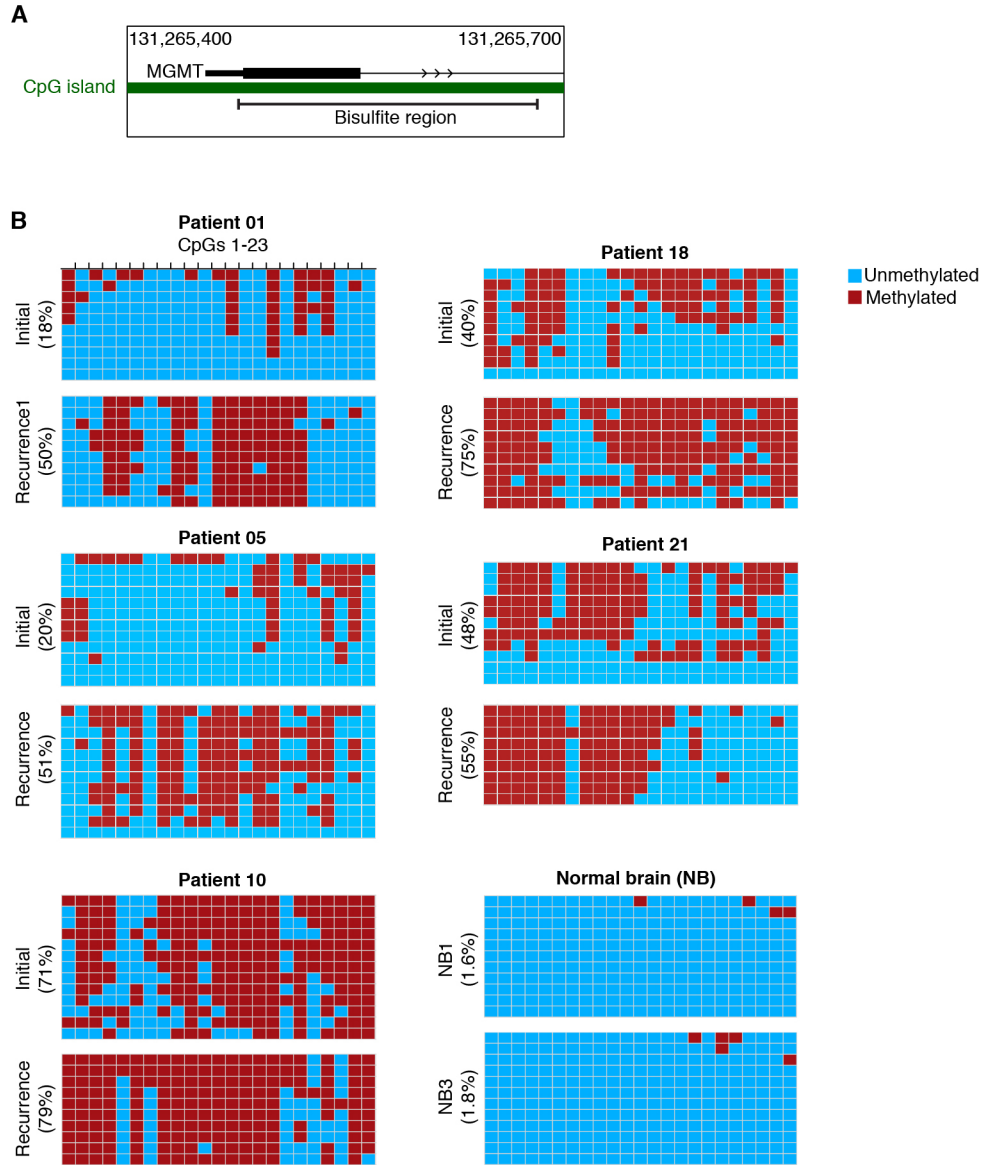
Figure 2.16 The evolution of DNA methylation affecting *MGMT* during malignant progression. (A) The position of the amplicon used to assess *MGMT* methylation levels. **(B)** Methylation status of CpG sites in individual clones of the PCR product from bisulfite-treated DNA from the initial and recurrent tumors of patients 01, 05, 10, 18, and 21 as well as two normal brain samples. Each row represents a single clone with each

CpG site marked as either methylated (red) or unmethylated (blue). The total methylation percentage of all clones is presented to the left of each panel.

FIGURE 2.17
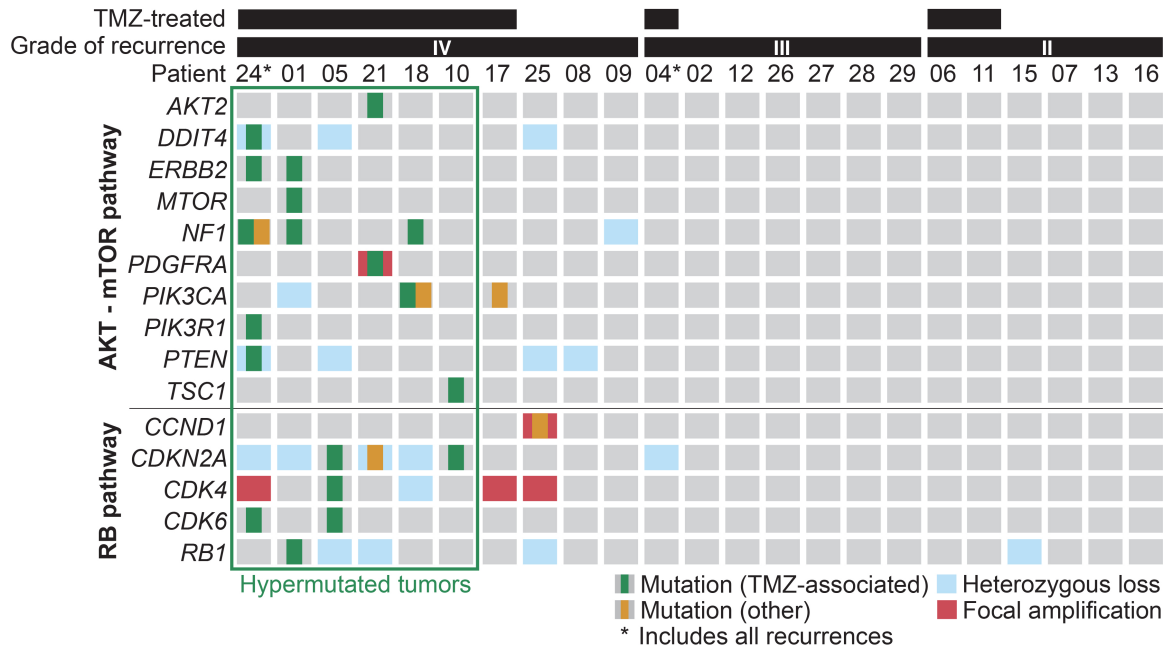
Figure 2.17 Recurrent tumors from patients treated with TMZ harbor genetic alterations in the RB and AKT-mTOR signaling pathways. Somatic mutations and CNAs acquired upon recurrence in key genes of pathways associated with GBM.

FIGURE 2.18
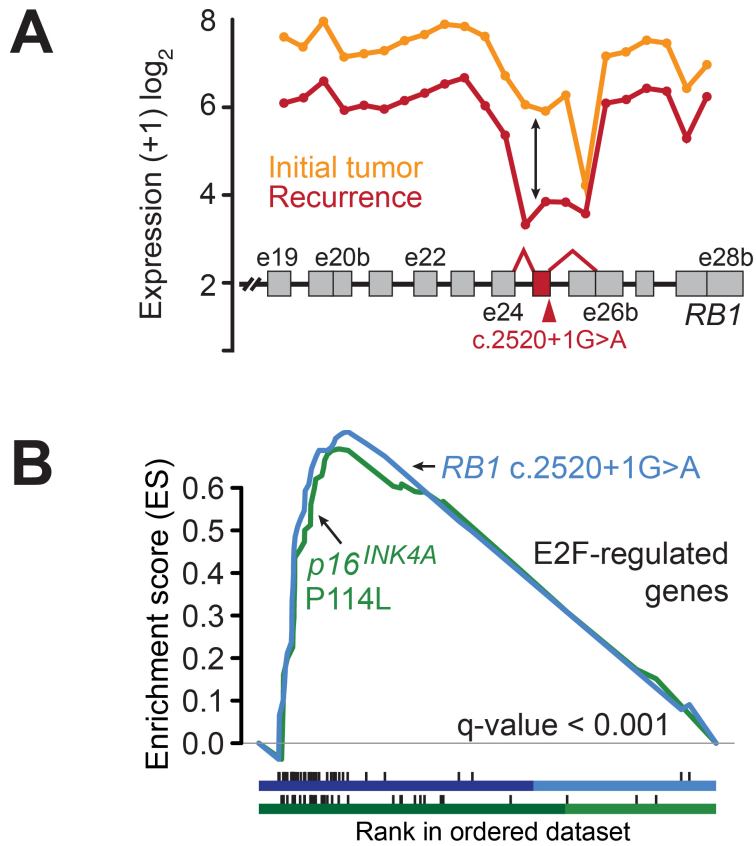
Figure 2.18 Functional consequences of TMZ-associated mutations in the RB pathway. (A) Expression level of *RB1* at each exon and exon-exon junction in the initial and recurrent tumor of patient 01 showing aberrant splicing of the *RB1* transcript in the recurrent tumor harboring the *RB1* c.2520+1G>A splice-site mutation. The *RB1* exon and exon junctions with significant differential usage (red) and the location of the splice-site mutation are shown. **(B)** Gene set enrichment analysis shows significant enrichment of genes down-regulated by *RB1* and up-regulated by *E2F* in the recurrent tumors of patients 01 (blue) and 10 (green), coincident with the acquisition of TMZ-associated mutations in the RB pathway.

FIGURE 2.19
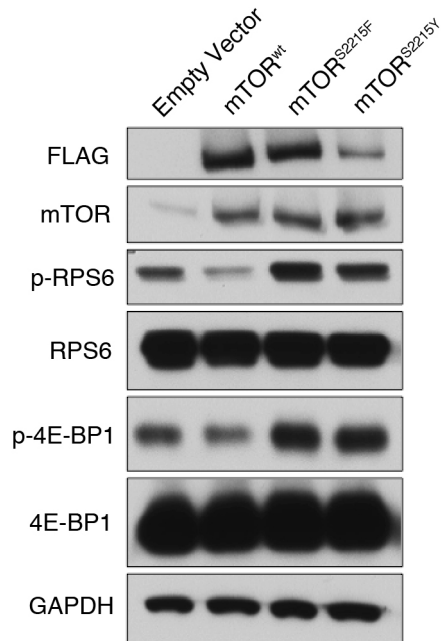
Figure 2.19 Functional assessment of *MTOR* mutations on mTORC1 signaling. Western blot on protein from HEK293 cells expressing wild-type or one of two mutant mTOR vectors. Constitutive phosphorylation of RPS6 and 4E-BP1 indicates that the *MTOR* S2215F mutation constitutively activates mTORC1 signaling, much like the previously characterized *MTOR* S2215Y mutation.

FIGURE 2.20
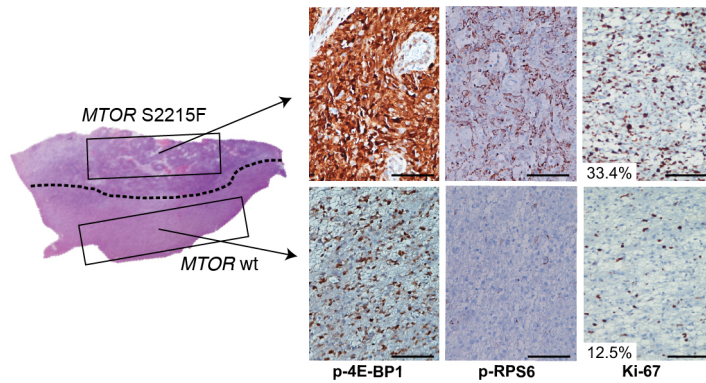
Figure 2.20 Heterogeneous mTORC1 activity in adjacent regions of the recurrent tumor of patient 01. Hematoxylin and eosin (H&E)-stained tumor sample from the first recurrent tumor of patient 01. A dotted line separates the two morphologically distinct regions. IHC for phospho-RPS6, phospho-4E-BP1 and Ki-67 show differential activation of mTORC1 targets and proliferation rates in the two adjacent regions. Bars represent 100 microns.

FIGURE 2.21
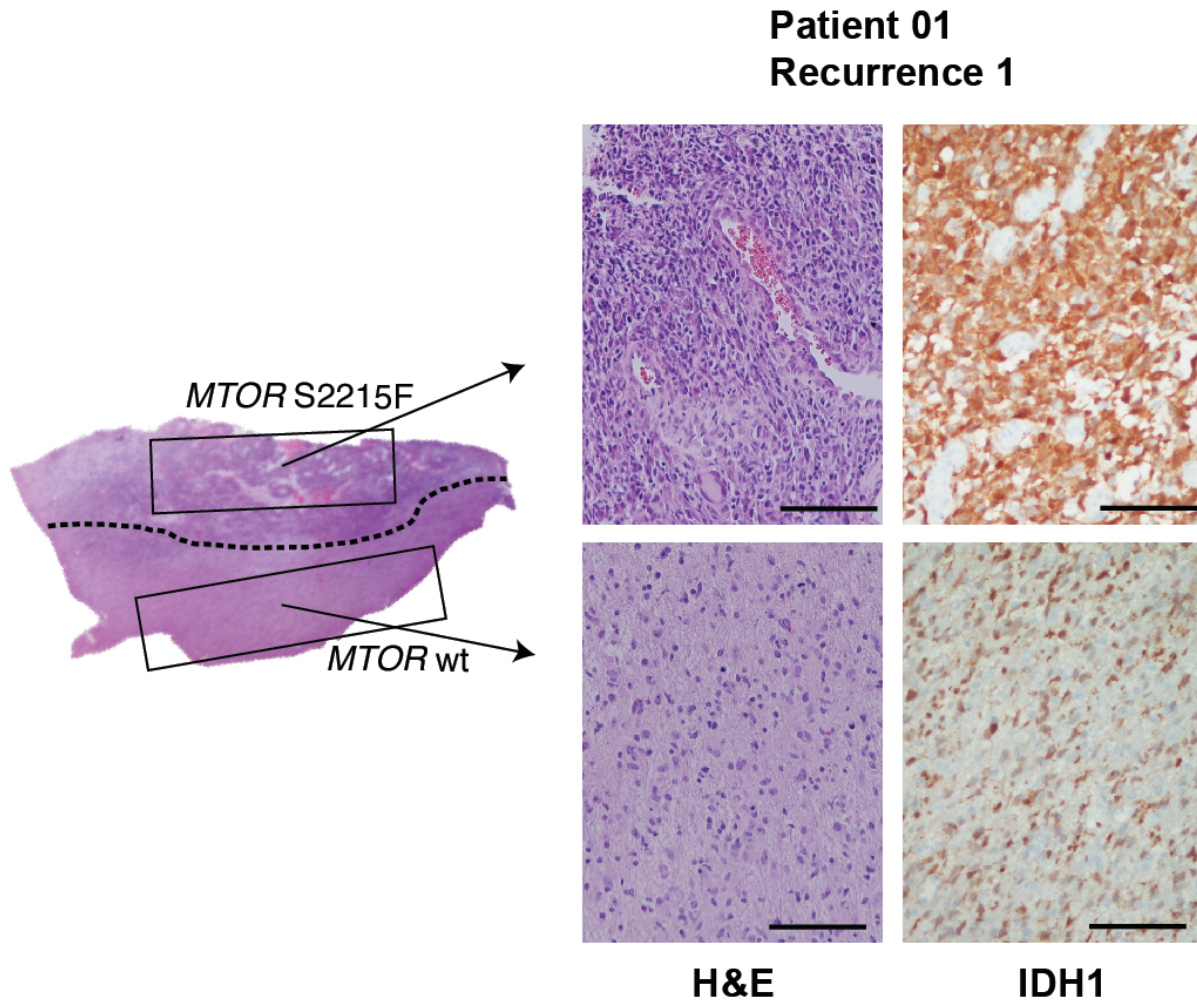
Figure 2.21 Comparison of tumor samples from the first recurrence of patient 01.

Hematoxylin and eosin (H&E)-stained tumor sample from the first recurrence of patient 01. A dotted line separates the two morphologically distinct regions. H&E-stained sections indicate that both regions are histologically GBM. IHC for mutant IDH1 in these same regions indicates comparable tumor content. Bars represent 100 microns.

FIGURE 2.22
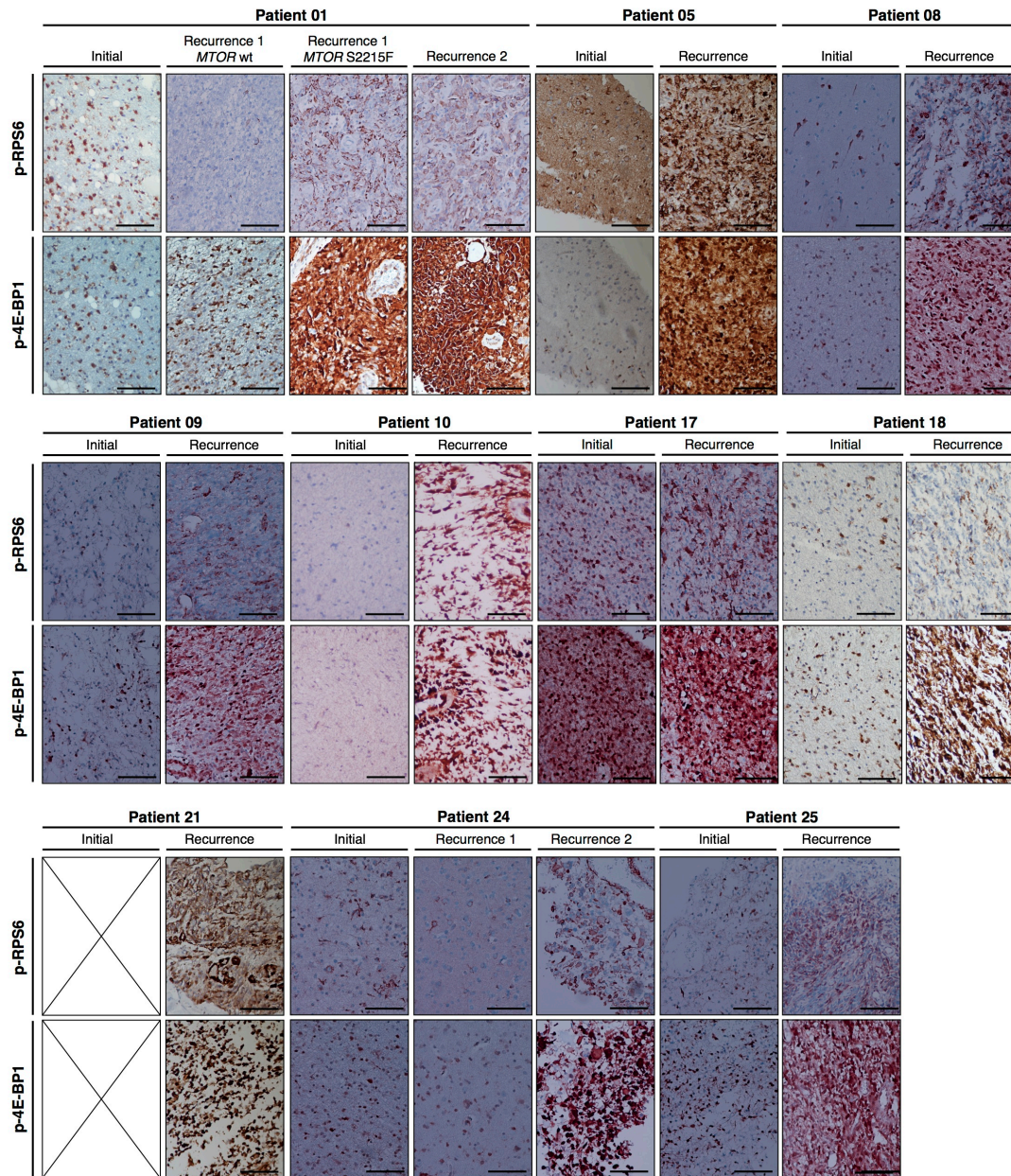
Figure 2.22 mTORC1 signaling in tumors at initial diagnosis and their GBM recurrences. Immunohistochemistry (IHC) for phospho-RPS6 and phospho-4E-BP1 in the initial and recurrent tumors of all patients that undergo malignant progression to GBM indicates an increase in mTORC1 signaling across GBMs relative to the patient-

matched initial tumors. Slides for the initial tumor from patient 21 were not available.

Bars in all panels represent 100 microns.

FIGURE 2.23
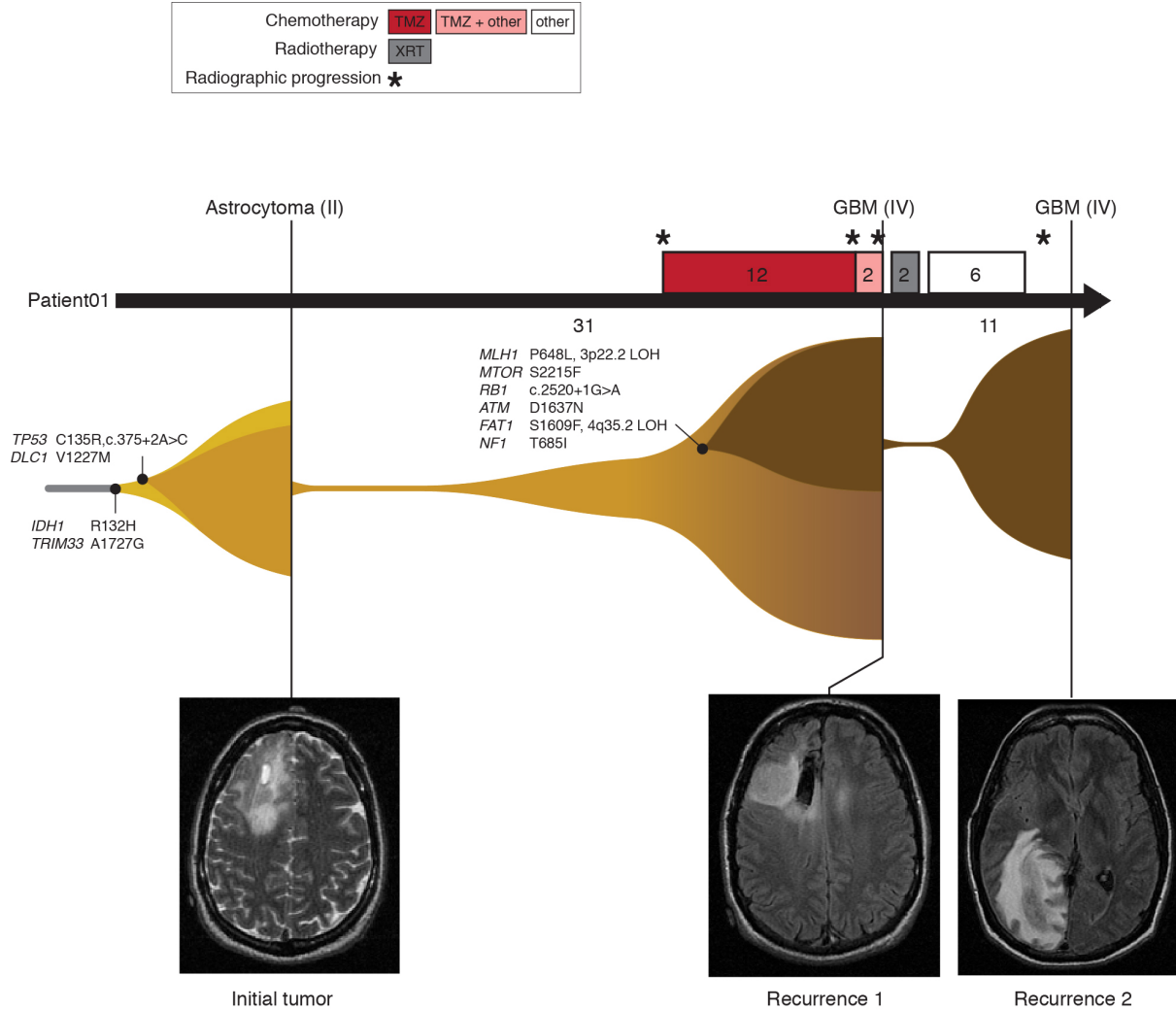
Figure 2.23 An integrated timeline of the treatment, imaging, and clonal evolution of a low-grade astrocytoma that underwent TMZ-associated malignant progression. A timeline of the treatment received by patient 01 (all intervals labeled in months). Vertical bars represent tumor resections and are labeled with their diagnosis and grade (top), as well as representative MRIs (bottom). A graphical representation of one model of the clonal evolution of these tumors (middle) begins with a founding clone with early mutations in *IDH1*, *TRIM33*, *TP53* and *DLC1*. Upon first recurrence, two morphologically distinct regions of GBM are present, with only one region harboring

63

TMZ-associated mutations in key functional cancer genes. This hypermutated clone then seeds the distal second recurrence.

FIGURE 2.24

Patient 01
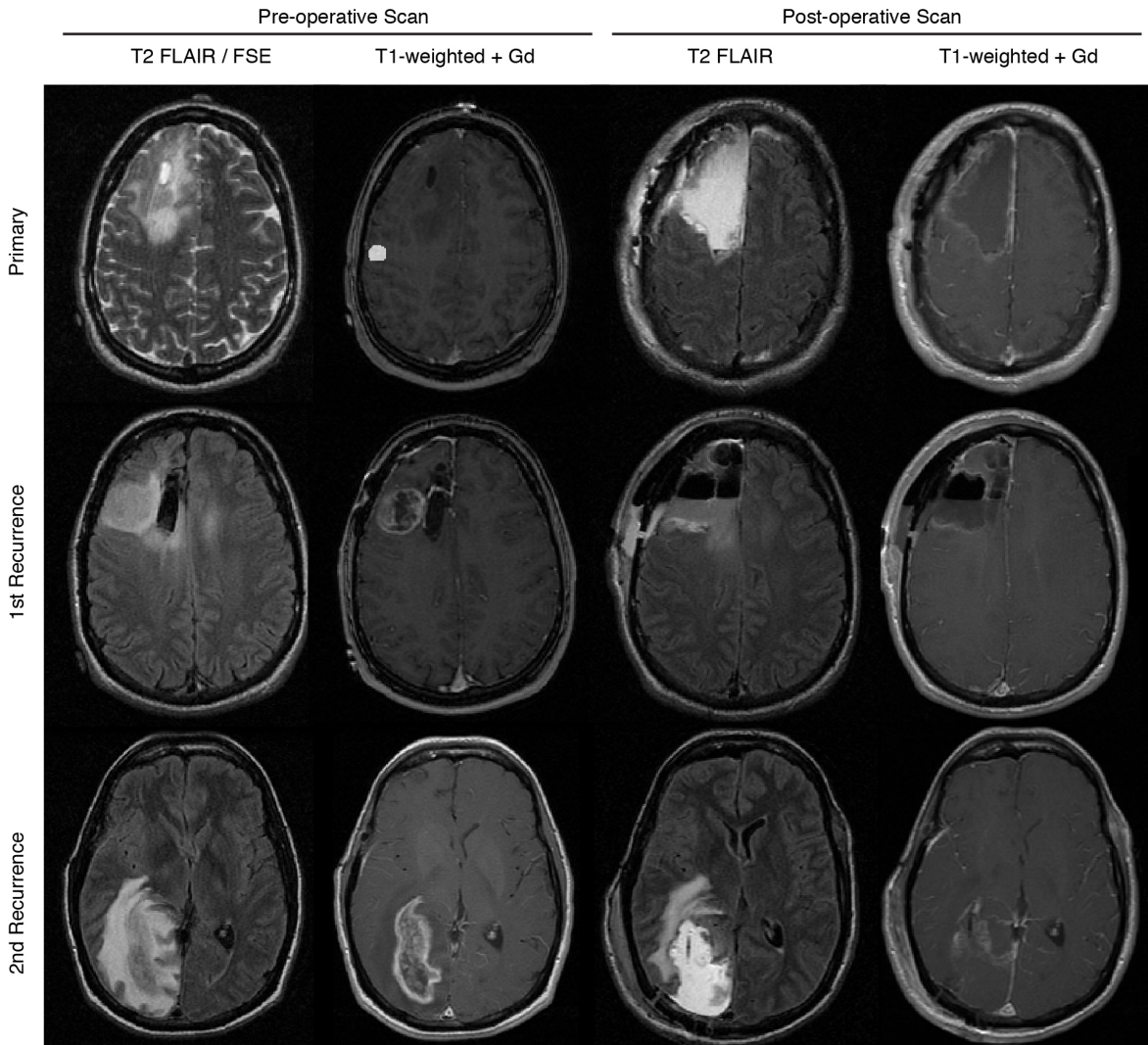
Figure 2.24 Pre- and post-surgical magnetic resonance imaging of patient 01. T1- and T2-weighted images representative of the tumor region throughout the course of treatment. At the time of initial resection, the tumor lesion appeared localized to the right frontal lobe in the pre-operative scan. The first tumor recurrence was at the posterior aspect of the initial resection site, and the second recurrence was found distally in the right temporal occipital region in a lower horizontal plane. The hyper-intense region in

the initial resection, pre-surgical spoiled gradient echo (SPGR), is a diffusion tensor imaging mask used for white matter tracking during surgery.

TABLE 2.1

Patient	Gender	Age	Sample	Diagnosis (WHO grade)	Surgical interval (months)	Non-surgical treatment (months)	Overall survival (months)	MGMT methylation	IDH1 status	1p/19q status	TP53, ATRX, CIC, FUBP1*
01	Male	28	Initial tumor	Astrocytoma (II)	31	TMZ (14)‡	58	Un-methylated	R132H	Intact	TP53, ATRX
			Recurrence	Glioblastoma (IV)				Methylated	R132H	19q deletion	TP53, ATRX
02	Female	26	Initial tumor	Oligoastrocytoma (II)	74	None	5 ‖	Methylated	R132H	19q deletion	TP53
			Recurrence	Anaplastic astrocytoma (III)				Un-methylated	R132H	19q deletion	TP53
04	Male	22	Initial tumor	Astrocytoma (II)	15	None	61	Unknown	R132C	Intact	TP53
			Recurrence 1	Anaplastic astrocytoma (III)	20	TMZ (7)		Unknown	R132C	Intact	TP53
			Recurrence 2	Anaplastic astrocytoma (III)	9	TMZ (6)		Unknown	R132C	Intact	TP53
			Recurrence 3	Anaplastic astrocytoma (III)				Unknown	R132C	Intact	TP53
05	Female	39	Initial tumor	Astrocytoma (II)	56	TMZ (12)	74	Methylated	R132H	Intact	TP53, ATRX
			Recurrence	Glioblastoma (IV)				Methylated	R132H	Intact	TP53, ATRX
06	Male	22	Initial tumor	Astrocytoma (II)	32	TMZ (6) §	87	Un-methylated	R132H	Intact	
			Recurrence	Astrocytoma (II)				Methylated	R132H	Intact	TP53, ATRX
07	Male	30	Initial tumor	Astrocytoma (II)	105	XRT (1)	148	Unknown	R132H	Intact	TP53, ATRX
			Recurrence	Astrocytoma (II)				Unknown	R132H	Intact	TP53, ATRX
08	Male	44	Initial tumor	Oligoastrocytoma (II)	40	None	103	Unknown	R132H	Intact	TP53, ATRX
			Recurrence	Glioblastoma (IV)				Unknown	R132H	19q deletion	TP53, ATRX
09	Male	28	Initial tumor	Astrocytoma (II)	35	XRT (1)	45	Methylated	R132H	Intact	TP53
			Recurrence	Glioblastoma (IV)				Methylated	R132H	Intact	TP53
10	Female	41	Initial tumor	Astrocytoma (II)	25	TMZ (9)	44	Methylated	R132H	Intact	TP53, ATRX
			Recurrence	Glioblastoma (IV)				Methylated	R132H	Intact	TP53, ATRX
11	Female	30	Initial tumor	Oligoastrocytoma (II)	132	XRT (1), TMZ (26)	186	Methylated	R132H	Intact	TP53, ATRX
			Recurrence	Oligoastrocytoma (II)				Methylated	R132H	Intact	TP53, ATRX
12	Male	35	Initial tumor	Astrocytoma (II)	17	None	82 ¶	Unknown	R132H	Intact	TP53, ATRX
			Recurrence	Anaplastic astrocytoma (III)				Unknown	R132H	Intact	TP53, ATRX
13	Male	24	Initial tumor	Oligoastrocytoma (II)	21	None	106	Un-methylated	R132G	Intact	TP53, ATRX
			Recurrence	Oligoastrocytoma (II)				Un-methylated	R132G	Intact	TP53, ATRX
15	Female	38	Initial tumor	Oligoastrocytoma (II)	119	None	143 ¶	Unknown	R132H	Co-deletion	
			Recurrence	Oligoastrocytoma (II)				Unknown	R132H	Co-deletion	CIC
16	Female	35	Initial tumor	Astrocytoma (II)	5 †	None	38	Methylated	R132H	Intact	TP53, ATRX
			Recurrence	Astrocytoma (II)				Methylated	R132H	Intact	TP53, ATRX

17	Male	27	Initial tumor	Oligodendroglioma (II)	30	TMZ (12)	59 ¶	Methylated	R132H	Intact	TP53, ATRX
			Recurrence	Glioblastoma (IV)				Un-methylated	R132H	Intact	TP53, ATRX
18	Male	49	Initial tumor	Oligoastrocytoma (II)	94	TMZ (11)	106 ¶	Methylated	R132H	Intact	TP53, ATRX
			Recurrence	Glioblastoma (IV)				Methylated	R132H	Intact	TP53, ATRX
21	Male	27	Initial tumor	Oligoastrocytoma (II)	21	TMZ (12)	35	Methylated	R132H	19q deletion	TP53, ATRX
			Recurrence	Glioblastoma (IV)				Methylated	R132H	Intact	TP53, ATRX
24	Male	34	Initial tumor	Astrocytoma (II)	88	XRT (1)	109	Un-methylated	R132H	Intact	TP53, ATRX
			Recurrence 1	Astrocytoma (II)	14	TMZ (12)		Un-methylated	R132H	Intact	TP53, ATRX
			Recurrence 2	Glioblastoma (IV)				Methylated	R132H	Intact	TP53, ATRX
25	Male	39	Initial tumor	Astrocytoma (II)	14	None	42 ¶	Methylated	R132H	Intact	ATRX
			Recurrence	Glioblastoma (IV)				Methylated	R132H	Intact	ATRX
26	Female	36	Initial tumor	Astrocytoma (II)	15	None	47 ¶	Methylated	R132H	Intact	TP53, ATRX
			Recurrence	Anaplastic astrocytoma (III)				Methylated	R132H	Intact	TP53, ATRX
27	Male	56	Initial tumor	Astrocytoma (II)	12	None	54 ¶	Methylated	R132H	Intact	TP53, ATRX
			Recurrence	Anaplastic astrocytoma (III)				Methylated	R132H	Intact	TP53, ATRX
28	Male	30	Initial tumor	Astrocytoma (II)	85	None	137 ¶	Methylated	R132H	19q deletion	TP53, ATRX
			Recurrence	Anaplastic astrocytoma (III)				Methylated	R132H	19q deletion	TP53, ATRX
29	Male	52	Initial tumor	Astrocytoma (II)	57	None	109	Methylated	R132H	Intact	TP53, ATRX
			Recurrence	Anaplastic astrocytoma (III)				Methylated	R132H	Intact	TP53, ATRX

* Non-silent mutations

† Recurrent surgery for residual disease, no evidence of radiographic progression

‡ Including a month each of TMZ plus either Accutane or Thalidomide

§ Patient received TMZ prior to initial resection only

|| Patient lost to follow-up

¶ Patient alive

Table 2.1 Clinical summaries of all patients. Summary of the clinical features, treatment history and molecular features of each tumor in the cohort.

TABLE 2.2

Patient ID	Sample Type	Aligned Reads	Percent Duplication	Agilent SureSelect Bait Set	PF Unique Reads Aligned	Mean Target Coverage	Percent Targets Zero Coverage	Percent Target Bases 30X Coverage
Patient01	Normal	164189752	0.52	Human All Exon 50mb	73268999	55.18	0.0440	0.65
Patient01	Initial	123191094	0.36	Human All Exon 50mb	71631056	55.03	0.0406	0.68
Patient01	Recurrence	152187820	0.40	Human All Exon 50mb	84006557	65.83	0.0380	0.73
Patient02	Normal	155497580	0.30	Human All Exon 50mb	100712175	64.57	0.0380	0.72
Patient02	Initial	130362234	0.44	Human All Exon 50mb	67316662	52.85	0.0473	0.63
Patient02	Recurrence	175262920	0.39	Human All Exon 50mb	98664035	79.45	0.0382	0.77
Patient04	Normal	369017302	0.65	Human All Exon 50mb	122144743	87.52	0.0294	0.86
Patient04	Initial	423149028	0.62	Human All Exon 50mb	149033959	108.56	0.0292	0.87
Patient04	Recurrence 1	388829972	0.50	Human All Exon 50mb	179237717	127.44	0.0297	0.86
Patient04	Recurrence 2	422622590	0.72	Human All Exon 50mb	109327464	76.52	0.0329	0.80
Patient04	Recurrence 3	411818172	0.56	Human All Exon 50mb	169340111	115.41	0.0289	0.86
Patient05	Normal	105960550	0.26	Human All Exon 50mb	72679670	62.00	0.0408	0.73
Patient05	Initial	115647024	0.44	Human All Exon 50mb	59514886	48.41	0.0734	0.52
Patient05	Recurrence	209762250	0.35	Human All Exon 50mb	123714928	105.95	0.0287	0.87
Patient06	Normal	122123454	0.42	Human All Exon 50mb	65149273	52.82	0.0576	0.59
Patient06	Initial	126528998	0.54	Human All Exon 50mb	53462276	45.65	0.0762	0.52
Patient06	Recurrence	112361636	0.41	Human All Exon 50mb	60725056	50.79	0.0655	0.55
Patient07	Normal	400920082	0.65	Human All Exon 50mb	130504743	92.45	0.0296	0.85
Patient07	Initial	398488840	0.48	Human All Exon 50mb	186969969	147.14	0.0271	0.89
Patient07	Recurrence	397446092	0.52	Human All Exon 50mb	172359540	134.21	0.0287	0.88
Patient08	Normal	378004132	0.58	Human All Exon 50mb	148134183	112.71	0.0285	0.87
Patient08	Initial	348591182	0.72	Human All Exon 50mb	91902268	64.63	0.0305	0.81
Patient08	Recurrence	384059252	0.57	Human All Exon 50mb	155227207	104.78	0.0298	0.84
Patient09	Normal	265686178	0.60	Human All Exon 50mb	99001945	76.37	0.0318	0.82
Patient09	Initial	368731284	0.72	Human All Exon 50mb	97645482	67.45	0.0310	0.80
Patient09	Recurrence	446906980	0.59	Human All Exon 50mb	171222128	112.72	0.0275	0.88
Patient10	Normal	386974478	0.57	Human All Exon 50mb	153915240	117.04	0.0303	0.88
Patient10	Initial	363569212	0.74	Human All Exon 50mb	89113474	56.05	0.0338	0.76
Patient10	Recurrence	349262384	0.53	Human All Exon 50mb	152272606	119.87	0.0302	0.88
Patient11	Normal	332902458	0.55	Human All Exon 50mb	139043307	105.76	0.0325	0.84

Patient11	Initial	437288102	0.61	Human All Exon 50mb	160052465	104.97	0.0315	0.86
Patient11	Recurrence	464429120	0.60	Human All Exon 50mb	174826967	111.94	0.0292	0.87
Patient12	Normal	399729530	0.59	Human All Exon 50mb	149009736	109.53	0.0278	0.87
Patient12	Initial	404170618	0.51	Human All Exon 50mb	181316672	141.54	0.0407	0.85
Patient12	Recurrence	396288996	0.51	Human All Exon 50mb	176766260	143.55	0.0282	0.89
Patient13	Normal	428823802	0.62	Human All Exon 50mb	149462438	112.50	0.0279	0.89
Patient13	Initial	375900864	0.57	Human All Exon 50mb	151991452	109.46	0.0290	0.86
Patient13	Recurrence	395698014	0.64	Human All Exon 50mb	133988496	102.04	0.0296	0.87
Patient15	Normal	356565546	0.69	Human All Exon 50mb	101923977	70.57	0.0322	0.83
Patient15	Initial	361842770	0.50	Human All Exon 50mb	170167006	122.04	0.0296	0.87
Patient15	Recurrence	324249284	0.66	Human All Exon 50mb	103127635	83.20	0.0334	0.82
Patient16	Normal	413818772	0.60	Human All Exon 50mb	153920547	103.69	0.0442	0.84
Patient16	Initial	366868764	0.68	Human All Exon 50mb	111294559	72.80	0.0323	0.83
Patient16	Recurrence	374388258	0.69	Human All Exon 50mb	108358244	75.66	0.0356	0.80
Patient17	Normal	410213150	0.62	Human All Exon 50mb	143137416	120.30	0.0294	0.86
Patient17	Initial A	432939976	0.50	Human All Exon 50mb	197954550	149.50	0.0283	0.88
Patient17	Initial B	282682304	0.34	Human All Exon 50mb	172706817	155.02	0.0294	0.88
Patient17	Initial C	262086408	0.34	Human All Exon 50mb	160023188	147.40	0.0299	0.87
Patient17	Recurrence A	434106670	0.55	Human All Exon 50mb	181195751	151.37	0.0287	0.88
Patient17	Recurrence B	221369134	0.26	Human All Exon 50mb	149300799	132.72	0.0286	0.87
Patient17	Recurrence C	212469564	0.19	Human All Exon 50mb	157206847	124.38	0.0277	0.86
Patient17	Recurrence D	192665284	0.15	Human All Exon 50mb	150388708	125.24	0.0283	0.86
Patient18	Normal	377796074	0.56	Human All Exon 50mb	156092218	135.47	0.0294	0.88
Patient18	Initial A	431458900	0.63	Human All Exon 50mb	148164517	120.08	0.0290	0.87
Patient18	Initial B	183170435	0.17	Human All Exon 50mb	139028086	125.30	0.0303	0.86
Patient18	Initial C	222901260	0.22	Human All Exon 50mb	159192535	143.28	0.0302	0.87
Patient18	Initial D	224755464	0.14	Human All Exon 50mb	178164963	162.41	0.0296	0.87
Patient18	Recurrence	413777728	0.56	Human All Exon 50mb	166488017	147.02	0.0288	0.88
Patient21	Normal	236557208	0.14	Human All Exon 50mb	185759526	157.45	0.0272	0.88
Patient21	Initial	232154134	0.40	Human All Exon 50mb	128220620	116.32	0.0299	0.85
Patient21	Recurrence	219025678	0.20	Human All Exon 50mb	160524299	142.22	0.0294	0.87
Patient24	Normal	291504104	0.32	Human All Exon 50mb	194079378	181.33	0.0511	0.85
Patient24	Initial	222865850	0.22	Human All Exon 50mb	171015094	160.38	0.0509	0.84
Patient24	Recurrence 1	239585468	0.14	Human All Exon 50mb	203306203	188.47	0.0478	0.86

Patient24	Recurrence 2	206208472	0.23	Human All Exon 50mb	155461755	146.81	0.0537	0.83
Patient25	Normal	263944886	0.15	Human All Exon 50mb	220616782	198.89	0.0440	0.86
Patient25	Initial	272637310	0.16	Human All Exon 50mb	226300494	208.45	0.0459	0.87
Patient25	Recurrence	278331906	0.19	Human All Exon 50mb	220670256	205.99	0.0478	0.85
Patient26	Normal	235450112	0.26	Human All Exon 50mb	170904446	164.20	0.0564	0.85
Patient26	Initial A	252423160	0.22	Human All Exon 50mb	192962251	176.03	0.0483	0.85
Patient26	Initial B	202072954	0.09	Human All Exon 50mb	182046280	156.63	0.0529	0.84
Patient26	Recurrence A	297876622	0.17	Human All Exon 50mb	243072156	230.40	0.0492	0.88
Patient26	Recurrence B	146455804	0.10	Human All Exon 50mb	130989039	114.68	0.0592	0.79
Patient27	Normal	276349302	0.28	Human All Exon 50mb	197384884	192.76	0.0527	0.86
Patient27	Initial A	274051470	0.28	Human All Exon 50mb	194508972	183.82	0.0514	0.86
Patient27	Initial B	129212828	0.08	Human All Exon 50mb	117837436	103.57	0.0582	0.77
Patient27	Recurrence A	237800232	0.26	Human All Exon 50mb	174652244	169.53	0.0546	0.84
Patient27	Recurrence B	175012226	0.09	Human All Exon 50mb	157511203	136.02	0.0529	0.81
Patient28	Normal	242922762	0.23	Human All Exon 50mb	183537404	172.10	0.0516	0.85
Patient28	Initial	279674136	0.28	Human All Exon 50mb	197100039	186.75	0.0503	0.86
Patient28	Recurrence	261646218	0.17	Human All Exon 50mb	212857278	212.54	0.0514	0.85
Patient29	Normal	302528350	0.33	Human All Exon 50mb	198828704	186.87	0.0507	0.86
Patient29	Initial	261084924	0.23	Human All Exon 50mb	196936334	185.18	0.0519	0.86
Patient29	Recurrence	318538994	0.14	Human All Exon 50mb	270007841	247.57	0.0443	0.88
Patient24	Normal	291504104	0.32	Human All Exon V4	194079378	206.67	0.0004	0.97
Patient24	Initial	222865850	0.22	Human All Exon V4	171015094	182.73	0.0004	0.96
Patient24	Recurrence 1	239585468	0.14	Human All Exon V4	203306203	215.22	0.0003	0.97
Patient24	Recurrence 2	206208472	0.23	Human All Exon V4	155461755	166.69	0.0005	0.95
Patient25	Normal	263944886	0.15	Human All Exon V4	220616782	227.72	0.0004	0.98
Patient25	Initial	272637310	0.16	Human All Exon V4	226300494	238.18	0.0003	0.98
Patient25	Recurrence	278331906	0.19	Human All Exon V4	220670256	235.59	0.0004	0.97
Patient26	Normal	235450112	0.26	Human All Exon V4	170904446	185.27	0.0016	0.96
Patient26	Initial A	252423160	0.22	Human All Exon V4	192962251	200.94	0.0015	0.97
Patient26	Initial B	202072954	0.09	Human All Exon V4	182046280	177.99	0.0017	0.96
Patient26	Recurrence A	297876622	0.17	Human All Exon V4	243072156	262.40	0.0014	0.98
Patient26	Recurrence B	146455804	0.10	Human All Exon V4	130989039	130.12	0.0019	0.92
Patient27	Normal	276349302	0.28	Human All Exon V4	197384884	219.61	0.0005	0.97
Patient27	Initial A	274051470	0.28	Human All Exon V4	194508972	208.77	0.0005	0.97

Patient27	Initial B	129212828	0.08	Human All Exon V4	117837436	117.06	0.0009	0.90
Patient27	Recurrence A	237800232	0.26	Human All Exon V4	174652244	192.07	0.0005	0.96
Patient27	Recurrence B	175012226	0.09	Human All Exon V4	157511203	154.88	0.0006	0.94
Patient28	Normal	242922762	0.23	Human All Exon V4	183537404	195.17	0.0004	0.97
Patient28	Initial	279674136	0.28	Human All Exon V4	197100039	212.96	0.0003	0.97
Patient28	Recurrence	261646218	0.17	Human All Exon V4	212857278	244.10	0.0003	0.97
Patient29	Normal	302528350	0.33	Human All Exon V4	198828704	212.74	0.0004	0.97
Patient29	Initial	261084924	0.23	Human All Exon V4	196936334	210.95	0.0003	0.97
Patient29	Recurrence	318538994	0.14	Human All Exon V4	270007841	283.59	0.0003	0.98

Table 2.2 Quality control metrics for exomes sequenced in this study. For comparison, quality control metrics for patients 24-29 are presented for both SureSelect bait sets.

TABLE 2.3

Patient ID	Total mutations in initial tumor	Mutations shared with recurrence	Percent shared	Major pattern of genetic evolution
Patient17	18	1	6%	branched
Patient05	36	6	17%	branched
Patient06	4	1	25%	branched
Patient07	126	44	35%	intermediate
Patient18	66	25	38%	intermediate
Patient12	22	10	45%	intermediate
Patient24	13	6	46%	intermediate
Patient25	46	22	48%	intermediate
Patient13	30	15	50%	intermediate
Patient15	26	13	50%	intermediate
Patient04	17	9	53%	intermediate
Patient01	48	26	54%	intermediate
Patient16	36	20	56%	intermediate
Patient21	27	15	56%	intermediate
Patient29	43	27	63%	intermediate
Patient02	26	17	65%	intermediate
Patient11	27	19	70%	intermediate
Patient08	24	17	71%	intermediate
Patient10	36	26	72%	intermediate
Patient28	20	15	75%	linear
Patient09	9	7	78%	linear
Patient26	27	23	85%	linear
Patient27	36	31	86%	linear

Table 2.3 Patterns of genetic evolution between initial and recurrent gliomas. The number of mutations identified in the initial tumor, the number and percent of those shared with the recurrence, and the major pattern of genetic evolution inferred.

TABLE 2.4

Gene	Contig	Position	Nucleotide	Protein	Patient	Tree branch	COSMIC gene frequency
CAND2	chr3	12858462	C2031T	D677D	04	Initial	10
OR10V1	chr11	59480502	C817T	R273W	04	Initial	1
RYR1	chr19	38939100	C906T	D302D	04	Initial	37
SGK223	chr8	8234869	c.1050_1051insAGCGGC	p.G350delinsGAA	04	Initial	0
TERF2IP	chr16	75690462	T1153C	F385L	04	Initial	1
TERF2IP	chr16	75690302	A993C	T331T	04	Initial	1
WDFY4	chr10	50004488	A4403G	N1468S	04	Initial	6
PSAPL1	chr4	7435803	C804T	A268A	04	Initial, Recurrence1	0
ACSF2	chr17	48541208	T1076G	M359R	04	Initial, Recurrence1-3	1
BOD1L	chr4	13604659	G3865A	V1289I	04	Initial, Recurrence1-3	11
CDH7	chr18	63481815	G600A	P200P	04	Initial, Recurrence1-3	13
IDH1	chr2	209113113	C394T	R132C	04	Initial, Recurrence1-3	3554
SLC9A4	chr2	103148842	C2092T	R698W	04	Initial, Recurrence1-3	7
TEAD3	chr6	35454288	C152T	P51L	04	Initial, Recurrence1-3	1
TP53	chr17	7577538	G347A	R116Q	04	Initial, Recurrence1-3	22675
ZNF107	chr7	64167377	C695G	T232S	04	Initial, Recurrence1-3	2
ADAM17	chr2	9630335	C2446T	R816C	04	Recurrence1	4
ADAM29	chr4	175898766	T2090A	L697H	04	Recurrence1	33
APOPT1	chr14	104040439	c.361_382AAGGAAAAAGAAGAATTTTTTAACC	NA	04	Recurrence1	0
ATXN2L	chr16	28840741	A761G	N254S	04	Recurrence1	5
C5orf54	chr5	159822214	C284T	S95L	04	Recurrence1	2
C6orf201	chr6	4087953	G78C	K26N	04	Recurrence1	0
CYP2C9	chr10	96702051	T434C	V145A	04	Recurrence1	9
DEFB126	chr20	126310	c.313_314del	p.105_105del	04	Recurrence1	0
FAM206A	chr9	111701942	T522C	I174I	04	Recurrence1	0
FUT11	chr10	75532510	A419G	Q140R	04	Recurrence1	0
HEY2	chr6	126080810	C876T	N292N	04	Recurrence1	1
KIAA1731	chr11	93432660	G4582C	E1528Q	04	Recurrence1	0
KRT83	chr12	52711478	G737A	R246Q	04	Recurrence1	9
LSG1	chr3	194369475	C1478T	T493M	04	Recurrence1	2
MACF1	chr1	39934319	T15609C	R5203R	04	Recurrence1	35
MGAT4C	chr12	86373731	G773C	G258A	04	Recurrence1	7
MRPL55	chr1	228295410	A295C	T99P	04	Recurrence1	1
MRPS6	chr21	35514779	T257C	I86T	04	Recurrence1	2
MUC16	chr19	9070009	G17437T	E5813X	04	Recurrence1	99
OR10T2	chr1	158368385	G872T	S291I	04	Recurrence1	5
PDZD2	chr5	32087897	A4343G	D1448G	04	Recurrence1	24
RAP1GAP2	chr17	2909313	C1337T	S446L	04	Recurrence1	2
RIMBP2	chr12	130926571	C1275T	N425N	04	Recurrence1	16
SPATA6	chr1	48764545	G1307C	G436A	04	Recurrence1	3
TDG	chr12	104373729	c.287_288insA	p.E96fs	04	Recurrence1	10
APOBEC4	chr1	183617696	C221G	S74C	04	Recurrence2-3	3
CFH	chr1	196694259	T1705C	C569R	04	Recurrence2-3	13
CLASP1	chr2	122182732	C2195G	P732R	04	Recurrence2-3	4
COL13A1	chr10	71684757	C1224T	G408G	04	Recurrence2-3	1
DPYSL4	chr10	134006219	C186G	G62G	04	Recurrence2-3	4
GABRE	chrX	151123975	C1002T	V334V	04	Recurrence2-3	2
GPR112	chrX	135453557	G7467T	E2489D	04	Recurrence2-3	22
GULP1	chr2	189449083	G701A	R234H	04	Recurrence2-3	3
LAMA3	chr18	21484018	G6272T	R2091L	04	Recurrence2-3	18
PHRF1	chr11	587424	C380G	A127G	04	Recurrence2-3	0

74

PSAP	chr10	73579333	c.1248_1249insCAAG	p.K416fs	04	Recurrence2-3	2
SLCO1B7	chr12	21200142	c.985delT	p.F329fs	04	Recurrence2-3	2
SNRPB	chr20	2443747	G547A	A183T	04	Recurrence2-3	2
SPIRE1	chr18	12449679	C1827G	P609P	04	Recurrence2-3	1
UBQLNL	chr11	5536309	C1363G	Q455E	04	Recurrence2-3	6
WDR72	chr15	54004993	G687A	L229L	04	Recurrence2-3	9
AKAP6	chr14	33242972	c.3461_3462insGCA	p.C1154delinsWH	04	Recurrence3	28
ARHGEF17	chr11	73076827	C5830T	L1944F	04	Recurrence3	2
ATXN3	chr14	92555132	c.252delT	p.G84fs	04	Recurrence3	1
C1orf124	chr1	231488849	c.1212_1214A	NA	04	Recurrence3	1
C5orf22	chr5	31541063	c.815_816del	p.272_272del	04	Recurrence3	3
C9orf84	chr9	114486071	NA	NA	04	Recurrence3	4
CASP10	chr2	202050641	c.141delC	p.V47fs	04	Recurrence3	7
CCR4	chr3	32994946	T32A	L11H	04	Recurrence3	4
CHRM1	chr11	62678364	C209G	A70G	04	Recurrence3	1
CNKSR3	chr6	154763244	G397A	A133T	04	Recurrence3	6
CRTC2	chr1	153921068	C1727T	P576L	04	Recurrence3	6
CUL9	chr6	43190286	c.6939_6949del	p.2313_2317del	04	Recurrence3	17
DDX60	chr4	169215051	T769C	S257P	04	Recurrence3	6
DGKI	chr7	137172402	A2336G	D779G	04	Recurrence3	7
DUOX1	chr15	45431646	c.1238_1241del	p.413_414del	04	Recurrence3	14
DYNC2H1	chr11	102984845	G380A	S127N	04	Recurrence3	3
DYNC2LI1	chr2	44021791	c.516delC	p.C172fs	04	Recurrence3	2
ERC1	chr12	1192504	c.844delT	p.F282fs	04	Recurrence3	9
FAM75D1	chr9	84606868	C1483A	H495N	04	Recurrence3	1
FIGNL1	chr7	50514933	A53T	Y18F	04	Recurrence3	4
FIGNL1	chr7	50514932	C54T	Y18Y	04	Recurrence3	4
GLMN	chr1	92713511	T1509C	N503N	04	Recurrence3	1
GRWD1	chr19	48955968	G1027A	G343S	04	Recurrence3	3
HMBOX1	chr8	28827573	A37C	M13L	04	Recurrence3	1
HPS4	chr22	26862199	G684T	Q228H	04	Recurrence3	2
HSP90AB1	chr6	44217180	A214G	K72E	04	Recurrence3	5
IK	chr5	140041897	c.1657delA	p.K553fs	04	Recurrence3	1
ITIH5L	chrX	54785050	T1457A	V486D	04	Recurrence3	12
KCTD16	chr5	143587110	NA	NA	04	Recurrence3	7
MBD4	chr3	129155548	c.939delA	p.K313fs	04	Recurrence3	4
MTTP	chr4	100521799	A1145G	K382R	04	Recurrence3	7
MUC5B	chr11	1253980	A2045G	D682G	04	Recurrence3	0
RFC3	chr13	34398063	c.235delA	p.K79fs	04	Recurrence3	0
SH3TC1	chr4	8242506	c.3835_3838del	p.1279_1280del	04	Recurrence3	7
SORCS1	chr10	108431048	c.2136delT	p.Y712X	04	Recurrence3	8
USP24	chr1	55591187	T3766C	L1256L	04	Recurrence3	18
WWC3	chrX	10046914	c.296delG	p.R99fs	04	Recurrence3	9
ZNF135	chr19	58579378	T1562C	L521P	04	Recurrence3	1
ZZEF1	chr17	3917753	C8202A	C2734X	04	Recurrence3	14
CD24	chrY	21154569	T27C	L9L	17	Initial A	0
MED20	chr6	41875026	NA	NA	17	Initial A	0
NOTCH4	chr6	32170335	C3273G	C1091W	17	Initial A	26
SLC4A3	chr2	220497665	T1292C	I431T	17	Initial A	7
SOX8	chr16	1035205	A1160G	Q387R	17	Initial A	2
ABCA10	chr17	67170804	A2992C	I998L	17	Initial A,B,C	9
ANKRD33	chr12	52283232	C198A	L66L	17	Initial A,B,C	2
ATRX	chrX	76937641	c.3103_3107del	p.1035_1036del	17	Initial A,B,C	36
C7orf10	chr7	40221586	T206G	L69X	17	Initial A,B,C	2
CD3EAP	chr19	45911872	c.646_647insA	p.K216fs	17	Initial A,B,C	5
CECR5	chr22	17619009	T1174C	C392R	17	Initial A,B,C	0
GPR128	chr3	100349558	G239C	C80S	17	Initial A,B,C	10
LRRC16B	chr14	24531921	C2572T	R858W	17	Initial A,B,C	12
RFX7	chr15	56385946	A3980G	N1327S	17	Initial A,B,C	1
TMEM131	chr2	98388775	C4433A	T1478K	17	Initial A,B,C	11
TP53	chr17	7578403	G131T	C44F	17	Initial A,B,C	22690

ZNF628	chr19	55993060	G488A	R163H	17	Initial A,B,C	0
IDH1	chr2	209113112	G395A	R132H	17	Initial A,B,C, Recurrence A,B,C,D	3554
ABCC9	chr12	21954093	C4535T	T1512M	17	Recurrence A,B,C,D	14
ADAMTSL1	chr9	18795416	c.3699delT	p.D1233fs	17	Recurrence A,B,C,D	7
ATP2B4	chr1	203677182	G1507T	A503S	17	Recurrence A,B,C,D	6
ATRX	chrX	76952141	c.287_294del	p.96_98del	17	Recurrence A,B,C,D	36
BCL11B	chr14	99641792	G1168A	D390N	17	Recurrence A,B,C,D	14
BRD4	chr19	15354224	C2656T	R886W	17	Recurrence A,B,C,D	2
CARD6	chr5	40852331	A897G	R299R	17	Recurrence A,B,C,D	7
CDHR3	chr7	105662691	G1873A	V625I	17	Recurrence A,B,C,D	1
CHORDC1	chr11	89943710	T429G	C143W	17	Recurrence A,B,C,D	0
CRTAP	chr3	33183903	A1169G	Y390C	17	Recurrence A,B,C,D	2
DIDO1	chr20	61513252	C4056T	D1352D	17	Recurrence A,B,C,D	21
FAT1	chr4	187518024	G12670A	A4224T	17	Recurrence A,B,C,D	27
HEPH	chrX	65409555	C1000A	P334T	17	Recurrence A,B,C,D	15
KIAA1383	chr1	232941658	T889G	S297A	17	Recurrence A,B,C,D	1
MDH1B	chr2	207621736	C299T	T100M	17	Recurrence A,B,C,D	6
MYO7B	chr2	128331590	G688A	A230T	17	Recurrence A,B,C,D	4
PIK3CA	chr3	178952085	A3140G	H1047R	17	Recurrence A,B,C,D	3709
RAD54B	chr8	95390425	G1946A	G649E	17	Recurrence A,B,C,D	6
SHISA9	chr16	13010641	C660T	N220N	17	Recurrence A,B,C,D	0
SHKBP1	chr19	41096697	G1830A	P610P	17	Recurrence A,B,C,D	6
SLC22A25	chr11	62951251	A869G	N290S	17	Recurrence A,B,C,D	6
SPAG17	chr1	118584652	A2828G	E943G	17	Recurrence A,B,C,D	13
TMEM63B	chr6	44122598	T2477C	I826T	17	Recurrence A,B,C,D	10
TP53	chr17	7578550	C380T	S127F	17	Recurrence A,B,C,D	22647
APLF	chr2	68765111	T912C	V304V	17	Recurrence A,C	3
ARNT	chr1	150795783	C1236A	F412L	17	Recurrence A,C	10
C19orf2	chr19	30503247	T1114C	S372P	17	Recurrence A,C	2
CLTC	chr17	57758404	A3051G	V1017V	17	Recurrence A,C	3
CUL4A	chr13	113889388	T777C	Y259Y	17	Recurrence A,C	4
GPR142	chr17	72363835	G191T	G64V	17	Recurrence A,C	4
HYAL4	chr7	123517035	A1272T	T424T	17	Recurrence A,C	6
IL23R	chr1	67724210	T1289C	V430A	17	Recurrence A,C	2
KCNK15	chr20	43379023	G537A	S179S	17	Recurrence A,C	2
SDAD1	chr4	76902575	A244G	K82E	17	Recurrence A,C	3
SPTLC1	chr9	94817753	T714C	T238T	17	Recurrence A,C	3
TNFSF9	chr19	6535032	G720T	V240V	17	Recurrence A,C	3
TSHB	chr1	115576706	C275A	A92D	17	Recurrence A,C	0
ZNF211	chr19	58152143	T289C	F97L	17	Recurrence A,C	4
ADAMTS3	chr4	73149155	A3316G	I1106V	17	Recurrence B,D	5
ASCC2	chr22	30198032	A1519T	N507Y	17	Recurrence B,D	0
AXL	chr19	41727930	T555C	G185G	17	Recurrence B,D	15
BRIP1	chr17	59876511	A1290G	I430M	17	Recurrence B,D	5
DNM1L	chr12	32861097	A308G	D103G	17	Recurrence B,D	2
ECI2	chr6	4133876	G30A	Q10Q	17	Recurrence B,D	1
FANCA	chr16	89862354	T966C	H322H	17	Recurrence B,D	9
FAT1	chr4	187531037	A9986G	N3329S	17	Recurrence B,D	27
FLAD1	chr1	154962825	C1084A	Q362K	17	Recurrence B,D	4
GORAB	chr1	170521320	T902C	V301A	17	Recurrence B,D	1
KAT6B	chr10	76790463	A5881G	M1961V	17	Recurrence B,D	0
MACC1	chr7	20199790	A194G	N65S	17	Recurrence B,D	6
MBD6	chr12	57921732	c.2338delG	p.G780fs	17	Recurrence B,D	4
PRKCH	chr14	61788905	T86C	L29P	17	Recurrence B,D	10
RGPD2	chr2	88125234	G15G	K5K	17	Recurrence B,D	0
SORCS2	chr4	7691261	G1537A	V513I	17	Recurrence B,D	7
SOX6	chr11	16068204	G1518A	Q506Q	17	Recurrence B,D	3
SP6	chr17	45924768	C1028T	A343V	17	Recurrence B,D	1
TLN2	chr15	63047743	G4489A	A1497T	17	Recurrence B,D	20
TMEM40	chr3	12779654	A405G	R135R	17	Recurrence B,D	0

TMPRSS11B	chr4	69095151	T770G	I257S	17	Recurrence B,D	1
TTN	chr2	179641275	T5316C	S1772S	17	Recurrence B,D	207
UGT3A1	chr5	35965819	G512T	G171V	17	Recurrence B,D	4
WFDC12	chr20	43752784	T202C	F68L	17	Recurrence B,D	0
FGFBP1	chr4	15937919	T337C	W113R	17	Recurrence D	0
PLEKHG1	chr6	151151933	C1686T	F562F	17	Recurrence D	6

Table 2.4 Mutations placed in phylogenetic trees. A list of all mutations included in the phylogenetic trees in Figure 2.8 and 2.12, and the phylogenetic tree branch on which each mutation lies.

TABLE 2.5

Patient ID	Sample Type	CpA	CpT	CpG	CpC	ApA	ApT	ApG	ApC	Overall
Patient01	Initial	1.41	0.72	6.19	3.24	1.09	0.65	1.44	2.09	1.73
Patient01	Recurrence	42.74	135.31	51.39	261.99	1.89	2.57	1.88	6.49	67.39
Patient02	Initial	0.49	0.50	6.88	1.45	0.56	0.67	0.25	0.73	0.93
Patient02	Recurrence	0.44	0.45	9.00	0.50	0.27	0.63	0.00	0.33	0.80
Patient04	Initial	0.41	0.21	4.64	0.00	0.00	0.92	0.21	0.00	0.49
Patient04	Recurrence 1	0.63	0.85	7.14	0.45	0.26	0.92	0.43	1.25	1.01
Patient04	Recurrence 2	1.07	1.31	4.41	0.70	0.00	0.62	0.00	0.32	0.80
Patient04	Recurrence 3	1.46	2.56	4.76	1.14	0.52	1.84	0.43	1.87	1.57
Patient05	Initial	2.01	0.89	9.20	0.74	0.30	1.09	0.59	3.81	1.57
Patient05	Recurrence	42.99	148.61	89.35	233.83	2.62	6.50	2.82	8.56	70.12
Patient06	Initial	0.00	0.00	3.52	0.00	0.30	0.00	0.00	0.00	0.18
Patient06	Recurrence	0.82	0.85	5.26	0.69	0.00	1.06	0.56	0.81	0.86
Patient07	Initial	2.68	4.20	9.74	2.44	0.78	2.13	2.94	8.30	3.61
Patient07	Recurrence	3.53	3.80	11.11	4.26	2.33	1.83	3.17	11.45	4.54
Patient08	Initial	0.42	1.08	3.72	0.00	0.78	0.31	0.43	0.32	0.66
Patient08	Recurrence	2.52	2.14	9.65	1.60	0.78	1.54	0.86	0.94	1.97
Patient09	Initial	0.21	0.00	1.26	0.47	0.26	0.31	0.43	0.00	0.30
Patient09	Recurrence	1.25	2.33	4.09	1.12	1.04	0.31	1.27	0.93	1.40
Patient10	Initial	0.65	0.44	11.51	0.24	0.79	1.24	0.44	0.64	1.18
Patient10	Recurrence	46.29	185.65	82.49	339.40	1.55	2.75	2.31	3.08	90.87
Patient11	Initial	0.42	0.21	5.91	0.90	0.26	0.61	1.06	0.31	0.85
Patient11	Recurrence	0.63	0.00	6.45	1.80	0.52	0.92	1.27	0.31	1.11
Patient12	Initial	0.43	0.22	4.02	0.48	0.00	0.62	0.44	0.96	0.61
Patient12	Recurrence	0.41	0.00	7.48	0.89	0.26	1.22	0.21	0.31	0.84
Patient13	Initial	0.21	0.63	3.50	0.67	0.00	0.61	0.00	0.62	0.55
Patient13	Recurrence	0.62	0.84	5.20	0.89	0.00	0.92	0.21	0.00	0.78
Patient15	Initial	0.42	0.42	6.99	0.90	0.26	0.00	0.21	0.31	0.75
Patient15	Recurrence	0.42	1.08	8.01	1.16	0.26	1.24	0.65	0.95	1.20
Patient16	Initial	0.21	0.22	8.89	0.94	0.79	1.24	0.65	0.95	1.10
Patient16	Recurrence	0.22	1.10	10.48	0.96	0.79	0.93	1.32	0.64	1.35
Patient17	Initial A	0.83	0.21	2.31	0.22	0.52	1.22	0.21	0.00	0.55
Patient17	Initial B	0.83	0.00	1.72	0.22	0.52	0.92	0.21	0.00	0.45
Patient17	Initial C	0.83	0.21	2.30	0.00	0.26	0.92	0.00	0.00	0.42
Patient17	Recurrence A	0.62	0.63	6.35	1.34	1.03	1.53	1.05	1.54	1.36
Patient17	Recurrence B	0.62	0.84	7.46	1.56	0.52	2.75	1.48	1.85	1.65
Patient17	Recurrence C	0.62	0.64	5.79	1.12	0.52	1.23	0.63	1.55	1.14
Patient17	Recurrence D	0.62	0.84	7.47	1.12	0.78	2.75	1.27	1.54	1.55
Patient18	Initial A	2.71	1.70	4.11	1.58	1.56	3.06	1.69	0.93	2.02
Patient18	Initial B	2.50	1.91	5.84	1.81	1.56	2.76	0.42	1.55	1.99
Patient18	Initial C	2.28	1.69	5.79	1.35	1.56	3.98	1.90	0.93	2.14
Patient18	Initial D	2.28	1.69	4.02	1.12	1.55	3.05	1.47	0.92	1.84
Patient18	Recurrence	53.69	176.51	77.24	290.79	1.29	5.19	3.57	4.61	83.78
Patient21	Initial	0.83	1.06	4.07	1.13	0.26	0.00	0.00	0.62	0.78
Patient21	Recurrence	31.22	69.48	35.95	91.67	0.26	2.14	2.31	4.31	31.94

Patient24	Initial	0.21	0.21	1.55	0.64	0.00	0.31	0.21	0.00	0.32
Patient24	Recurrence 1	0.20	0.62	4.11	0.64	0.26	0.31	0.21	0.31	0.60
Patient24	Recurrence 2	47.58	171.75	55.34	278.01	0.79	3.11	1.68	4.32	79.54
Patient25	Initial	1.23	0.62	6.15	1.06	0.79	0.93	0.21	0.91	1.14
Patient25	Recurrence	1.64	2.08	16.00	2.56	1.05	1.55	1.46	0.61	2.52
Patient26	Initial A	0.41	0.42	3.61	0.21	0.53	1.55	0.83	0.31	0.76
Patient26	Initial B	0.41	0.21	3.65	0.22	0.53	1.24	1.26	1.54	0.90
Patient26	Recurrence A	0.82	0.62	6.14	0.64	1.05	1.23	1.04	0.61	1.17
Patient26	Recurrence B	0.63	0.21	5.90	0.44	0.53	0.94	1.28	1.88	1.11
Patient27	Initial A	0.82	0.62	5.66	0.85	0.52	0.93	0.42	1.22	1.05
Patient27	Initial B	1.48	0.86	7.57	2.00	0.80	0.95	0.43	1.26	1.51
Patient27	Recurrence A	1.03	1.04	6.21	1.71	0.79	0.93	1.04	1.23	1.44
Patient27	Recurrence B	0.83	0.85	5.27	1.52	0.79	0.94	0.63	1.55	1.26
Patient28	Initial	0.00	0.00	2.57	1.07	0.26	0.93	0.42	0.31	0.54
Patient28	Recurrence	0.00	0.63	4.65	0.86	0.79	0.62	0.83	0.00	0.80
Patient29	Initial	1.03	0.83	8.76	0.85	0.26	1.24	0.00	1.22	1.24
Patient29	Recurrence	1.22	1.03	6.65	1.06	0.52	0.62	0.62	0.91	1.23

Table 2.5 Overall and dinucleotide-specific mutation rates. Mutation rates in each tumor at each dinucleotide context and overall in the exome. Mutation rates are given in number of mutations/Mb of sequence.

TABLE 2.6

Patient ID	Mutation	Additional initial tumor pieces	Mutational Status
Patient01	MTOR S2215F	6	Absent
Patient01	ERBB2 D989N	6	Absent
Patient01	RB1 c.2520+1G>A	6	Absent
Patient01	NF1 T685I	6	Absent
Patient05	CDK4 K84N	6	Absent
Patient05	CDK6 D311N	6	Absent
Patient05	CDKN2A P114L	6	Absent
Patient10	CDKN2A P114L	3	Absent
Patient10	TSC1 E646K	3	Absent
Patient18	NF1 L1475F	3	Absent
Patient18	NF1 T1951I	3	Absent
Patient18	PIK3CA E542K	3	Absent

Table 2.6 Sanger sequencing results of TMZ-associated mutations.

CHAPTER 3.

MATERIALS AND METHODS

3.1 SAMPLE ACQUISITION

All initial and recurrent tumor samples were collected during surgical resection and were either snap frozen in liquid nitrogen and stored at -80° C, or were formalin fixed and paraffin embedded (FFPE). In cases where more than one sample from a tumor was investigated, those samples were independent, geographically distinct pieces derived from multiple time points during surgery. Two neuropathologists independently confirmed the clinical diagnosis from H&E-stained smear preparations or FFPE tissues prior to library construction. Patient-matched normal samples were peripheral blood mononuclear cells or muscle tissue. Samples from patients 01-21 were obtained from the Neurosurgery Tissue Bank at the University of California San Francisco (UCSF). Sample use was approved by the Committee on Human Research at UCSF and research was approved by the institutional review board at UCSF. Samples from patients 24-29 were collected at the University of Tokyo hospital and the study was approved by the Ethics Committee of the University of Tokyo. All patients provided informed written consent. Snap frozen normal human post-mortem brain tissue from two males (55 and 56 years of age respectively) was obtained from the National Disease Research Interchange (NDRI) and frontal cerebral cortex gray matter was macrodissected.

3.2 RADIOLOGIC ANALYSIS

Magnetic resonance imaging was acquired from the electronic radiology archives at UCSF. T1- and T2-weighted images representative of the tumor region were obtained from pre-surgical and post-surgical scans performed at either UCSF or outside

institutions. T1-weighted images were acquired from a spoiled gradient echo (SPGR) pulse sequence after an injection of a paramagnetic gadolinium contrast agent. T2-weighted imaging was acquired from a fluid attenuated inversion recovery (FLAIR) sequence when available, and a standard fast spin echo (FSE) sequence when unavailable.

3.3 DNA AND RNA ISOLATION

Genomic DNA was extracted with either a QIAGEN DNA extraction kit (Qiagen, Valencia, CA) following the manufacturer's instructions or isolated by PCI extraction. For PCI extraction, tissues were digested with 1mg/ml proteinase K in lysis buffer (50mM Tris, pH 8.0, 1mM EDTA pH 8.0, 0.5% SDS) overnight at 55C. After RNase treatment, DNA was phenol/chloroform extracted, precipitated with ethanol and resuspended in TE. For DNA extraction from FFPE, PCI extractions were preceded by xylene washes to remove paraffin. RNA was isolated with Trizol (Invitrogen, Carlsbad, CA, USA) according to manufacturer's instruction.

3.4 HYBRID CAPTURE AND SEQUENCING

Exome capture was performed using the Agilent SureSelect Target Enrichment System Protocol (Version 1.0, September 2009) according to manufacturer's protocol. The SureSelect Human All Exon 50Mb kit (Agilent Technologies) was used on samples from patients 01-21, and the SureSelect Human All Exon V4 kit (Agilent Technologies) was used on samples from patients 24-29. All sequencing reported here acquired paired-end reads of 76bp or 100bp in length from Illumina HiSeq 2000 and 2500 instrumentation.

3.5 EXOME ALIGNMENT AND MUTATION IDENTIFICATION

Paired-end sequencing data from exome capture libraries were aligned to the reference human genome (build hg19) with the Burrows-Wheeler Aligner (*134*). All sequenced and aligned libraries (uniquely aligned reads only) were further processed with both the Picard suite (http://picard.sourceforge.net/) and the Genome Analysis Toolkit (*135, 136*), including de-duplication, base quality recalibration, and multiple-sequence realignment, all performed prior to mutation detection. BAM files were coordinate-sorted and processed for both point mutations and small insertions and deletions (indels) less than 50bp in length. Single-nucleotide variants (SNVs) were detected with MuTect, a Bayesian framework for the detection of somatic mutations (*137*). SNVs with less than a 10% variant frequency in the tumor, with more than 5 variant reads in the patient-matched normal, or greater than a 10% variant frequency in the patient-matched normal were excluded from further analysis. Indels were detected with Pindel (*138*), and those with fewer than 6 supporting reads in the tumor, any supporting reads or less than 14 total reads in the patient-matched normal, and replacements for which the deletion and non-template inserted sequence were of the same length were excluded. If multiple indels were present at the same genomic coordinates, only the indel with the most supporting reads was retained. All indels and SNVs were annotated for their mutational context and effect using ANNOVAR (*139*). Only protein-coding or splice-site mutations were retained for further analysis. Mutations were additionally annotated for their presence in dbSNP (Build ID: 132) (http://www.ncbi.nlm.nih.gov/SNP/) or 1000Genomes (Phase 1, November 2010 release) (*140*) data sets.

In the original exomes from the initial and recurrent gliomas of patients 26 and 27, a total of 44 mutations were categorized as private. After the generation of additional exomes from distinct regions of each tumor, 3 mutations that were formerly private were now shared: 1 mutation in the recurrence of patient 26 and 2 mutations in the recurrence of patient 27 were called in the additional exomes of their patient-matched initial gliomas, for an overall misclassification rate of 3/44=7%.

3.6 IDENTIFICATION OF TMZ-ASSOCIATED MUTATIONS

TMZ-associated mutations were defined as C>T/G>A transition mutations at any CpN dinucleotide context which were unique to a TMZ-treated hypermutated recurrent tumor. To ensure this was a conservative determination, any TMZ-associated mutation identified in a recurrence that showed evidence of the alternate allele (1 or more reads of base quality greater than or equal to 20) in the patient-matched initial tumor (or first recurrent tumor for patient 24) or failed Sanger validation were not labeled candidate TMZ-associated mutations for the purposes of further analysis. Nevertheless, it is possible that a subset of candidate TMZ-associated mutations were misattributed as such, having existed in the initial tumor but were not identified from exome sequence data due to intratumoral heterogeneity. Therefore, we compared the TMZ-associated mutations identified in the recurrent tumor of patient 18 with exome sequencing data from three additional samples from geographically distinct regions of the initial tumor and from eight other non-patient matched initial tumor exomes with similar coverage (patients 04, 07, 12, 13, 15, 17, 24, and 26). The number of mutations that were

misattributed as TMZ-associated was small and did not vary significantly between the patient-matched (1.7±0.08%) and non-patient-matched (1.5±0.6%) comparisons (p-value = 0.5; Wilcoxon rank sum test).

3.7 TRANSCRIPTOME SEQUENCING

PolyA+ RNA was purified using the MACS mRNA isolation kit (Miltenyi Biotec, Bergisch Gladbach, Germany), from 2-4ug of total RNA as per the manufacturer's instructions. The process included on-column DNaseI treatment (Invitrogen). Following extraction, RNA integrity was measured on an Agilent bioanalyzer with a minimum RIN of 7 required before proceeding. cDNA was synthesized from the purified polyA+ RNA using the Superscript II Double-Stranded cDNA Synthesis kit (Invitrogen) and 200ng random hexamers (Invitrogen). After first strand synthesis, dNTPs were removed using 2 volumes of AMPure XP beads. Second strand synthesis was performed with the GeneAmp 12.5mM dNTPs blend (2.5mM dCTP, 2.5mM dGTP, 2.5mM dATP, 5.0mM dUTP) leading to the incorporation of dUTP in this strand only. Double stranded cDNA was purified using 2 volumes of Ampure XP beads, fragmented using Covaris E series shearing (Covaris Inc. Woburn, MA, USA; 20% duty cycle, Intensity 5, 55 seconds), and used for paired-end sequencing library preparation following indexed plate-based library construction (*141*) with the following modifications: ligation reaction was extended to 2h, just before library amplification uridine digestion was performed at 37°C for 30min following with 10min at 95°C in Qiagen Elution buffer (Qiagen Inc., Toronto, ON, Canada; 10mM Tris-Cl, pH 8.5) with 5 units of Uracil-N-Glycosylase (AmpErase UNG, Invitrogen). This leads to the selective degradation of the dUTP-marked second strand.

3.8 TRANSCRIPTOME SEQUENCING ANALYSIS

All transcriptome sequencing data from initial and recurrent tumor pairs were aligned with TopHat (v1.4.0) (*142*), with parameters –r30 –library-type fr-firststrand. To estimate transcript abundance, aligned data was processed with Cufflinks (v1.3.0) (*143*), with parameters –b hg19.fa –G refGene_HG19.gtf –library-type fr-firststrand. Alternative splicing was analyzed with ALEXA-seq (*144*). Gene set enrichment analysis (*145*) was performed using the MSigDB genetic and chemical perturbation gene sets (v3.0) of size 15-500, 1000 gene set permutations, the weighted enrichment statistic, and the log2 ratio of classes as the gene ranking metric.

3.9 VALIDATION OF MUTATIONS

Candidate mutations were validated with PCR amplification of genomic DNA followed by Sanger biochemistry according to conventional protocols. While most primers were designed with Primer3 (*146*), primers for the IDH1 mutation were taken from Christensen et al (*147*). All primer sequences are available upon request. PCR was performed using either the KOD-plus (TOYOBO) or Phusion (New England Biolabs) high-fidelity DNA polymerases under optimized thermal conditions. PCR products were evaluated on agarose gels and sequenced in both directions by Quintara Biosciences. Additional sequencing was performed using Big Dye Terminator reactions and subsequent loading on an ABI 3130xl capillary sequencer (Applied Biosystems).

To confirm mutations of interest as well as the large number of somatic mutations in the hypermutated recurrent tumors, we used Sanger sequencing and validated 50 of 51 randomly selected mutations and 213 of 291 targeted mutations, many of which were assayed for their likely false-positive status (table S3). To expand the number of loci assayed, we used available transcriptome sequencing data for the initial and recurrent tumors of eight patients as a second orthogonal means of confirming somatic mutations. Of those putative mutations with at least 10 transcriptome sequencing reads, we confirmed 3,385 of 3,812 coding somatic point mutations (table S3). Our overall validation rate of 88% compares favorably with many recent cancer sequencing studies (*148, 149*).

3.10 DROPLET DIGITAL PCR

TaqMan assays against mutations in MLH1 and TP53 were designed and synthesized by Applied Biosystems: (1) fwd primer: CCTGATTGGATTACCCCTTCTGATT, rev primer: CAGTGGCTAGTCGAAGAATGAAGAT, VIC (wt) probe: ACTATGTGCCCCCTTTG, FAM (mut) probe: AACTATGTGCTCCCTTTG for mutation MLH1 chr3:37090054 C>T identified in patient 01 recurrence (2) fwd primer: TCCCTTGTCCTTTTTCCTGCAA, rev primer: GATAGGCAGTCCCTCCAAAGG, VIC (wt) probe: CTGATTGGATTACCCCTTC, FAM (mut) probe: CTGATTGGATTATCCCTTC for mutation MLH1 chr3:37090029 C>T identified in patient 10 recurrence (3) fwd primer: GCCAGTTGGCAAAACATCTTGT, rev primer: TGACTTTCAACTCTGTCTCCTTCCT, VIC (wt) probe: CCTACAGTACTCCCCTGCC, FAM (mut) probe: CCTACAGTACTTCCCTGCC for mutation TP53 chr17:7578550 G>A

identified in patient 17 recurrence. A TaqMan assay against BRAF V600E was synthesized by Applied Biosystems from primer and probe sequences described in BioRad Bulletin 6260: fwd primer: CTACTGTTTTCCTTTACTTACTACACCTCAGA, rev primer: ATCCAGACAACTGTTCAAACTGATG, VIC (mut) probe: TTGGTCTAGCTACAGAGAAAT, FAM (wt) probe: TTGGTCTAGCTACAGTGAAAT

All reactions were set up with the droplet PCR supermix and the QX100 Droplet Digital PCR system from Bio-Rad (Hercules, CA) according to manufacturer guidelines and analyzed using the QuantaSoft software in rare event detection (RED) mode. Assays were first optimized through a temperature gradient to maximize separation between the mutant and wild-type signals. Assays were then subject to titration experiments to determine if mutant allele detection was robust down to 0.1%.

The assays were then tested in genomic DNA from the tumors of interest. In all cases, genomic DNA was first subject to restriction enzyme digest (MluCI (patients 01, 10, 18) and AluI (patient 17), New England BioLabs) at 37°C for 15 minutes. Each assay was run with digested DNA from the tumor in which the mutation was identified (positive control), normal DNA from a different patient (negative control, in duplicate), the patient-matched tumor in which the mutation was not detected (in quadruplicate) and a no-DNA water control.

3.11 PCR ANALYSIS OF ATRX DELETION

Genomic DNA from the initial and recurrent tumors for patient 17 was amplified using the following primers: forward ACGCATCTTCATTTACAGTTTCA and reverse AACAAAGTATGTAGAATCAGATGATGA. These primers flank the 8bp deletion found in the recurrence, allowing for amplification of both the wild-type and deletion alleles. The PCR products were resolved on a 15% TBE polyacrylamide gel, stained with SybrSafe (Invitrogen) for 30min and then imaged. To determine the limit of detectability for the deletion allele, a dilution series (30ng down to 30pg) was performed with genomic DNA from the recurrent tumor.

3.12 PHYLOGENETIC TREES

We constructed phylogenetic trees using mutations from exome sequencing data (*150*) of all samples of tumor tissue from patients 04 and 17, inferring ancestral relationships by clonal ordering (*94, 123*). A subset of the coding SNVs and indels from each branch was subject to validation by Sanger sequencing and their locations in the tree were adjusted (false negatives) or removed (false positives). One mutation (patient 04, *MUC4* p.3894_3910del) could not be assessed for technical reasons and was excluded. At least one mutation from each branch was confirmed by Sanger sequencing to validate the structure of the tree. The length of each branch in the phylogenetic tree is proportional to the number of mutations. Labeled genes are those for which there are more than 20 entries in the COSMIC database (version 58, March 2012 release) (*129*).

To confirm that the initial and recurrent tumors of patient 17 derived from a common cell of origin rather than being independently arising tumors, we identified non-coding mutations shared by all geographically distinct samples of the initial and recurrent tumor and validated 3 of them by Sanger sequencing.

3.13 MUTATION RATES

Mutation rates were determined for each tumor from the total number of SNVs detected and the total number of base pairs sequenced to a sufficient depth and quality for mutations to be called by MuTect. Only mutations and sequencing data in protein coding regions and splice-sites were used.

Though it is not possible to determine with certainty whether any single mutation was directly induced by TMZ exposure, one can estimate the proportion of mutations attributable to such an event. Given the mechanisms of action of TMZ and its near-exclusive induction of C>T/G>A transitions across all CpN dinucleotide contexts (*60, 69, 74*), we can estimate R and P, which are the C>T/G>A mutation rates for the TMZ-treated recurrent tumor (R) and the TMZ-naïve initial tumor (P). Here, R is a mixture of both the spontaneous mutation rate of the tumor (measured as P) and the rate of mutation due to TMZ exposure (R-P). Then, (R-P)/R estimates the proportion of C>T/G>A mutations in the TMZ-treated recurrent tumor attributable solely to TMZ exposure. Therefore, we determined that 98.7% to 99.8% of the mutations we identified in the TMZ-treated hypermutated tumors were attributable to TMZ-associated mutagenesis. Though other factors not modeled here could influence the recurrent

tumor mutation rate, the relative stability of mutation rates between initial and recurrent tumors in the untreated patients strongly suggests this is not the case.

3.14 COPY NUMBER ANALYSIS

Copy number segmentation was performed on all samples from exome sequence data with an adaptation of CBS segmentation (*151*). For each tumor (initial or recurrence) and matched normal pair, total aligned coverage was determined for each baited exon from the hybrid selection assay. After excluding exons from the analysis with coverage levels in the matched normal sample of fewer than 10 reads, a log2 ratio of read coverage levels from the tumor-to-normal was determined and scaled by the total aligned sequence in each library. These were segmented with CBS and change-points were reverted if the standard deviation between the means of adjacent segments was less than 1.5. Segmented profiles were then normalized and copy number alterations determined with the RAE framework (*152*).

3.15 TUMOR CELL FRACTION ANALYSIS

Purity (fraction of cells in the sequenced sample that were tumor) and ploidy in each tumor were estimated with ASCAT (*153*) using B allele frequencies inferred for all heterozygous SNPs genotyped as non-reference in tumor and normal exome pairs. At each of these variant sites and in each sample, a log2 copy number ratio was assigned from the average read coverages of the host exon. ASCAT was run with default parameters and the allelic frequencies of all somatic SNVs were converted into the fraction of tumor cells bearing that mutation as previously described (*154*). Calculation

of tumor cell fraction does not adjust for hemizygosity in the normal, so SNVs on the X chromosome in male patients were excluded. One SNV (TP53 R213P, Patient 05) was miscalled as absent in the primary due to low coverage at the locus, but was validated as somatic in both tumors by Sanger sequencing, and is therefore presented as a shared variant. Indel variant frequencies were not available and therefore were excluded from this analysis. Purity and ploidy estimates for the first recurrence of patients 06 and 24 could not be estimated by ASCAT likely due to low tumor purity. Subclonal CNAs, including those arising in rare cell populations, were distinguished from intrinsic experimental noise in the copy number inference from tumor/normal exome coverage levels by comparing all lesions to the minimum allele frequencies (MAF) of heterozygous SNPs spanned by the event. Subclonal CNAs have a decrease in their log2 copy number ratio that is accompanied by a similar change in MAF.

3.16 MGMT BISULFITE SEQUENCING ANALYSIS

In total, 1ug of DNA was bisulfite converted as previously described (*155*). Converted DNA was amplified with PCR using the following primers: forward GGATATGTTGGGATAGTT and reverse TAAAAATCAAAACRACCCCACACC. Amplified DNA was gel extracted, cloned using the TOPO TA sequencing kit (Invitrogen) and 10-15 clones were sequenced. Bisulfite sequence data at the *MGMT* locus (*156*) was analyzed with BISMA (*157*).

3.17 MGMT METHYLATION-SPECIFIC PCR

Genomic DNA samples (250-1000ng each) were used for bisulfite reactions using the EZ DNA Methylation Kit (Zymo Research, Irvine, CA, USA) according to the manufacturer's protocol. DNA methylation status of the O6-methylguanine methyltransferase (*MGMT*) promoter was then determined by methylation-specific PCR as previously described (*156*).

3.18 EXPRESSION OF EXOGENOUS MTOR AND WESTERN BLOTS

The pcDNA-FLAG-mTOR plasmid was obtained (a generous gift of Davide Ruggero Lab, UCSF) and mutated by site directed mutagenesis per the Quickchange II XL kit using primer sets (S2215F - CTGGCCAATGACCCAACATTTCTTCGGAAAAACCTC and GAGGTTTTTCCGAAGAAATGTTGGGTCATTGGCCAG; S2215Y - CTGGCCAATGACCCAACATATCTTCGGAAAAACCTC and GAGGTTTTTCCGAAGATATGTTGGGTCATTGGCCAG). HEK293 cells were transfected with pcDNA-FLAG-mTOR, S2215F, S2215Y, or pcDNA empty vector using Lipofectamine 2000 reagent overnight. Cells were then serum and nutrient starved by incubation in DMEM/0.1% FBS for 47hrs and then in sterile PBS for 1hr prior to harvest. Cells were lysed in Cell Lysis Buffer (Cell Signaling). Western blots were probed with the following antibodies FLAG-M2 (Cell Signaling #8146), mTOR (#2983), RPS6 (#2217s), p-4E-BP1 (#2855s), 4E-BP1 (#9644s), p-RPS6 (#2211s), and GAPDH (Millipore mab374).

3.19 IMMUNOHISTOCHEMISTRY

The following antibodies were used for immunohistochemistry: IDH1 (1:100 Dianova #DIAH09), Phospho-4E-BP1 (1:400 Cell Signaling #2855), and Phospho-S6 (1:200 Cell Signaling #2215). Ki-67 staining was performed with a Ventana Benchmark XT (Confirm anti-Ki-67 30-9, #790-4286).

CHAPTER 4.

DISCUSSION

4.1 GLIOMA GENOME EVOLUTION

4.1.i Mutations in newly diagnosed low-grade gliomas

Newly diagnosed low-grade astrocytic gliomas frequently contain driver mutations in *IDH1*, *TP53*, and *ATRX* (*22*). In the initial grade II astrocytomas and oligoastrocytomas from this study, we identified somatic mutations in *IDH1* all 22 cases, *TP53* in 19 cases, and *ATRX* in 17 cases (Figure 2.2) (Table 2.1). Mutations in the *IDH1* gene occur at a single codon, and were present in all low-grade gliomas from this study. In contrast, there are multiple exons that are recurrently mutated in *TP53* and mutations/indels in *ATRX* are more dispersed throughout the gene, requiring comprehensive coverage of their exons to rule out the presence of a somatic mutation (*22*). Additionally, the genetic alterations in these two genes are frequently indels, which are a significant challenge to accurately identify even in high-coverage next-generation sequencing data. Thus, the absence of *TP53* and/or *ATRX* mutations in the initial low-grade astrocytic gliomas from patients 02, 04, 06, and 25 could be a false negative.

Despite initial appearances, driver events outside of *IDH1* can be subclonal in low-grade astrocytic gliomas. While the trio of driver mutations in *IDH1*, *TP53*, and *ATRX* appear to be fully clonal in all the initial tumors from this study in which they were identified, the recurrent tumor of patient 17 had different driver mutations in *TP53* and *ATRX* than its patient-matched initial tumor. Thus, genetic alterations in *TP53* and *ATRX* were acquired after the mutation of *IDH1* and tumor cells without these two driver mutations were present at initial diagnosis. This raises the possibility that this order of events may be the same for other low-grade astrocytomas. Indeed, Sanger sequencing confirmed

that the *TP53* and *ATRX* mutations in the recurrent tumor of patient 06 were absent from its patient-matched initial tumor, which supports this hypothesis.

A similar pattern was discovered for the fourth most frequently mutated gene in this cohort, the putative tumor suppressor *SMARCA4* (*119, 120*), which had mutations that were private to either the initial or recurrent tumor in six of the seven patients in which they were identified. While mutations in *SMARCA4* may occur frequently in low-grade astrocytic gliomas, the paired nature of the data from this study can be leveraged to show that these mutations are usually late events in tumor evolution, are therefore not an initiator of tumorigenesis, and are also not required for tumor growth. While driver events such as those identified in *SMARCA4* or *BRAF* may accelerate tumor growth, this data suggests their clonal outgrowth may be spatially restricted and thus surgically curable. Thus, they may make poor therapeutic targets. Distinguishing between early and late driver events that may otherwise appear clonal is a key advantage of using longitudinal data and may help gain new insights into the frequently mutated genes identified by the TCGA and ICGC. In addition to longitudinal comparisons, detailed analyses of intratumoral heterogeneity from a single surgical time point provides similar and complementary insight into event ordering, therapeutic value of targets, and improved understanding of the basic mechanisms underlying human tumorigenesis.

Prior studies and data from this study can be used to propose a tentative order of key events in the tumorigenesis of initial astrocytic gliomas. First, germline variants like the SNP rs55705857 at 8q24.21 predispose somatic cells in the brain to malignant

transformation (*29*). This may occur through disruption of a novel microRNA or alterations to long-range chromosomal interactions with this highly conserved region. The exact mechanisms by which this gene poor region contributes to gliomagenesis are unknown. Second, an IDH1 mutation is acquired leading to widespread 2HG-dependent epigenetic remodeling, an inhibition of gliogenic differentiation, and the clonal outgrowth of the cell (*15, 17*). Third, secondary driver mutations or indels in *TP53* and *ATRX* are acquired through strong selective pressure. Additional copy number alterations frequently lead to copy-neutral loss of heterozygosity for the *TP53* gene at 17p13. Inactivation of *TP53* prevents cell cycle arrest and/or apoptosis, while the loss of *ATRX* helps to maintain the telomere length of actively dividing cells through ALT (*23*). Fourth, a subclone may acquire one or more tertiary driver mutations in genes such as *SMARCA4* and *BRAF* that increase their evolutionary fitness leading to subclonal outgrowth. The result of this sequential process is a genetically heterogeneous grade II glioma that develops through the successive acquisition of three or more driver events. Follow-up studies with greater numbers of initial-recurrent tumor pairs and intratumoral samples are currently being performed and will help refine this model to more accurately decipher the temporal accumulation of genetic events and successive clonal evolution found in low-grade gliomas. Extending this type of analysis to grade II oligodendrogliomas will be particularly interesting because they have a different set of common driver mutations, along with unique histology, potentially different cells of origin, and significantly greater sensitivity to chemotherapy.

4.1.ii The genetic relatedness of initial-recurrent tumor pairs

There is a broad spectrum of genetic relatedness between initial low-grade gliomas and their subsequent patient-matched recurrences (Table 2.3). The fraction of mutations shared between initial and recurrent tumors is heavily dependent on the genetic makeup of the tumor cells beyond the surgical margin that seed recurrences. The data from this study show that these cells can originate from either linear or branching patterns of clonal evolution. At one extreme, the tumors from patient 17 shared only the *IDH1* mutation, suggesting that a population of tumor cells with this single mutation expanded before the initial tumor was formed. These *IDH1*-mutant cells may have infiltrated into the surrounding normal tissue before surgical resection, or they may have remained in place with the initial tumor mass growing in an adjacent region. At the other extreme, 86% of the mutations in the initial tumor from patient 27 were detected in the subsequent recurrence. This may be a direct consequence of the subtotal resection performed on this patient, where unresected portions of the initial tumor regrew resulting in a linear pattern of clonal evolution. Indeed, the patient with the next most genetically similar initial-recurrent tumor pair also received a subtotal resection. While the cohort in this study is small and surgical details are incomplete, the pattern of linear clonal evolution after subtotal resection might have been anticipated and future investigations may find a similar relationship between the extent of surgical resection and the mutational burden of the recurrent tumor. In contrast, the early branching pattern of clonal evolution was unexpected in the context of a local recurrence and merits further investigation.

Intratumoral heterogeneity is a major confounding factor in studying the genetic relatedness between initial and recurrent tumors. The ancestral relationship between any two tumor cell populations can be inferred by comparing their mutational burden. However, insufficient sampling of either the initial or recurrent tumor gives an incomplete picture of the tumor cells present at a given time point. If substantial intratumoral heterogeneity is actually present, the estimates of heterogeneity between the initial and recurrent tumor may be inaccurate. The confounding nature of intratumoral heterogeneity in longitudinal sample comparisons is illustrated in the genetic relationships between different pieces of patient 17's initial and recurrent tumors (Figure 2.8). While the data from our study supports intratumoral heterogeneity in every tumor examined, only a small minority of the mutations private to one tumor could be identified in additional samples from its patient-matched pair. This suggests intratumoral heterogeneity can confound the number and identity of the mutations that differ between two patient-matched, longitudinally collected gliomas, but a single sample from each tumor is sufficient to estimate the number of mutations shared. This may be the result of a strong founder effect in both the initial and recurrent tumors. If the clonal expansion of a single subclone is responsible for establishing the bulk of a tumor, then every daughter cell will retain nearly the same number of shared mutations regardless of the acquisition of new clonal or subclonal genetic alterations. An in-depth investigation of the patterns of intratumoral heterogeneity in low-grade gliomas may therefore give some insight into the mechanisms by which recurrences arise. This information may in turn allow inference of the mutational characteristics of residual disease, the target of adjuvant therapy.

4.2 HYPERMUTATION

4.2.i The beginnings of hypermutation

Mutations in *MSH6* and other MMR pathway genes enable resistance to alkylating agent therapy, leading to tumor recurrence (*75*). While the accelerated mutagenesis and subsequent hypermutation of gliomas appears to be a consequence of this mechanism of resistance (*74*), hypermutation has now also been associated with the mechanism of malignant progression of low-grade gliomas to GBM (*116*). As such, the temporal relationship between the exposure of tumor cells to alkylating agents and the inactivation of the MMR pathway is of particular interest.

Two models of the relationship between alkylating agent treatment and MMR pathway inactivation can be drawn based on the data reported in this dissertation. One possibility is that genetic alterations in MMR pathway genes may already exist in the initial, untreated tumor. Treatment with TMZ or other alkylating agents would then present a strong selective pressure for the outgrowth of these MMR deficient cells while simultaneously resulting in their hypermutation. There is only scant evidence to support this model. Across the six hypermutated recurrent tumors presented in this study, we identified eight non-silent mutations in MMR genes. Only the *MSH6* C1158Y mutation identified in the second recurrent tumor of patient 24 showed any evidence of existing in the patient-matched initial tumor, appearing in 2 of 188 high quality reads (Q>20). The depth of coverage in the initial tumors for the other seven MMR mutations ranged from 26 to 261. Furthermore, ddPCR of the *MLH1* P648L and P640S mutations identified in

the recurrent tumors of patients 01 and 10, respectively, showed that they were not present at a variant frequency of at least 0.1% in three pieces of each patient-matched initial tumor (Figure 2.7). Similarly, other groups have identified *MSH6* mutations in recurrent gliomas, but have failed to find any evidence of those mutations in patient-matched untreated initial tumors (*75, 158*). Interestingly, we identified a frameshift deletion in the MMR gene *MLH3* in the initial tumor from patient 07. While this suggests non-silent somatic variants in MMR genes can exist in untreated low-grade gliomas, this patient did not receive treatment with TMZ, and neither the *MLH3* indel nor any signs of hypermutation were detected in the recurrent grade II astrocytoma. Given the intratumoral heterogeneity and incomplete sampling of these initial tumors, we cannot rule out the possibility that infiltrative, unresected tumor cells have a MMR mutation of interest prior to treatment with an alkylating agent. Future experiments to better estimate the baseline mutation rate and true genetic diversity of initial low-grade gliomas may shed additional light on whether or not these mutations were present in tumor cells prior to TMZ exposure.

Alternatively, mutations that cause MMR dysfunction may be induced by exposure to alkylating agents. The inactivation of the MMR pathway normally results in C>T/G>A transition mutations as a result of O6-methyl guanine mispairing with thymine, but the mutation rate ensuing from this mismatch in the presence of an intact MMR pathway is unclear. TMZ treatment of a sufficiently large number of tumor cells may enable a rare event of MMR gene mutation in previously MMR intact cells, which then further enables the outgrowth of TMZ-resistant cells that acquire many more mutations (i.e.

hypermutation). This model is supported by the observation that all eight MMR mutations identified in our recurrent hypermutated tumors, and nearly all of the MMR mutations in the hypermutated GBMs from other groups (*60, 75*), were C>T/G>A transitions. This possibility is further supported by *in vitro* experiments in which *MSH6* wild-type GBM cells were exposed to TMZ and derived resistant clones with *MSH6* mutations (*75*). Similarly, MMR intact rat fibroblast cell lines have been used to study the mutagenicity of a number of alkylating agents (*69, 159-161*). There are several factors that may increase the mutation rate of tumor cells exposed to TMZ. First, pre-existing copy-number alterations may lower the capacity of the MMR pathway activity. Partial inactivation of MMR pathway genes may have functional consequences, as heterozygous point mutations in *MSH6* have been associated with TMZ resistance in GBMs (*60, 75*). Examples of copy-number alterations in MMR genes can be seen in the hypermutated tumors of patients 01, 05, 10, and 18 that showed heterozygous deletion of either the *MLH1* or *MSH2/MSH6* loci upon recurrence. Only patient 10 showed evidence of this heterozygous deletion in the untreated initial tumor, however the other deletions may have been initially present and undetected either because they were subclonal or the tumor was insufficiently sampled. Second, MMR efficiency may experience an age-related decrease (*8, 162*). While age at diagnosis over 40 years is already a major negative prognostic factor for patients with low-grade glioma (*6, 7*), older patients may also be more susceptible to alkylating agent-induced mutagenesis. Third, the TP53 DNA-damage response pathway has been shown to synergize with the MMR pathway to increase the cytotoxicity and limit the mutagenicity of chemotherapeutic agents (*163*). Biallelic inactivation of *TP53* is one of the genetic

hallmarks of grade II astrocytomas and appears to be a common feature of all hypermutated recurrent tumors presented in this study (Table 2.1).

In both models, the activity of MGMT may play an important role in modulating the extent of hypermutation. The methyl group adducts on the O^6 position of guanine induced by TMZ are removed by MGMT. The activity of MGMT therefore prevents TMZ-induced mutations and must be compromised or overwhelmed by adducts before hypermutation occurs (*164*). Evidence of how this occurs can also be seen in the hypermutated tumors from our study. Each of the five hypermutated tumors assessed showed increased and significant levels of DNA methylation at the *MGMT* promoter region (Figure 2.16), which is associated with transcriptional silencing of *MGMT (87-89, 156)*. A further four out of six hypermutated GBMs studied by the TCGA project showed promoter hypermethylation of *MGMT* as well (*60, 75*). Additionally, patients 01, 05, 21, and 24 from our study each showed heterozygous loss of the *MGMT* locus in their hypermutated recurrent tumor. This copy-number alteration was clearly present in the initial untreated tumors from patients 01 and 21, and may have contributed to lower levels of MGMT protein in the tumor cells. Finally, we identified a clonal *MGMT* A114T mutation in the hypermutated recurrent tumor of patient 18. Whether this mutation has any functional consequence on MGMT protein function is unclear, but like the clonal mutations in *MSH3* and *MSH5*, it was present in the founder cell that gave rise to the hypermutated recurrent tumor. Unfortunately, it is unclear whether this MGMT mutation preceded the two mutations in the MMR pathway. As this mutation is a C>T/G>A transition, it may have even been induced by TMZ itself.

Together, these data illustrate the diverse mechanisms that may influence how hypermutation initially arises in these TMZ-treated tumors and gives some initial clues as to the order of the events. Both of the models described above seem likely to occur, albeit in different patients. The inactivation of MGMT by mutation, copy-number alteration, or DNA hypermethylation also appears to be an early event during hypermutation, with some evidence that copy-number loss of the MGMT locus precedes the inactivation of the MMR pathway.

4.2.ii Hypermutation and malignant progression

The data presented in this study show an association between TMZ treatment and subsequent acquisition of new mutations in the RB and AKT-mTOR pathways that directly implicate TMZ-induced hypermutation as a driver of malignant progression. There remains the possibility, however, that hypermutation occurred in a cell that had already undergone malignant progression and was in the process of forming a recurrent high-grade tumor. Whether high-grade tumor cells were already present when TMZ therapy was administered is not known. Nevertheless, the order in which these events occur is particularly relevant in understanding this newly discovered risk associated with TMZ treatment. Based of the data from ten patients that received treatment with TMZ, there are four potential explanations for the interrelationships among TMZ treatment, hypermutation, and malignant progression are possible (Figure 4.1).

The first possibility is that the tumor cells comprising residual disease do not contain a high-grade component. TMZ treatment leads to the induction of apoptosis in some cells and hypermutation in others. The acquisition of TMZ-associated mutations in the RB and AKT-mTOR pathways then leads to malignant progression in one tumor cell. This hypermutated tumor cell then outcompetes the surrounding low-grade cells and forms a recurrent high-grade tumor with fully clonal TMZ-associated mutations. In this situation, the recurrent tumor becomes resistant to TMZ therapy and TMZ-induced mutagenesis is the primary event responsible for malignant progression. The hypermutated recurrences from patients 05, 10, 18, and 21 all appear to fit this pattern, with fully clonal hypermutated high-grade tumors. Interestingly, the second recurrent tumor from patient 24 initially appeared to not fit within this pattern and showed predominantly subclonal TMZ-associated mutations. However, this tumor had a pattern of subclonal mutations, including multiple hits to the MMR pathway gene *MSH6* (G571D and C1158Y) and the tumor suppressor *PTEN* (A121T and G493A), that suggested the recurrence was actually composed of two independent hypermutated subclones that independently lost MMR activity and underwent malignant progression to GBM. Unfortunately, the low variant frequency of mutations within this tumor sample makes an analysis of its subclonal composition with the currently available data very difficult. Additional sequencing experiments, including either increased exome coverage or targeted amplification of identified somatic mutations, would aid in a dissection of the pattern of clonal evolution that occurred here.

The second possibility is that only low-grade tumor cells are exposed to TMZ, resulting in some cellular cytotoxicity but not hypermutation-driven malignant progression. The recurrent tumor that subsequently develops remains low-grade and shows no signs of TMZ-induced mutagenesis. This appears to be the case with the recurrent tumor from patient 11, which recurred as a non-hypermutated grade II oligoastrocytoma after 26 months of TMZ therapy. Patient 06 also fell within this category, having received 6 months of TMZ treatment prior to an initial resection. Both the initial and recurrent tumor from this patient remained grade II, and neither showed any signs of hypermutation. It is possible that after TMZ therapy, these residual low-grade tumor cells may undergo malignant progression. In this case, spontaneous mutations and copy number alterations potentially accelerated by genomic instability are assumed to be the primary driver of malignant progression. This is potentially what happened in the tumor of patient 17, where the tumor recurred after 12 months of TMZ treatment as a GBM without any signs of TMZ-induced mutagenesis.

The third possibility is that initially low-grade tumor cells had already undergone malignant progression when TMZ therapy was administered. While there may be a cytotoxic response to TMZ therapy in the residual tumor cells, it is not the driver of malignant progression. This situation seems more likely to occur when TMZ is given at the time of radiographic progression rather than immediately after surgical resection. Patient 04 clearly fell within this category having received TMZ therapy after surgical resection of a recurrent grade III anaplastic astrocytoma. No evidence of TMZ-induced mutagenesis was detected in any of the two subsequent grade III tumors resected from

this patient. It is also possible this is what happened to the recurrent tumor of patient 17 instead of undergoing malignant progression after TMZ therapy. The presence or absence of high-grade tumor cells is often difficult to know for certain without a biopsy, and whether patient 17's tumor had already undergone malignant progression by the time TMZ treatment was started is unknown.

If malignant progression has already occurred by the time TMZ treatment is given, there is a fourth possibility. Here, TMZ can induce hypermutation in a high-grade tumor cell, potentially conferring a selective advantage that allows for its clonal outgrowth. As non-hypermutated high-grade glioma cells also rapidly divide, the resulting recurrent tumor is heterogeneous with a subclonal hypermutated component. The recurrent tumor from patient 01 was a clear example of this, where two clonally related but histologically distinct high-grade components were present within the tumor, yet only one of them was hypermutated. The intratumoral heterogeneity that results from this sequence of events also makes it more difficult to appropriately classify these recurrent tumors. Incomplete sampling could lead to either sequencing a tumor sample that does not contain the hypermutated subclone or appears clonally hypermutated. In the latter case, this may lead to the misattribution of malignant progression to TMZ therapy. This situation could also be exacerbated if TMZ-associated mutations lead to a dramatically higher replication rate and thus a higher proportion of cells in the recurrent tumor. This appears to be exactly the situation with the recurrent tumor from patient 01, where the initial sample sequenced from this recurrent tumor appeared to be clonally hypermutated.

Indeed, IHC for Ki-67 revealed the hypermutated portion of the tumor had almost triple the proliferation index of the non-hypermutated component (Figure 2.20).

Depicted within this model is the hypermutation of low-grade cells that do not succumb to apoptosis, but also do not undergo malignant progression or expand and outcompete other tumor cells. Whether such cells exist *in vivo* is unknown. No evidence of hypermutated low-grade tumor cells was identified in this study. All six hypermutated recurrent tumors underwent malignant progression to GBM, and both TMZ-treated low-grade recurrences showed no signs of TMZ-induced mutagenesis. While this suggests hypermutation invariably leads to malignant progression, that conclusion is complicated by the fact that low-grade glioma patients are typically treated with multiple doses of TMZ over a period of time (*38, 54*). This may allow for low-grade tumor cells with inactive MMR pathways to undergo many rounds of cell division and TMZ-induced mutation, making it unlikely that at least one daughter cell from the hypermutated subclone does not undergo malignant progression during the course of this accelerated evolution. Additionally, it is possible that TMZ-associated mutations in some hypermutated cells do not affect the appropriate pathways to drive clonal outgrowth without also inducing malignant progression. The detection of minor subclones in post-treatment samples that have not been selected for is very difficult. Indeed, the somatic mutations identified within this study had a minimum variant frequency of 10%. Single-cell sequencing experiments may be able to identify these populations if they are sufficiently common.

All four of the patterns of recurrence after TMZ treatment described above occur in the tumors of patients described in this study. Key to understanding the risks inherent in treating low-grade glioma patients with TMZ will be larger studies that characterize how often TMZ treatment induces clonal and subclonal hypermutation in high-grade recurrent tumors. The potential consequences of TMZ-induced hypermutation seem less dire if malignant progression has already occurred, and may represent the scenario where patients have the most to benefit from TMZ therapy. The further development of methods to non-invasively detect high-grade tumor cells may help guide the clinical use of TMZ in the future.
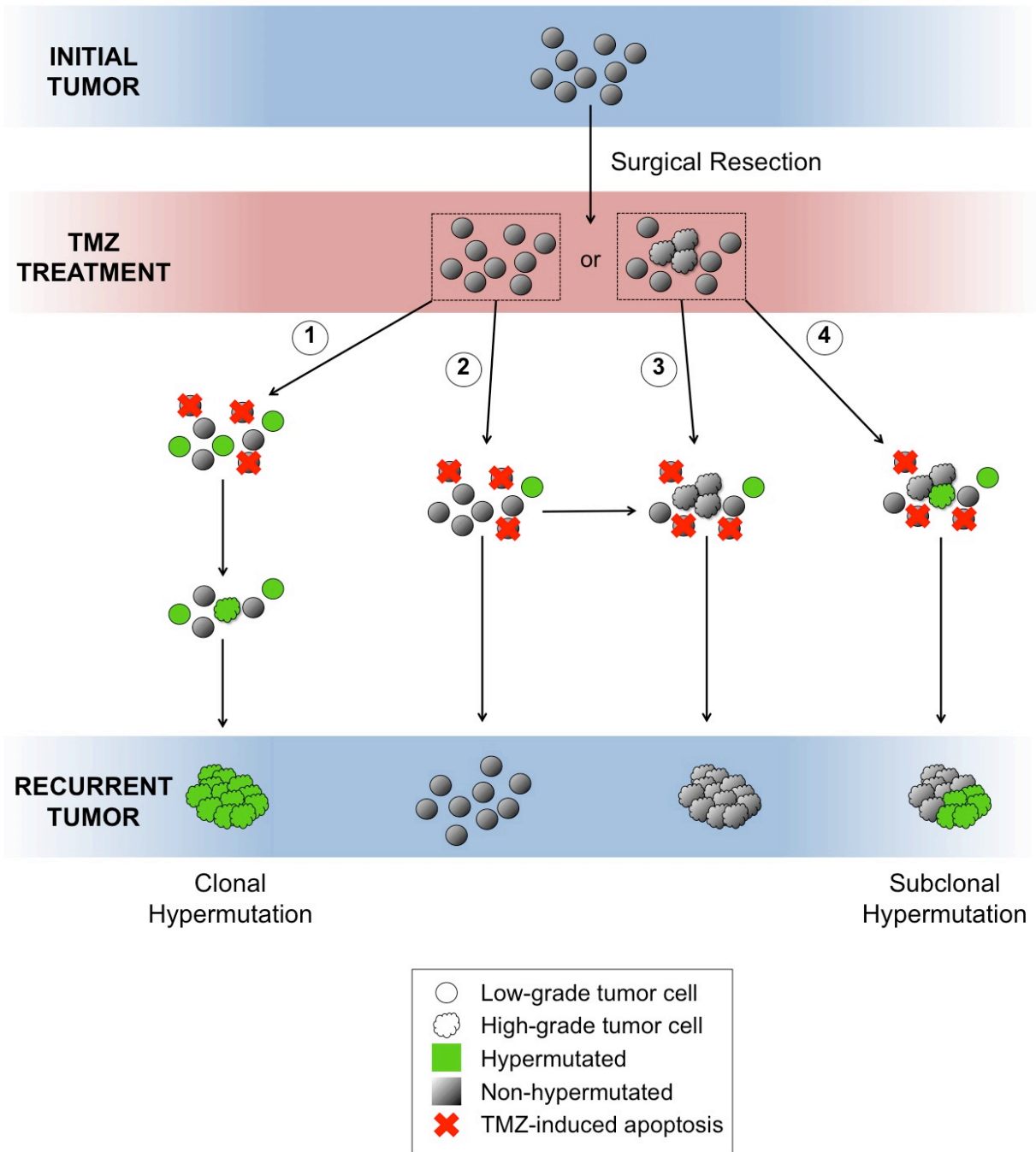
FIGURE 4.1

Figure 4.1 Four models of the relationship between TMZ treatment, hypermutation, and malignant progression in low-grade glioma.

4.2.iii The clonality of TMZ-associated mutations

The fraction of cancer cells harboring each TMZ-associated mutation may lend insight into the patterns of evolution that give rise to hypermutated recurrent tumors. Patients with low-grade gliomas are often treated with TMZ over an extended period (*38, 54*), creating the possibility for TMZ-associated mutations to be progressively accumulated over the course of many cell divisions. Mutations acquired during the initial hypermutation of a MMR deficient cell will be clonal, while those acquired later in time will be unique to daughter cells and subclonal. The relative cancer cell fraction of TMZ-associated mutations is thus related to the order of their accumulation. In reality, however, this is complicated by the clonal outgrowth of subclones with advantageous mutations, which can mask their temporal ordering. Furthermore, the possibility of intratumoral heterogeneity means the calculated cancer cell fraction values may not be representative of the entire tumor. While some conclusions can be drawn from this data, caution must be exercised to avoid over interpretation.

The TMZ-associated mutations identified in the six hypermutated tumors from this study had cancer cell fractions with three distinct distributions (Figure 4.2). The TMZ-associated mutations from the recurrent tumors of patients 05, 10, and 18 appeared to be almost uniformly clonal with little heterogeneity. This suggests one hypermutated cell was responsible for nearly the entire genotype of the recurrent tumor. This pattern could result from many situations, including 1) a single hypermutated subclone dramatically outcompeting a heterogeneous pool of hypermutated cells, 2) TMZ-induced mutagenesis only occurring in a limited number of cells, or 3) the regional outgrowth of

many hypermutated subclones leading to the appearance genetic homogeneity. In contrast, the TMZ-associated mutations from the recurrent tumor of patient 24 were mostly subclonal. As discussed earlier, this tumor may be composed of two or more hypermutated subclones with significant genetic differences. The presence of a small number of clonal TMZ-associated mutations suggests these hypermutated subclones were descended from the same ancestral cell and may indicate they diverged from one another soon after the beginning of TMZ-induced mutagenesis. Finally, the pattern of hypermutation in the recurrent tumors of patients 01 and 21 was somewhere between these two extremes, with a large number of both clonal and subclonal TMZ-associated mutations. While a single hypermutated ancestral cell gave rise to these recurrences, this may be the direct consequence of TMZ-induced mutagenesis occurring over an extended period during active cell division. Together, these data provide a tantalizing yet incomplete picture of the patterns of clonal evolution that give rise to hypermutated tumors. The sequencing of additional samples from these tumors would help identify any intratumoral heterogeneity and may allow for the identification of TMZ-associated mutations with correlated cancer cell fractions that represent distinct subclonal populations (*101*).

The order in which key TMZ-associated mutations in the RB and AKT-mTOR pathways are acquired may provide some insight into the process of malignant progression. Most *in vivo* studies of malignant progression have relied on cohorts of unpaired tumor samples, resulting in models based on correlations between common genetic alterations and tumor grade (*110-113*). In this study, non-silent TMZ-associated

mutations in genes implicated in malignant progression were identified (Figure 2.17), and the fraction of cancer cells in each recurrent tumor bearing these mutations was estimated (Table 4.1). The clonal expansion of a single genotype in the recurrent tumors of patients 05, 10, and 18 masked the majority of any ordering information that might otherwise have been available. Nevertheless, the *CDK6* D311N and *TSC1* E646K mutations in the tumors from patients 05 and 10, respectively, do appear to be subclonal and thus later acquisitions. In the recurrent tumors from patients 01 and 21 a majority of the TMZ-associated mutations looked subclonal, yet the only key subclonal mutations were the *ERBB2* D989N missense and *AKT2* splice-site mutations. While these four mutations had sufficiently low cancer cell fractions to make them likely subclonal, there was no clear evidence that any cause functional consequences to the proteins they encode or their associated pathways. On the other hand, TMZ-associated mutations in these five recurrent tumors that were earlier shown to have functional consequences to the RB and AKT-mTOR pathways had high cancer cell fractions, as would be expected of mutations that drive malignant progression and thus clonal outgrowth. The cancer cell fraction of mutations acquired after an initial resection may therefore be a useful tool for discriminating early drivers of malignant progression from passenger mutations or subclonal drivers. This approach is less successful in the recurrent tumor from patient 24, however, as the majority of key mutations had such a low cancer cell fraction that it was unclear whether or not they existed within the same tumor cells. Only the *MSH6* G571D and *NF1* A1139T mutations appeared to be clonal. All other key TMZ-associated mutations had cancer cell fractions that only place them in up to half the tumor cells. If two independent hypermutated subclones underwent

115

malignant progression independently as hypothesized, then ordering mutations based on their cancer cell fraction is not possible until they are shown to coexist within the same tumor cells. Again, sequencing the exomes of additional tumor samples from this patient would aid in the genetic definition of subclonal populations.

A more careful analysis of the clonality of mutations in the recurrent tumors from this study is currently hampered by the resolution of the data. The variables needed to estimate the fraction of cancer cells bearing a mutation include the sample purity, the locus-specific copy number of the tumor and patient-matched normal, and the variant frequency of the mutation (*154*). Differentiating clonal from subclonal mutations or delineating the order of genetic events at cancer cell fractions that are close together relies on highly accurate measurements. A degree of uncertainty currently exists in the necessary data from this study. First, purity in this data set was assessed with ASCAT (*153*), but potentially more accurate algorithms such as ABSOLUTE are currently available (*165*). Second, genome-wide copy number alterations were inferred from exome sequencing coverage. While these copy number estimates generally agree with the results of array CGH experiments on the same tumor samples (unpublished data), this data is lower resolution and generally less accurate than methods intended to assess copy number. Other studies investigating clonal evolution have relied on copy number data from genome-wide human SNP arrays (*101, 154*). Finally, the variant frequency estimates for each mutation are the result of variable sequencing depths across the exome. In this study, the sequencing depth at TMZ-associated mutations has an average of 131-fold coverage, but ranges from 12 to 942 reads. Ultra-deep coverage

from targeted sequencing experiments results in a higher minimum coverage and thus more accurate variant frequency estimates. This approach has been used successfully in other studies of clonal evolution (*114, 150*). Therefore, caution must be used during the interpretation of the cancer cell fraction data. As a consequence, the patterns of clonal evolution discussed in this study frequently rely on the use of multiple samples from a single patient, using the presence or absence of a mutation to make some inference about its order of acquisition during clonal evolution.
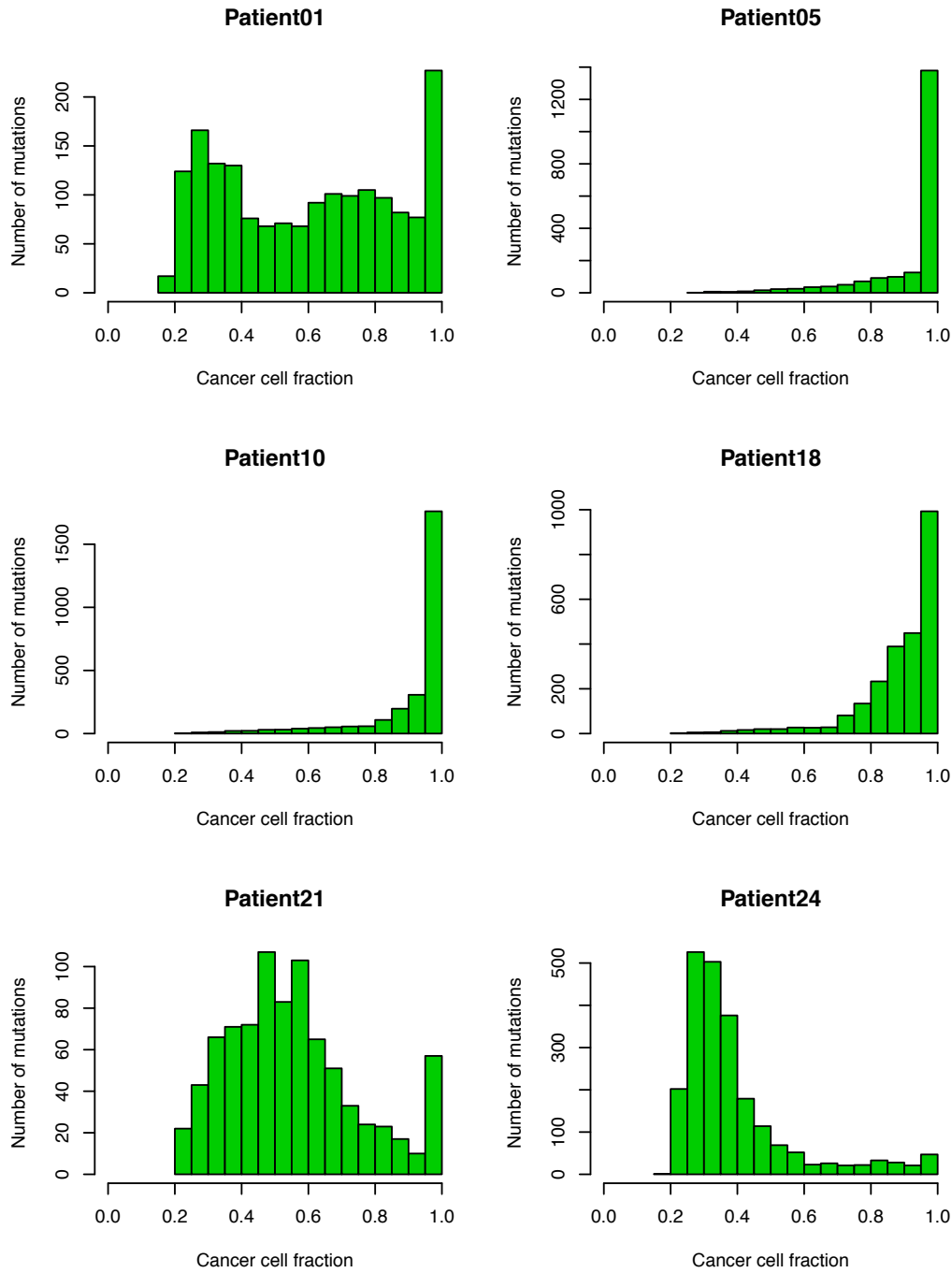
FIGURE 4.2

Figure 4.2 The clonal distribution of all TMZ-associated mutations. A histogram is shown for each hypermutated recurrent tumor graphing the distribution of the cancer cell fraction for all TMZ-associated mutations identified.

TABLE 4.1

Patient ID	Gene	Protein	Context	Cancer cell fraction
Patient01	ERBB2	D989N	exonic	0.72
Patient01	NF1	T685I	exonic	0.86
Patient01	MTOR	S2215F	exonic	0.92
Patient01	RB1	NA	splicing	0.96
Patient01	MLH1	P648L	exonic	1.00
Patient05	CDK6	D311N	exonic	0.66
Patient05	CDK4	K84N	exonic	0.79
Patient05	MSH6	P1077S	exonic	1.00
Patient05	CDKN2A	P114L	exonic	1.00
Patient10	TSC1	E646K	exonic	0.67
Patient10	MLH1	P640S	exonic	1.00
Patient10	CDKN2A	P114L	exonic	1.00
Patient18	NF1	L1475F	exonic	0.76
Patient18	NF1	T1951I	exonic	0.80
Patient18	MSH3	NA	splicing	0.82
Patient18	MSH5	NA	splicing	0.92
Patient18	PIK3CA	E542K	exonic	0.96
Patient21	AKT2	NA	splicing	0.61
Patient21	PDGFRA	E229K	exonic	1.00
Patient24	DDIT4	S198F	exonic	0.50
Patient24	ERBB2	G965D	exonic	0.23
Patient24	MSH5	E121K	exonic	0.31
Patient24	MSH6	G571D	exonic	0.88
Patient24	NF1	A1139T	exonic	1.00
Patient24	PIK3R1	G45E	exonic	0.34
Patient24	PTEN	A121T	exonic	0.52
Patient24	PTEN	G165R	exonic;splicing	0.52
Patient24	CDK6	G273D	exonic	0.27

Table 4.1 The clonality of key TMZ-associated mutations in the MMR, RB, and AKT-mTOR pathways.

4.3 CLINICAL IMPLICATIONS

4.3.i Personalizing medicine

The genetic landscape of each glioma is unique and constantly evolving. Analyses of histologically homogeneous collections of primary low and high-grade gliomas have identified common somatic genetic alterations, yet have also revealed their profound genetic intertumoral heterogeneity (*60, 116*). Even within a low-grade glioma from a single patient, there can be substantial intratumoral heterogeneity at the time of diagnosis (*102, 107*). Furthermore, separate components of these initial tumors can have different evolutionary trajectories (*109*), leading to the development of recurrent tumors which are genetically distinct from their patient-matched initial tumors (*116*). These findings demonstrate the need to adapt the way low-grade glioma patients are diagnosed and treated by investigating and responding to the unique genetics and evolutionary trajectories of each individual tumor with personalized medicine (*166*).

Ascertaining the mutational burden of an individual patient's tumor is complicated by the possibility of intratumoral heterogeneity, and thus requires an analysis of multiple spatially distinct tumor samples. The number and minimum spatial separation of samples required to capture the majority of the genetic alterations present within a given glioma is currently unknown and may vary by patient, tumor grade, or any number of other factors. Sample acquisition during surgical resection is thus a critical component of accurately genotyping a tumor, but can be hindered by surgical constraints and the necessity of putting a safe, maximal resection before all other concerns. The use of image-guided biopsies to acquire samples for genomic analysis is currently being

explored and may help minimize the impact of intratumoral heterogeneity on identifying the true mutational burden of a tumor.

After an initial resection, the treatment of low-grade glioma patients is aimed at managing the residual tumor cells that have the potential to form a recurrent glioma. By definition, the genetic alterations present within this population are inaccessible to initial sequencing-based analyses and may only be inferred from subsequent recurrent tumors. The data presented in this study illustrate the broad spectrum of genetic differences that can arise between initial tumors and their patient-matched recurrences. Thus, the genetic alterations identified in an initial low-grade glioma do not necessarily reflect the mutational burden of either the residual tumor cells or the recurrent tumor to which they give rise. Acquiring tumor tissue at progression is therefore critical for updating the genetic information used to inform treatment decisions. A paradigm of serial genomic surveillance appears to be the best option for keeping abreast of the clonal evolution and shifting genetic landscape of recurrent glioma.

Identifying the genetic alterations present within an initial tumor and understanding how they change over time can help to guide therapy decisions. Actionable mutations include driver events that have predictive implications for specific therapies, but they may not be present throughout the course of a patient's disease. An example identified in this study was the *BRAF* V600E mutation present in the initial tumor of patient 18. Vemurafenib, a small-molecule *BRAF* V600E kinase inhibitor used to treat late-stage melanoma, has shown some effectiveness in pediatric low and high-grade gliomas and

may have been a therapeutic option for patient 18 (*167, 168*). Interestingly, this mutation was subclonal in the initial tumor and completely absent from the subsequent recurrence, providing a prime example of actionable information changing after initial diagnosis. The value of subclonal driver mutations in making treatment decisions is complicated and unclear. While treating a subset of tumor cells is less than ideal, patients may still benefit from targeted therapy against subclones likely to expand (*101*). Other potentially actionable mutations may be identified only in recurrent tumors. For example, the recurrent tumor of patient 10 had a *BRCA1* splice-site mutation and the recurrent tumor of patient 18 had non-silent mutations in both *BRCA1* and *BRCA2*. Although these were all TMZ-associated mutations completely absent from the patient-matched initial tumors, they nevertheless appear to be clonal in the recurrence. These patients may therefore have benefitted from therapy with poly(ADP-ribose) polymerase (PARP) inhibitors, as they have cytotoxic effects on *BRCA* mutated tumors defective in homologous recombination repair and have already shown some effectiveness in sensitizing high-grade gliomas to radiation (*169*).

The presence of hypermutation in a glioma may also be clinically useful information. Hypermutation has been regarded as a side effect of resistance to alkylating agents and its identification in a tumor suggests that a patient will no longer benefit from this type of chemotherapeutic. In addition, the large mutational burden of these tumors may have other consequences that necessitate regarding hypermutated gliomas as distinct clinical entities in the future. For example, the high rate of mutagenesis induced by TMZ acts on each MMR pathway deficient cell independently. The resulting accelerated evolution

may facilitate the development of resistance to targeted therapies given concurrently with alkylating agents. An extended time course of TMZ therapy additionally suggests a larger degree of intratumoral heterogeneity in hypermutated versus non-hypermutated tumors, as MMR pathway deficient cells have been selected for and given time to expand while being subjected to TMZ-induced mutagenesis. Intratumoral heterogeneity is a genetic reservoir for adaptability, raising the likelihood that subclones resistant to targeted therapies delivered after TMZ therapy may already exist. It is currently unclear what the best treatment paradigm will be for balancing alkylating agents with other targeted therapies. As discussed earlier in this study with patient 01, hypermutation may also lead to the development of more proliferative GBMs (Figure 2.20), signaling the need for more aggressive treatment. The ways in which hypermutated gliomas clinically diverge from histologically similar, non-hypermutated gliomas is currently unclear. Understanding how to alter treatment based on this new molecular marker will be greatly aided if future clinical trials incorporate routine tests for hypermutation in recurrent tumors exposed to alkylating agents.

There is a dramatic need for new therapeutic alternatives for patients diagnosed with both low and high-grade gliomas. The use of next-generation sequencing in modern cancer genomics has enabled an unprecedented ability to subset and stratify histologically similar gliomas. The unique mutational burden of each tumor presents an opportunity to use this data to guide the customization of treatment strategies for patients diagnosed with low-grade gliomas. Much work is currently being done to understand and interpret the functional consequences of mutations identified through

exome or whole genome sequencing. Unfortunately, the application of this insight is also currently hobbled by the available therapeutic options for patients with gliomas. The treatments currently available are largely limited to surgery, radiation therapy, and a short list of chemotherapeutic agents. Thus, there is a serious need for the development of new therapeutic alternatives before the insight gleaned from genomics can be appropriately leveraged.

4.3.ii Delaying and preventing malignant progression

Low-grade gliomas frequently undergo malignant progression, resulting in a significantly worse prognosis for the patient. Delaying or preventing malignant progression is therefore an important goal in the adjuvant treatment of low-grade gliomas after an initial resection. The initial goal of this study was to aid in the prediction of which patients initially diagnosed with a low-grade glioma would have a subsequent high-grade recurrence. No molecular marker present in the initial tumors that would predict malignant progression was immediately apparent in the data generated for this study. Previous work has shown malignant progression is associated with the acquisition of genetic alterations in the RB and AKT-mTOR pathways (*28, 60*). Instead of identifying biomarkers of malignant progression, the work presented in this study identifies functional TMZ-associated mutations in these same pathways, suggesting TMZ-induced mutagenesis may be responsible driving malignant progression in some patients. The identification of a potential new cause for malignant progression also opens up new strategies for delaying or preventing the transition from low to high-grade glioma.

The development of a recurrent high-grade glioma occurs through the clonal expansion of tumor cells that have acquired genetic alterations in the RB and AKT-mTOR pathways. Treatments to combat malignant progression must therefore either prevent the acquisition of these genetic alterations or inhibit the clonal outgrowth of high-grade tumor cells. The identification of TMZ-associated mutations in the RB and AKT-mTOR pathways suggests that removing alkylating agents from the adjuvant treatment setting may help to delay the acquisition of key mutations by not artificially inflating the rate of random mutagenesis within residual tumor cells. The RTOG 9802 has reported an increased overall survival benefit for high-risk low-grade glioma patients when treated with adjuvant PCV, but whether this applies to all low-grade glioma patients is currently unknown. Similarly, the high frequency with which genetic alterations in the RB and AKT-mTOR pathways are acquired in GBMs suggests that the use of therapies targeted against these two key pathways may delay the clonal outgrowth of any malignantly transformed cells.

A new phase II clinical trial at UCSF will be using conclusions drawn from this study and exploring a related therapeutic strategy in patients with newly diagnosed low-grade gliomas (ClinicalTrials.gov Identifier NCT02023905). This clinical trial will be evaluating the adjuvant use of everolimus (RAD001) with and without TMZ in grade II astrocytomas, oligodendrogliomas, and oligoastrocytomas. Everolimus is a derivative of rapamycin that selectively inhibits mTOR signaling resulting in decreased tumor cell growth and vascularity. The use of everolimus in this patient population is motivated by the observation that activation of the AKT-mTOR pathway, as measured by

phosphorylation of PRAS40, may be frequently driven by promoter DNA hypermethylation of *PTEN* in low-grade gliomas *(170)*. In this trial, patients will be first stratified by the 1p/19q status of their tumors. As 1p/19q co-deletion is a favorable prognostic marker, these patients will receive adjuvant treatment with everolimus as a single agent. Tumors with 1p/19q intact will be evaluated for their p-PRAS40 status, and those with positive results will be treated with everolimus as they presumably have an activated AKT-mTOR pathway. Patients with tumors that are 1p/19q intact but negative for p-PRAS40 represent the prognostically least favorable group here and are also the least likely to benefit from everolimus as a single agent. With inspiration drawn from the study presented in chapter two, these patients will be given TMZ with the addition of everolimus in an attempt to prevent the clonal outgrowth of high-grade tumor cells with TMZ-induced mutations.

While this clinical trial will help assess the efficacy of adjuvant treatment with everolimus in low-grade glioma patients, it does have several drawbacks. First, this trial does not administer alkylating agents to patients with 1p/19q co-deleted tumors. This is paradoxically the patient population most likely to benefit from that therapy (*49, 50*). With the preliminary results of RTOG 9802 recently being made public, adjuvant chemotherapy with PCV or TMZ may become the standard of care for high-risk low-grade glioma patients. Second, the administration of everolimus to patients with 1p/19q intact, p-PRAS40 negative tumors is given with the primary objective of assessing the progression-free survival of these patients. It is not designed to assess whether everolimus is effective in suppressing the clonal outgrowth of hypermutated subclones

with TMZ-associated mutations in key pathways. Clinical trials incorporating alkylating agents may find an improved progression free survival is associated with their use, but a simultaneously higher rate of therapy-induced malignant progression may actually lead to a decrease in overall survival. As this study is the first directly linking therapy-induced hypermutation to malignant progression in glioma, no controlled study has been performed investigating the rate at which adjuvant TMZ treatment leads to hypermutated recurrent GBMs. This could be addressed with an additional control arm consisting of 1p/19q intact, p-PRAS40 negative low-grade gliomas treated with TMZ as a single agent. A mutational analysis of the tumor samples from this clinical trial will aid in the study of the evolution of low-grade glioma genomes, but any conclusions drawn about the impact of everolimus on TMZ-induced mutagenesis may remain anecdotal.

The association between TMZ-induced mutagenesis and recurrent GBMs raises many questions about the process of malignant progression. Whether targeted therapies like everolimus will inhibit the growth of hypermutated high-grade tumor cells is unknown, but of clear interest. An *in vitro* model of malignant progression based on the common genetic features of low-grade gliomas does not currently exist, but would be of great use in both dissecting the process of TMZ-associated malignant progression and investigating the interplay between TMZ and other targeted therapies.

4.3.iii Treating patients with TMZ

The role of alkylating chemotherapeutics in the treatment of patients with low-grade gliomas is still being defined (*8*). In the adjuvant setting, low-risk patients are usually

untreated and put under surveillance. With the preliminary results of RTOG 9802, high-risk patients are now recommended to receive adjuvant radiation and PCV therapy. As PCV is not tolerated well by many patients, TMZ therapy may become more common in practice. Therapy with alkylating agents is also considered for patients with progressive or recurrent gliomas if they are symptomatic or there are signs of malignant progression. The decision to treat low-grade gliomas with radiation or chemotherapy is not undertaken lightly, as these therapies can have significant long-term side effects in a patient population that can live a decade or more.

The results from two clinical trials may soon offer additional guidance on which patients clearly benefit from therapy with alkylating agents. The RTOG 9802 clinical trial has been evaluating a combination of radiation therapy plus PCV against radiation therapy alone for patients with high-risk low-grade gliomas. While initial results only found an increase in progression free survival for patients receiving the combination therapy, a recent press release has announced a statistically significant increase in overall survival of 5.5 years. This result is practice changing, and now suggests high-risk patients should receive adjuvant radiation and PCV therapy. An analysis of the molecular markers for this study has yet to be released and it is unclear whether the study will be powered to detect differences in survival between the various genetically distinct subtypes of low-grade glioma. While the 1p/19q co-deleted gliomas seem likely to benefit from this treatment (*46-50*), 1p/19q intact gliomas have not previously shown the same level of response to alkylating agents. On the other hand, the EORTC 22033-26033 clinical trial has been directly comparing TMZ therapy alone against radiation

therapy alone for high-risk or progressive low-grade glioma patients. Although not enough time has passed yet to fully analyze and publish the results, early trends for patients treated with TMZ have been reported. Patients with 1p intact tumors seem to trend towards inferior progression free survival, while those with 1p deleted tumors trend towards improved overall survival. This seems to follow the same pattern in which 1p/19q co-deleted gliomas respond much better to alkylating agent therapy than 1p/19q intact gliomas (*46-50*).

The results presented in this study reveal a new adverse consequence of alkylating agent therapy, but much work still needs to be done to fully define the potential risks. For example, it is unknown how the rate of hypermutation changes with different TMZ dosing regimens. Similarly, the length of time it takes to develop a hypermutated recurrent tumor after exposure to alkylating agents is a key variable in the cost to benefit calculation performed whenever therapy decisions are made. In the cohort presented here, the time between the initiation of TMZ treatment and the radiographic progression of an ultimately hypermutated tumor ranged from 12 to 90 months. The insight that can be drawn from this study is limited, however, as the cohort is relatively small and was not originally selected for uniformity of treatment. Nevertheless, it may be ethically responsible to inform patients about these new potential side effects despite the current gaps in our knowledge.

Not all patients who receive therapy with alkylating agents show evidence of TMZ-induced mutagenesis and malignant progression (*60, 116*). It will thus be critical to use

a larger set of samples to identify biomarkers that predict whether individual patient tumors are susceptible to hypermutation and should therefore be considered for radiation therapy instead. However, predicting the hypermutation response on a case-by-case basis may be very difficult if the underlying susceptibility is multifactorial or a matter of random chance. Stratifying patients with common low-grade glioma biomarkers may reveal significant differences in the rate of hypermutation and malignant progression after TMZ therapy.

This study demonstrates the adverse effect adjuvant TMZ therapy can have on the course of tumor evolution and suggests that TMZ may therefore be contraindicated for some low-grade astrocytic gliomas because of its potential to drive malignant progression. Future work on understanding the interplay between TMZ treatment, hypermutation, and malignant progression will help to refine treatment strategies for patients with low-grade gliomas.

BIBLIOGRAPHY

1. D. N. Louis, International Agency for Research on Cancer., World Health Organization., *WHO classification of tumours of the central nervous system*. World Health Organization classification of tumours (International Agency for Research on Cancer, Lyon, ed. 4th, 2007), pp. 309 p.

2. T. Scholzen, J. Gerdes, The Ki-67 protein: from the known and the unknown. *J Cell Physiol* **182**, 311 (Mar 1, 2000).

3. D. N. Louis *et al.*, The 2007 WHO classification of tumours of the central nervous system. *Acta Neuropathol* **114**, 97 (Aug 1, 2007).

4. M. Westphal, K. Lamszus, The neurobiology of gliomas: from cell biology to the development of therapeutic approaches. *Nat Rev Neurosci* **12**, 495 (Sep 1, 2011).

5. J. S. Smith *et al.*, Role of extent of resection in the long-term outcome of low-grade hemispheric gliomas. *J Clin Oncol* **26**, 1338 (Mar 10, 2008).

6. A. B. Karim *et al.*, A randomized trial on dose-response in radiation therapy of low-grade cerebral glioma: European Organization for Research and Treatment of Cancer (EORTC) Study 22844. *Int J Radiat Oncol Biol Phys* **36**, 549 (Oct 1, 1996).

7. A. B. M. F. Karim *et al.*, Randomized trial on the efficacy of radiotherapy for cerebral low-grade glioma in the adult: European Organization for Research and Treatment of Cancer Study 22845 with the Medical Research Council study BRO4: an interim analysis. *Int J Radiat Oncol Biol Phys* **52**, 316 (Feb 1, 2002).

8. N. Sanai, S. Chang, M. S. Berger, Low-grade gliomas in adults. *J Neurosurg* **115**, 948 (Nov 1, 2011).

9. M. Westphal, K. Lamszus, The neurobiology of gliomas: from cell biology to the development of therapeutic approaches. *Nature reviews. Neuroscience* **12**, 495 (Sep, 2011).

10. C. Hartmann *et al.*, Type and frequency of IDH1 and IDH2 mutations are related to astrocytic and oligodendroglial differentiation and age: a study of 1,010 diffuse gliomas. *Acta Neuropathol* **118**, 469 (Oct 1, 2009).

11. P. S. Ward *et al.*, The common feature of leukemia-associated IDH1 and IDH2 mutations is a neomorphic enzyme activity converting alpha-ketoglutarate to 2-hydroxyglutarate. *Cancer Cell* **17**, 225 (Mar 16, 2010).

12. W. Xu *et al.*, Oncometabolite 2-hydroxyglutarate is a competitive inhibitor of alpha-ketoglutarate-dependent dioxygenases. *Cancer Cell* **19**, 17 (Jan 18, 2011).

13. S. Turcan *et al.*, IDH1 mutation is sufficient to establish the glioma hypermethylator phenotype. *Nature* **483**, 479 (Mar 22, 2012).

14. H. Noushmehr *et al.*, Identification of a CpG island methylator phenotype that defines a distinct subgroup of glioma. *Cancer Cell* **17**, 510 (May 18, 2010).

15. D. Rohle *et al.*, An Inhibitor of Mutant IDH1 Delays Growth and Promotes Differentiation of Glioma Cells. *Science (New York, NY)*, (Apr 4, 2013).

16. M. E. Figueroa *et al.*, Leukemic IDH1 and IDH2 Mutations Result in a Hypermethylation Phenotype, Disrupt TET2 Function, and Impair Hematopoietic Differentiation. *Cancer cell*, (Dec 2, 2010).

17. T. Watanabe, S. Nobusawa, P. Kleihues, H. Ohgaki, IDH1 mutations are early events in the development of astrocytomas and oligodendrogliomas. *The American journal of pathology* **174**, 1149 (Apr 1, 2009).

18.   P. J. Killela *et al.*, The genetic landscape of anaplastic astrocytoma. *Oncotarget*, (Oct 16, 2013).

19.   P. J. Killela *et al.*, TERT promoter mutations occur frequently in gliomas and a subset of tumors derived from cells with low rates of self-renewal. *Proc Natl Acad Sci USA* **110**, 6021 (Apr 9, 2013).

20.   Y. Okamoto *et al.*, Population-based study on incidence, survival rates, and genetic alterations of low-grade diffuse astrocytomas and oligodendrogliomas. *Acta Neuropathol* **108**, 49 (Jul 1, 2004).

21.   M. Olivier, M. Hollstein, P. Hainaut, TP53 mutations in human cancers: origins, consequences, and clinical use. *Cold Spring Harb Perspect Biol* **2**, a001008 (Jan 1, 2010).

22.   Y. Jiao *et al.*, Frequent ATRX, CIC, and FUBP1 mutations refine the classification of malignant gliomas. *Oncotarget* **3**, 709 (Jul 1, 2012).

23.   C. M. Heaphy *et al.*, Altered telomeres in tumors with ATRX and DAXX mutations. *Science (New York, NY)* **333**, 425 (Jul 22, 2011).

24.   C. Molinari *et al.*, Chromosome 1p and 19q evaluation in low-grade oligodendrogliomas: a descriptive study. *Int J Mol Med* **25**, 145 (Jan 1, 2010).

25.   R. B. Jenkins *et al.*, A t(1;19)(q10;p10) mediates the combined deletions of 1p and 19q and predicts a better prognosis of patients with oligodendroglioma. *Cancer research* **66**, 9852 (Oct 15, 2006).

26.   C. Bettegowda *et al.*, Mutations in CIC and FUBP1 Contribute to Human Oligodendroglioma. *Science (New York, NY)*, (Aug 4, 2011).

27.   F. W. Huang *et al.*, Highly recurrent TERT promoter mutations in human melanoma. *Science (New York, NY)* **339**, 957 (Feb 22, 2013).

28.   D. N. Louis, Molecular pathology of malignant gliomas. *Annu Rev Pathol* **1**, 97 (Jan 1, 2006).

29.   R. B. Jenkins *et al.*, A low-frequency variant at 8q24.21 is strongly associated with risk of oligodendroglial tumors and astrocytomas with IDH1 or IDH2 mutation. *Nature genetics* **44**, 1122 (Oct 1, 2012).

30.   K. L. Chaichana, M. J. McGirt, J. Laterra, A. Olivi, A. Quiñones-Hinojosa, Recurrence and malignant degeneration after resection of adult hemispheric low-grade gliomas. *J Neurosurg* **112**, 10 (Jan 1, 2010).

31.   A. S. Jakola *et al.*, Comparison of a strategy favoring early surgical resection vs a strategy favoring watchful waiting in low-grade gliomas. *JAMA* **308**, 1881 (Nov 14, 2012).

32.   R. Cavaliere, M. B. S. Lopes, D. Schiff, Low-grade gliomas: an update on pathology and therapy. *Lancet Neurol* **4**, 760 (Nov 1, 2005).

33.   E. G. Shaw *et al.*, Recurrence following neurosurgeon-determined gross-total resection of adult supratentorial low-grade glioma: results of a prospective clinical trial. *J Neurosurg* **109**, 835 (Nov 1, 2008).

34.   M. C. Chamberlain, Does RTOG 9802 change practice with respect to newly diagnosed low-grade glioma? *J Clin Oncol* **31**, 652 (Feb 10, 2013).

35.   E. G. Shaw *et al.*, Randomized trial of radiation therapy plus procarbazine, lomustine, and vincristine chemotherapy for supratentorial adult low-grade glioma: initial results of RTOG 9802. *J Clin Oncol* **30**, 3065 (Sep 1, 2012).

36. M. J. van den Bent *et al.*, Long-term efficacy of early versus delayed radiotherapy for low-grade astrocytoma and oligodendroglioma in adults: the EORTC 22845 randomised trial. *Lancet* **366**, 985 (Jan 1, 2005).

37. M. Brada *et al.*, Phase II study of primary temozolomide chemotherapy in patients with WHO grade II gliomas. *Ann Oncol* **14**, 1715 (Dec 1, 2003).

38. J. A. Quinn *et al.*, Phase II trial of temozolomide in patients with progressive low-grade glioma. *J Clin Oncol* **21**, 646 (Feb 15, 2003).

39. A. Pace *et al.*, Temozolomide chemotherapy for progressive low-grade glioma: clinical benefits and radiological response. *Ann Oncol* **14**, 1722 (Dec 1, 2003).

40. E. M. B.-t. Stege *et al.*, Successful treatment of low-grade oligodendroglial tumors with a chemotherapy regimen of procarbazine, lomustine, and vincristine. *Cancer* **103**, 802 (Feb 15, 2005).

41. J. C. Buckner *et al.*, Phase II trial of procarbazine, lomustine, and vincristine as initial therapy for patients with low-grade oligodendroglioma or oligoastrocytoma: efficacy and associations with chromosomal abnormalities. *J Clin Oncol* **21**, 251 (Jan 15, 2003).

42. M. J. van den Bent *et al.*, Phase II study of first-line chemotherapy with temozolomide in recurrent oligodendroglial tumors: the European Organization for Research and Treatment of Cancer Brain Tumor Group Study 26971. *J Clin Oncol* **21**, 2525 (Jul 1, 2003).

43. A. Tosoni *et al.*, Temozolomide three weeks on and one week off as first line therapy for patients with recurrent or progressive low grade gliomas. *J Neurooncol* **89**, 179 (Sep 1, 2008).

44. M. J. van den Bent, K. Jaeckle, B. Baumert, W. Wick, RTOG 9802: good wines need aging. *J Clin Oncol* **31**, 653 (Feb 10, 2013).

45. A. Ng, G. M. Taylor, O. B. Eden, Treatment-related leukaemia--a clinical and scientific challenge. *Cancer Treat Rev* **26**, 377 (Oct, 2000).

46. M. J. van den Bent *et al.*, Adjuvant procarbazine, lomustine, and vincristine chemotherapy in newly diagnosed anaplastic oligodendroglioma: long-term follow-up of EORTC brain tumor group study 26951. *J Clin Oncol* **31**, 344 (Jan 20, 2013).

47. G. Cairncross *et al.*, Phase III trial of chemoradiotherapy for anaplastic oligodendroglioma: long-term results of RTOG 9402. *J Clin Oncol* **31**, 337 (Jan 20, 2013).

48. M. C. M. Kouwenhoven *et al.*, 1p/19q loss within oligodendroglioma is predictive for response to first line temozolomide but not to salvage treatment. *Eur J Cancer* **42**, 2499 (Oct 1, 2006).

49. G. Kaloshi *et al.*, Temozolomide for low-grade gliomas: predictive impact of 1p/19q loss on response and outcome. *Neurology* **68**, 1831 (May 22, 2007).

50. K. Hoang-Xuan *et al.*, Temozolomide as initial treatment for adults with low-grade oligodendrogliomas or oligoastrocytomas and correlation with chromosome 1p deletions. *J Clin Oncol* **22**, 3133 (Aug 1, 2004).

51. M. E. Hegi *et al.*, MGMT gene silencing and benefit from temozolomide in glioblastoma. *N Engl J Med* **352**, 997 (Mar 10, 2005).

52. W. Wick *et al.*, Prognostic or predictive value of MGMT promoter methylation in gliomas depends on IDH1 mutation. *Neurology* **81**, 1515 (Oct 22, 2013).

53. S. Everhard *et al.*, MGMT methylation: a marker of response to temozolomide in low-grade gliomas. *Ann Neurol* **60**, 740 (Dec 1, 2006).

54. W. Taal *et al.*, First-line temozolomide chemotherapy in progressive low-grade astrocytomas after radiotherapy: molecular characteristics in relation to response. *Neuro-oncology* **13**, 235 (Feb 1, 2011).

55. D. W. Parsons *et al.*, An integrated genomic analysis of human glioblastoma multiforme. *Science* **321**, 1807 (Sep 26, 2008).

56. C. Houillier *et al.*, IDH1 or IDH2 mutations predict longer survival and response to temozolomide in low-grade gliomas. *Neurology* **75**, 1560 (Oct 26, 2010).

57. H. J. Dubbink *et al.*, IDH1 mutations in low-grade astrocytomas predict survival but not response to temozolomide. *Neurology* **73**, 1792 (Nov 24, 2009).

58. J. Rees *et al.*, Volumes and growth rates of untreated adult low-grade gliomas indicate risk of early malignant transformation. *Eur J Radiol* **72**, 54 (Oct 1, 2009).

59. N. Sanai, M.-Y. Polley, M. S. Berger, Insular glioma resection: assessment of patient morbidity, survival, and tumor progression. *J Neurosurg* **112**, 1 (Jan 1, 2010).

60. Cancer Genome Atlas Research Network, Comprehensive genomic characterization defines human glioblastoma genes and core pathways. *Nature* **455**, 1061 (Oct 23, 2008).

61. M. S. Song, L. Salmena, P. P. Pandolfi, The functions and regulation of the PTEN tumour suppressor. *Nat Rev Mol Cell Biol* **13**, 283 (May 1, 2012).

62. C. D. James *et al.*, Clonal genomic alterations in glioma malignancy stages. *Cancer research* **48**, 5546 (Oct 1, 1988).

63. H. Wang *et al.*, Analysis of the activation status of Akt, NFkappaB, and Stat3 in human diffuse gliomas. *Lab Invest* **84**, 941 (Aug 1, 2004).

64. E. C. Holland *et al.*, Combined activation of Ras and Akt in neural progenitors induces glioblastoma formation in mice. *Nature genetics* **25**, 55 (May 1, 2000).

65. H. Rayess, M. B. Wang, E. S. Srivatsan, Cellular senescence and tumor suppressor gene p16. *Int J Cancer* **130**, 1715 (Apr 15, 2012).

66. M. Wolter *et al.*, Oligodendroglial tumors frequently demonstrate hypermethylation of the CDKN2A (MTS1, p16INK4a), p14ARF, and CDKN2B (MTS2, p15INK4b) tumor suppressor genes. *J Neuropathol Exp Neurol* **60**, 1170 (Dec 1, 2001).

67. W. A. Weiss *et al.*, Genetic determinants of malignancy in a mouse model for oligodendroglioma. *Cancer research* **63**, 1589 (Apr 1, 2003).

68. A. Xiao, H. Wu, P. P. Pandolfi, D. N. Louis, T. Van Dyke, Astrocyte inactivation of the pRb pathway predisposes mice to malignant astrocytoma development that is accelerated by PTEN mutation. *Cancer cell* **1**, 157 (Mar 1, 2002).

69. W. J. Bodell, N. W. Gaikwad, D. Miller, M. S. Berger, Formation of DNA adducts and induction of lacI mutations in Big Blue Rat-2 cells treated with temozolomide: implications for the treatment of low-grade adult and pediatric brain tumors. *Cancer Epidemiol Biomarkers Prev* **12**, 545 (Jun 1, 2003).

70. A. Loveless, Possible relevance of O-6 alkylation of deoxyguanosine to the mutagenicity and carcinogenicity of nitrosamines and nitrosamides. *Nature* **223**, 206 (Jul 12, 1969).

71. W. P. Roos *et al.*, Apoptosis in malignant glioma cells triggered by the temozolomide-induced DNA lesion O6-methylguanine. *Oncogene* **26**, 186 (Jan 11, 2007).

72. K. S. Ellison, E. Dogliotti, T. D. Connors, A. K. Basu, J. M. Essigmann, Site-specific mutagenesis by O6-alkylguanines located in the chromosomes of mammalian cells: influence of the mammalian O6-alkylguanine-DNA alkyltransferase. *Proc Natl Acad Sci U S A* **86**, 8620 (Nov, 1989).

73. C. Greenman *et al.*, Patterns of somatic mutation in human cancer genomes. *Nature* **446**, 153 (Mar 8, 2007).

74. C. Hunter *et al.*, A hypermutation phenotype and somatic MSH6 mutations in recurrent human malignant gliomas after alkylator chemotherapy. *Cancer research* **66**, 3987 (Apr 15, 2006).

75. S. Yip *et al.*, MSH6 mutations arise in glioblastomas during temozolomide therapy and mediate temozolomide resistance. *Clin Cancer Res* **15**, 4622 (Jul 15, 2009).

76. D. H. Christiansen, M. K. Andersen, J. Pedersen-Bjergaard, Mutations with loss of heterozygosity of p53 are common in therapy-related myelodysplasia and acute myeloid leukemia after exposure to alkylating agents and significantly associated with deletion or loss of 5q, a complex karyotype, and a poor prognosis. *J Clin Oncol* **19**, 1405 (Mar 1, 2001).

77. P. M. Nolan, A. Hugill, R. D. Cox, ENU mutagenesis in the mouse: application to human genetic disease. *Brief Funct Genomic Proteomic* **1**, 278 (Oct 1, 2002).

78. H. Druckrey, S. Ivanković, R. Preussmann, Teratogenic and carcinogenic effects in the offspring after single injection of ethylnitrosourea to pregnant rats. *Nature* **210**, 1378 (Jun 25, 1966).

79. B. C. Zook, S. J. Simmens, R. V. Jones, Evaluation of ENU-induced gliomas in rats: nomenclature, immunochemistry, and malignancy. *Toxicol Pathol* **28**, 193 (Jan 1, 2000).

80. D. Fink, S. Aebi, S. B. Howell, The role of DNA mismatch repair in drug resistance. *Clin Cancer Res* **4**, 1 (Jan 1, 1998).

81. P. Karran, J. Offman, M. Bignami, Human mismatch repair, drug-induced DNA damage, and secondary cancer. *Biochimie* **85**, 1149 (Nov 1, 2003).

82. A. Umar *et al.*, Correction of hypermutability, N-methyl-N'-nitro-N-nitrosoguanidine resistance, and defective DNA mismatch repair by introducing chromosome 2 into human tumor cells with mutations in MSH2 and MSH6. *Cancer research* **57**, 3949 (Sep 15, 1997).

83. T. Lettieri *et al.*, Effect of hMSH6 cDNA expression on the phenotype of mismatch repair-deficient colon cancer cell line HCT15. *Carcinogenesis* **20**, 373 (Mar 1, 1999).

84. D. P. Cahill *et al.*, Loss of the mismatch repair protein MSH6 in human glioblastomas is associated with tumor progression during temozolomide treatment. *Clin Cancer Res* **13**, 2038 (Apr 1, 2007).

85. M. E. Hegi *et al.*, Correlation of O6-methylguanine methyltransferase (MGMT) promoter methylation with clinical outcomes in glioblastoma and clinical strategies to modulate MGMT activity. *J Clin Oncol* **26**, 4189 (Sep 1, 2008).

86.   S. L. Gerson, Clinical relevance of MGMT in the treatment of cancer. *J Clin Oncol* **20**, 2388 (May 1, 2002).

87.   J. F. Costello, B. W. Futscher, R. A. Kroes, R. O. Pieper, Methylation-related chromatin structure is associated with exclusion of transcription factors from and suppressed expression of the O-6-methylguanine DNA methyltransferase gene in human glioma cell lines. *Mol Cell Biol* **14**, 6515 (Oct 1, 1994).

88.   J. F. Costello, B. W. Futscher, K. Tano, D. M. Graunke, R. O. Pieper, Graded methylation in the promoter and body of the O6-methylguanine DNA methyltransferase (MGMT) gene correlates with MGMT expression in human glioma cells. *J Biol Chem* **269**, 17228 (Jun 24, 1994).

89.   G. S. Watts *et al.*, Methylation of discrete regions of the O6-methylguanine DNA methyltransferase (MGMT) CpG island is associated with heterochromatinization of the MGMT transcription start site and silencing of the gene. *Mol Cell Biol* **17**, 5612 (Sep 1, 1997).

90.   M. J. Bello *et al.*, Hypermethylation of the DNA repair gene MGMT: association with TP53 G:C to A:T transitions in a series of 469 nervous system tumors. *Mutat Res* **554**, 23 (Oct 4, 2004).

91.   P. C. Nowell, The clonal evolution of tumor cell populations. *Science (New York, NY)* **194**, 23 (Oct 1, 1976).

92.   M. Greaves, C. C. Maley, Clonal evolution in cancer. *Nature* **481**, 306 (Jan 19, 2012).

93.   S. Aparicio, C. Caldas, The implications of clonal genome evolution for cancer medicine. *N Engl J Med* **368**, 842 (Feb 28, 2013).

94.   M. Gerlinger *et al.*, Intratumor heterogeneity and branched evolution revealed by multiregion sequencing. *N Engl J Med* **366**, 883 (Mar 8, 2012).

95.   X. Wu *et al.*, Clonal selection drives genetic divergence of metastatic medulloblastoma. *Nature* **482**, 529 (Feb 23, 2012).

96.   A. G. Knudson, Mutation and cancer: statistical study of retinoblastoma. *Proc Natl Acad Sci USA* **68**, 820 (Apr 1, 1971).

97.   W. K. Cavenee *et al.*, Expression of recessive alleles by chromosomal mechanisms in retinoblastoma. *Nature* **305**, 779 (Jan 1, 1983).

98.   N. Ishii *et al.*, Cells with TP53 mutations in low grade astrocytic tumors evolve clonally to malignancy and are an unfavorable prognostic factor. *Oncogene* **18**, 5870 (Oct 21, 1999).

99.   D. Sidransky *et al.*, Clonal expansion of p53 mutant cells is associated with brain tumour progression. *Nature* **355**, 846 (Feb 27, 1992).

100.   M. Gerlinger, C. Swanton, How Darwinian models inform therapeutic failure initiated by clonal heterogeneity in cancer medicine. *Br J Cancer* **103**, 1139 (Oct 12, 2010).

101.   D. A. Landau *et al.*, Evolution and impact of subclonal mutations in chronic lymphocytic leukemia. *Cell* **152**, 714 (Feb 14, 2013).

102.   A. L. Vital *et al.*, Intratumoral patterns of clonal evolution in gliomas. *Neurogenetics* **11**, 227 (May 1, 2010).

103.   K. Harada *et al.*, Intratumoral cytogenetic heterogeneity detected by comparative genomic hybridization and laser scanning cytometry in human gliomas. *Cancer research* **58**, 4694 (Oct 15, 1998).

104. J. R. Shapiro, W. K. Yung, W. R. Shapiro, Isolation, karyotype, and clonal growth of heterogeneous subpopulations of human malignant gliomas. *Cancer research* **41**, 2349 (Jun 1, 1981).

105. V. Jung *et al.*, Evidence of focal genetic microheterogeneity in glioblastoma multiforme by area-specific CGH on microdissected tumor cells. *J Neuropathol Exp Neurol* **58**, 993 (Sep 1, 1999).

106. M. Snuderl *et al.*, Mosaic Amplification of Multiple Receptor Tyrosine Kinase Genes in Glioblastoma. *Cancer Cell*, (Nov 30, 2011).

107. S. W. Coons, P. C. Johnson, J. R. Shapiro, Cytogenetic and flow cytometry DNA analysis of regional heterogeneity in a low grade human glioma. *Cancer research* **55**, 1569 (Apr 1, 1995).

108. Z.-P. Ren *et al.*, Molecular genetic analysis of p53 intratumoral heterogeneity in human astrocytic brain tumors. *J Neuropathol Exp Neurol* **66**, 944 (Oct 1, 2007).

109. J. R. Shapiro, W. R. Shapiro, The subpopulations and isolated cell types of freshly resected high grade human gliomas: their influence on the tumor's evolution in vivo and behavior and therapy in vitro. *Cancer Metastasis Rev* **4**, 107 (Jan 1, 1985).

110. H. Ohgaki *et al.*, Genetic pathways to glioblastoma: a population-based study. *Cancer research* **64**, 6892 (Oct 1, 2004).

111. H. Ohgaki, B. Schäuble, A. zur Hausen, K. von Ammon, P. Kleihues, Genetic alterations associated with the evolution and progression of astrocytic brain tumours. *Virchows Arch* **427**, 113 (Jan 1, 1995).

112. A. von Deimling, D. N. Louis, O. D. Wiestler, Molecular pathways in the formation of gliomas. *Glia* **15**, 328 (Nov 1, 1995).

113. V. P. Collins, C. D. James, Gene and chromosomal alterations associated with the development of human gliomas. *FASEB J* **7**, 926 (Jul 1, 1993).

114. L. Ding *et al.*, Clonal evolution in relapsed acute myeloid leukaemia revealed by whole-genome sequencing. *Nature* **481**, 506 (Jan 26, 2012).

115. S. Yachida *et al.*, Distant metastasis occurs late during the genetic evolution of pancreatic cancer. *Nature* **467**, 1114 (Oct 28, 2010).

116. B. E. Johnson *et al.*, Mutational analysis reveals the origin and therapy-driven evolution of recurrent glioma. *Science (New York, NY)* **343**, 189 (Jan 10, 2014).

117. A full list of the somatic mutations identified in this study along with RNA-seq and Sanger validation status can be downloaded at http://www.sciencemag.org/content/suppl/2013/12/11/science.1239947.DC1/1239947s.xls.

118. K. Watanabe *et al.*, Incidence and timing of p53 mutations during astrocytoma progression in patients with multiple biopsies. *Clin Cancer Res* **3**, 523 (Apr 1, 1997).

119. P. P. Medina *et al.*, Frequent BRG1/SMARCA4-inactivating mutations in human lung cancer cell lines. *Hum Mutat* **29**, 617 (May 1, 2008).

120. S. Glaros, G. M. Cirrincione, A. Palanca, D. Metzger, D. Reisman, Targeted knockout of BRG1 potentiates lung cancer development. *Cancer research* **68**, 3689 (May 15, 2008).

121. N. J. Szerlip *et al.*, Intratumoral heterogeneity of receptor tyrosine kinases EGFR and PDGFRA amplification in glioblastoma defines subpopulations with distinct growth factor response. *Proceedings of the National Academy of Sciences of the United States of America* **109**, 3041 (Feb 21, 2012).

122. A. Sottoriva *et al.*, Intratumor heterogeneity in human glioblastoma reflects cancer evolutionary dynamics. *Proceedings of the National Academy of Sciences of the United States of America* **110**, 4009 (Mar 5, 2013).

123. L. M. F. Merlo, J. W. Pepper, B. J. Reid, C. C. Maley, Cancer as an evolutionary and ecological process. *Nat Rev Cancer* **6**, 924 (Dec 1, 2006).

124. G. Reifenberger, J. Reifenberger, K. Ichimura, P. S. Meltzer, V. P. Collins, Amplification of multiple genes from chromosomal region 12q13-14 in human malignant gliomas: preliminary mapping of the amplicons shows preferential involvement of CDK4, SAS, and MDM2. *Cancer research* **54**, 4299 (Aug 15, 1994).

125. T. Tsai *et al.*, Rapid identification of germline mutations in retinoblastoma by protein truncation testing. *Arch Ophthalmol* **122**, 239 (Feb 1, 2004).

126. C. Houdayer *et al.*, Comprehensive screening for constitutional RB1 mutations by DHPLC and QMPSF. *Hum Mutat* **23**, 193 (Feb 1, 2004).

127. X. Q. Qin, T. Chittenden, D. M. Livingston, W. G. Kaelin, Identification of a growth suppression domain within the retinoblastoma gene product. *Genes Dev* **6**, 953 (Jun 1, 1992).

128. J. Koh, G. H. Enders, B. D. Dynlacht, E. Harlow, Tumour-derived p16 alleles encoding proteins defective in cell-cycle inhibition. *Nature* **375**, 506 (Jun 8, 1995).

129. S. A. Forbes *et al.*, The Catalogue of Somatic Mutations in Cancer (COSMIC). *Curr Protoc Hum Genet* **Chapter 10**, Unit 10.11 (Apr 1, 2008).

130. M. C. Fargnoli *et al.*, CDKN2a/p16INK4a mutations and lack of p19ARF involvement in familial melanoma kindreds. *J Invest Dermatol* **111**, 1202 (Dec 1, 1998).

131. S. Kang, A. G. Bader, P. K. Vogt, Phosphatidylinositol 3-kinase mutations identified in human cancer are oncogenic. *Proc Natl Acad Sci USA* **102**, 802 (Jan 18, 2005).

132. S. Y. Han *et al.*, Functional evaluation of PTEN missense mutations using in vitro phosphoinositide phosphatase assay. *Cancer research* **60**, 3147 (Jun 15, 2000).

133. T. Sato, A. Nakashima, L. Guo, K. Coffman, F. Tamanoi, Single amino-acid changes that confer constitutive activation of mTOR are discovered in human cancer. *Oncogene* **29**, 2746 (May 6, 2010).

134. H. Li, R. Durbin, Fast and accurate short read alignment with Burrows-Wheeler transform. *Bioinformatics* **25**, 1754 (Jul 15, 2009).

135. A. McKenna *et al.*, The Genome Analysis Toolkit: a MapReduce framework for analyzing next-generation DNA sequencing data. *Genome Res* **20**, 1297 (Sep 1, 2010).

136. M. A. Depristo *et al.*, A framework for variation discovery and genotyping using next-generation DNA sequencing data. *Nature genetics*, (Apr 10, 2011).

137. K. Cibulskis *et al.*, Sensitive detection of somatic point mutations in impure and heterogeneous cancer samples. *Nat Biotechnol*, (Feb 10, 2013).

138. K. Ye, M. H. Schulz, Q. Long, R. Apweiler, Z. Ning, Pindel: a pattern growth approach to detect break points of large deletions and medium sized insertions from paired-end short reads. *Bioinformatics* **25**, 2865 (Nov 1, 2009).

139. K. Wang, M. Li, H. Hakonarson, ANNOVAR: functional annotation of genetic variants from high-throughput sequencing data. *Nucleic Acids Research* **38**, e164 (Sep 1, 2010).

140. 1000 Genomes Project Consortium, A map of human genome variation from population-scale sequencing. *Nature* **467**, 1061 (Oct 28, 2010).

141. K. C. Wiegand *et al.*, ARID1A mutations in endometriosis-associated ovarian carcinomas. *N Engl J Med* **363**, 1532 (Oct 14, 2010).

142. C. Trapnell, L. Pachter, S. L. Salzberg, TopHat: discovering splice junctions with RNA-Seq. *Bioinformatics* **25**, 1105 (May 1, 2009).

143. C. Trapnell *et al.*, Transcript assembly and quantification by RNA-Seq reveals unannotated transcripts and isoform switching during cell differentiation. *Nat Biotechnol* **28**, 511 (May 1, 2010).

144. M. Griffith *et al.*, Alternative expression analysis by RNA sequencing. *Nature Methods* **7**, 843 (Oct 1, 2010).

145. A. Subramanian *et al.*, Gene set enrichment analysis: a knowledge-based approach for interpreting genome-wide expression profiles. *Proc Natl Acad Sci USA* **102**, 15545 (Oct 25, 2005).

146. S. Rozen, H. Skaletsky, Primer3 on the WWW for general users and for biologist programmers. *Methods Mol Biol* **132**, 365 (Jan 1, 2000).

147. B. C. Christensen *et al.*, DNA methylation, isocitrate dehydrogenase mutation, and survival in glioma. *J Natl Cancer Inst* **103**, 143 (Jan 19, 2011).

148. M. F. Berger *et al.*, The genomic complexity of primary human prostate cancer. *Nature* **470**, 214 (Feb 10, 2011).

149. M. A. Chapman *et al.*, Initial genome sequencing and analysis of multiple myeloma. *Nature* **471**, 467 (Mar 24, 2011).

150. P. J. Campbell *et al.*, Subclonal phylogenetic structures in cancer revealed by ultra-deep sequencing. *Proceedings of the National Academy of Sciences of the United States of America* **105**, 13081 (Sep 2, 2008).

151. E. S. Venkatraman, A. B. Olshen, A faster circular binary segmentation algorithm for the analysis of array CGH data. *Bioinformatics* **23**, 657 (Mar 15, 2007).

152. B. S. Taylor *et al.*, Functional copy-number alterations in cancer. *PLoS ONE* **3**, e3179 (Jan 1, 2008).

153. P. Van Loo *et al.*, Allele-specific copy number analysis of tumors. *Proc Natl Acad Sci USA* **107**, 16910 (Sep 28, 2010).

154. S. Nik-Zainal *et al.*, The life history of 21 breast cancers. *Cell* **149**, 994 (May 25, 2012).

155. A. K. Maunakea *et al.*, Conserved role of intragenic DNA methylation in regulating alternative promoters. *Nature* **466**, 253 (Jul 8, 2010).

156. M. Esteller, S. R. Hamilton, P. C. Burger, S. B. Baylin, J. G. Herman, Inactivation of the DNA repair gene O6-methylguanine-DNA methyltransferase by promoter

hypermethylation is a common event in primary human neoplasia. *Cancer research* **59**, 793 (Feb 15, 1999).

157. C. Rohde, Y. Zhang, R. Reinhardt, A. Jeltsch, BISMA--fast and accurate bisulfite sequencing data analysis of individual clones from unique and repetitive sequences. *BMC Bioinformatics* **11**, 230 (Jan 1, 2010).

158. J. A. Maxwell *et al.*, Mismatch repair deficiency does not mediate clinical resistance to temozolomide in malignant glioma. *Clin Cancer Res* **14**, 4859 (Aug 1, 2008).

159. D. M. Zimmer, X. B. Zhang, P. R. Harbach, J. K. Mayo, C. S. Aaron, Spontaneous and ethylnitrosourea-induced mutation fixation and molecular spectra at the lacI transgene in the Big Blue rat-2 embryo cell line. *Environmental and molecular mutagenesis* **28**, 325 (1996).

160. D. L. Wyborski, S. Malkhosyan, J. Moores, M. Perucho, J. M. Short, Development of a rat cell line containing stably integrated copies of a lambda/lacI shuttle vector. *Mutat Res* **334**, 161 (Apr 1, 1995).

161. C. N. Sprung *et al.*, Induction of lacI mutations in Big Blue Rat-2 cells treated with 1-(2-hydroxyethyl)-1-nitrosourea: a model system for the analysis of mutagenic potential of the hydroxyethyl adducts produced by 1,3-bis (2-chloroethyl)-1-nitrosourea. *Mutat Res* **484**, 77 (Dec 12, 2001).

162. S. Neri *et al.*, Mismatch repair system and aging: microsatellite instability in peripheral blood cells from differently aged participants. *J Gerontol A Biol Sci Med Sci* **60**, 285 (Mar 1, 2005).

163. X. Lin *et al.*, P53 modulates the effect of loss of DNA mismatch repair on the sensitivity of human colon cancer cells to the cytotoxic and mutagenic effects of cisplatin. *Cancer research* **61**, 1508 (Feb 15, 2001).

164. M. J. Bello *et al.*, Hypermethylation of the DNA repair gene MGMT: association with TP53 G:C to A:T transitions in a series of 469 nervous system tumors. *Mutat Res* **554**, 23 (Oct 4, 2004).

165. S. L. Carter *et al.*, Absolute quantification of somatic DNA alterations in human cancer. *Nat Biotechnol* **30**, 413 (May 1, 2012).

166. J. T. Huse *et al.*, Where are we now? And where are we going? A report from the Accelerate Brain Cancer Cure (ABC2) low-grade glioma research workshop. *Neuro-oncology* **16**, 173 (Jan 1, 2014).

167. F. Bautista *et al.*, Vemurafenib in pediatric patients with BRAFV600E mutated high-grade gliomas. *Pediatr Blood Cancer* **61**, 1101 (Jun 1, 2014).

168. Abstracts of the 15th International Symposium on Pediatric Neuro-Oncology. June 24-27 2012. Toronto, Ontario, Canada. *Neuro-oncology* **14 Suppl 1**, i1 (Jun 1, 2012).

169. D. G. van Vuurden *et al.*, PARP inhibition sensitizes childhood high grade glioma, medulloblastoma and ependymoma to radiation. *Oncotarget* **2**, 984 (Dec 1, 2011).

170. J. K. Wiencke *et al.*, Methylation of the PTEN promoter defines low-grade gliomas and secondary glioblastoma. *Neuro-oncology* **9**, 271 (Jul 1, 2007).

PUBLISHING AGREEMENT

It is the policy of the University to encourage the distribution of all theses, dissertations, and manuscripts. Copies of all UCSF theses, dissertations, and manuscripts will be routed to the library via the Graduate Division. The library will make all theses, dissertations, and manuscripts accessible to the public and will preserve these to the best of their abilities, in perpetuity.

I hereby grant permission to the Graduate Division of the University of California, San Francisco to release copies of my thesis, dissertation, or manuscript to the Campus Library to provide access and preservation, in whole or in part, in perpetuity.

Author Signature _____ Date _06/05/14_